Report 524-02-79-CR

(2) LEVEL II

AD A080459

A Battlefield Obscuration Model

(Smoke & Dust)

FINAL REPORT

By:

Ralph Zirkind

October 1979

OPERATIONS ANALYSIS GROUP

GENERAL RESEARCH CORPORATION

A SUBSIDIARY OF FLOW GENERAL INC.

7655 Old Springhouse Road, McLean, Virginia 22102

Prepared for:

U.S. Army ERADCOM
Night Vision and EO Laboratory
Fort Belvoir, Virginia

Contract DAAK02-76-C-0366

Report 524-02-79-CR

A Battlefield Obscuration Model

(Smoke & Dust)

FINAL REPORT

By:

Ralph Zirkind

October 1979

OPERATIONS ANALYSIS GROUP

GENERAL RESEARCH CORPORATION

A SUBSIDIARY OF FLOW GENERAL INC

7655 Old Springhouse Road, McLean, Virginia 22102

Prepared for:

U.S. Army ERADCOM
Night Vision and EO Laboratory
Fort Belvoir, Virginia

Contract DAAK02-76-C-0366

SECURITY CLASSIFICATION OF THIS PAGE (When Data Entered)

REPORT DOCUMENTATION PAGE

READ INSTRUCTIONS BEFORE COMPLETING FORM

1 REPORT NUMBER: GRC-524-02-79-CR	2 GOVT ACCESSION NO.
3 RECIPIENT'S CATALOG NUMBER: Pepti	
4 TITLE (and Subtitle): A BATTLEFIELD OBSCURATION MODEL (Smoke & Dust)	5 TYPE OF REPORT & PERIOD COVERED: Final, July 77 — Oct 79
	6 PERFORMING ORG. REPORT NUMBER
7 AUTHOR(s): Ralph Zirkind	8 CONTRACT OR GRANT NUMBER(s): DAAK02-76-C-0366
9 PERFORMING ORGANIZATION NAME AND ADDRESS: General Research Corporation, Operations Analysis Group, 7655 Old Springhouse Road, McLean, Virginia 22102	10 PROGRAM ELEMENT, PROJECT, TASK AREA & WORK UNIT NUMBERS: 62709A; 1L162709DR95, OV, 023CJ; 65713A; LX765713DF26, OV, 009CJ
11 CONTROLLING OFFICE NAME AND ADDRESS: Director (DELNV-VI) Night Vision and Electrooptics Laboratory Fort Belvoir, Virginia 22060	12 REPORT DATE: Oct 79
	13 NUMBER OF PAGES: 206
14 MONITORING AGENCY NAME & ADDRESS (if different from Controlling Office): 12) 212	15 SECURITY CLASS (of this report): Unclassified
	15a DECLASSIFICATION/DOWNGRADING SCHEDULE

16 DISTRIBUTION STATEMENT (of this Report)

Distribution of this document is unlimited.

DISTRIBUTION STATEMENT A
Approved for public release;
Distribution Unlimited

17 DISTRIBUTION STATEMENT (of the abstract entered in Block 20, if different from Report)

17) OV

18 SUPPLEMENTARY NOTES

19 KEY WORDS (Continue on reverse side if necessary and identify by block number)

Obscurants
Smoke Model
Aerosol Properties
Explosive Dust Model
Vehicle Dust Model

20 ABSTRACT (Continue on reverse side if necessary and identify by block number)

This report presents a semi-empirical (non-Gaussian) model for the obscurants that may be generated by military activity. These include smoke and obscuring aerosol munitions, dust clouds generated by non-nuclear explosive munitions, and dust generated by military-like vehicles. The field data and some laboratory experiments are discussed, and numerous validations are provided.

DD FORM 1473 EDITION OF 1 NOV 65 IS OBSOLETE

SECURITY CLASSIFICATION OF THIS PAGE (When Data Entered)

441 050

SUMMARY

This report presents a semi-empirical (non-Gaussian) model for the obscurants that may be generated by military activity. These include smoke and obscuring aerosol munitions, dust clouds generated by non-nuclear explosive munitions, and dust generated by military-like vehicles. The field data and some laboratory experiments are discussed.

Basically the approach adopted here is to generate a predictive model that will permit the analyst, as well as the field operator, to establish the thermal and space-time history of the obscurant cloud and the concentration of the obscurant therein. The input data for the predictions are readily available to the user. In a similar vein, the explosive dust model subsumes the smoke dispersion model.

The basis, justification, and validation for the various algorithms are presented, and the mathematical expressions to find the mean values and the deviations of the obscurant concentration spatial-temporal behavior. Directions for model improvement are discussed.

Lastly, an attempt is made here to present, at the ends of sections, a calculational scheme to compute the necessary parameters to establish the effect of the various obscurants on battlefield electro-optical systems.

CONTENTS

SECTION		PAGE
	SUMMARY	i
	INTRODUCTION	1
	1.1 Background	3
	1.2 Approach	4
	PART 1 - SMOKES AND OBSCURING AEROSOL MODEL	7
1	MODEL DEVELOPMENT SYNOPSIS	9
	1.1 Introduction	9
	1.2 Model Extension and Modification	9
2	BASIC CONCEPTS	14
	2.1 General	14
	2.2 Source Characteristics	14
	2.3 Data Problems	27
	2.4 Aerosol Diffusion	39
	2.5 Cloud History	47
	2.6 Multiple and Array Sources	58
	2.7 Validation Tests	61
3	MODEL STRUCTURE	71
	3.1 Computation Scheme for Cloud Concentration of Smokes/Obscuring Aerosols	71
	3.2 Method for WR/WP - Wicks, Wedges, Plasticized Material	77
	3.3 Method for HC Smoke Concentration Time History	81
	3.4 Method for Fog Oil Generator	85
	PART 2 - EXPLOSIVE DUST OBSCURATION MODEL	89
1	INTRODUCTION	91
2	BASIC CONSIDERATIONS	92
	2.1 The Soil Medium	92
	2.2 Particle Size Distribution	96

CONTENTS (Cont.)

SECTION		PAGE
	2.3 Dust Optical Properties	108
	2.4 Explosive Effects	112
3	CLOUD DEVELOPMENT MODEL	117
	3.1 Cratering Effects	117
	3.2 Thermal Effects	128
	3.3 Cloud Dispersal	137
	3.4 Initial Cloud Volume	138
	3.5 Growth of Main Cloud and Stem	138
	3.6 Cloud Dispersion	140
	3.7 Mass Distribution	142
	3.8 Mass Concentration	143
4	VALIDATION TESTS	149
5	MODEL STRUCTURE FOR EXPLOSIVE DUST	163
	5.1 Ground Input Data	163
	PART 3 - VEHICULAR DUST OBSCURANT MODEL	175
1	INTRODUCTION	177
2	TECHNICAL DISCUSSION	178
3	MODEL STRUCTURE	182
APPENDIX		
A	MUNITIONS CHARACTERISTICS	183
B	A STABILITY CLASSIFICATION BASED ON HOURLY AIRPORT OBSERVATIONS	191
C	CONTINUOUS VALUES FOR PLUME DISPERSION PARAMETERS PLUME HEIGHT	195
D	ADDITIONAL CRATERING DATA	197

FIGURES

NO.		PAGE
	PART 1 - SMOKES AND OBSCURING AEROSOL MODEL	
1	Source Sigmas vs. WP Fill Weights	16
2	Cloud Rise History	17
3	Axial Dispersion of Bulk WP	20
4	Submunition Burn Rate, 105 mm Canister (HC)	22
5	Submunition Burn Rate, 6-in Wick (WP)	23
6	Submunition Burn Rate, Navy 155 mm Wedge (RP)	24
7	Proportion of Particles in Various Ranges as a Function of Time Based on Number	31
8	Extinction Coefficient vs. Wavelength	35
9	Trial 9 (DP1-002), 23 September 1977, 13:03:00, WP Smoke	38
10	Prevalence of Pasquill Stability Categories Over the Netherlands	43
11	1/L as a Function of Pasquill Classes and z_0	46
12	Cloud ΔT as a Function of Relative Humidity	57
13	Multi-Munition Schematic	59
14	Trial 4 (DP1-002), 19 November 1977, 12:38:00, HC Smoke	62
15	C · L History Determined by Aerosol Photometers	63
16	C · L Values Versus Time for Row 0	65
17	C · L History from Aerosol Samplers (+ Model Predictions)	66
18	C · L History Calculated from Transmissometers	67
19	C · L Time History; Trial 10, DP1-002, 4-4.2" Mortars	69
20	C · L Time History; Trial DP1-002, 1-155 mm WP	70

FIGURES (Cont.)

NO.		PAGE
	PART 2 - EXPLOSIVE DUST OBSCURATION MODEL	
1	Extinction Coefficient for Ft. Benning and Ft. McClellan	97
2	Typical Grain Size Distribution Curve for DIRT-I Test Area	102
3	Extinction Coefficient as a Function of Particle Diameter	111
4	Significant Blast Parameters	114
5	Definitions of Charge Placement	118
6	Typical Half-Crater Profile and Nomenclature for Near-Surface Burst	119
7	Crater Radii and Depth Versus Depth of Burst Relation for Various Earth Materials	121
8	Apparent Crater Dimensions Versus Charge Yield for Mixed Company Scaled Overburden ST Even. MC-3, MC-2, and MCC-5; Middle Gust Wet and Dry Site ST Events; and Spherical Charge ST Events Conducted at the DRES Site	123
9	Apparent Crater Volume Versus Charge Yield for Mixed Company Scaled Overburden ST Events MC-3, MC-2, and MCC-5; Middle Gust Wet and Dry Site ST Events; and Spherical Charge ST Events Conducted at the DRES Site	124
10	Crater Shape Factors for Conventionally Shaped Craters in Solid and Rock as Compared with Those for Events MC-1, MC-2, and MC-3; the Middle Gust Events; and the Events Conducted at DRES	125
11	Cratering Efficiency as a Function of Height of Burst (Charge Radii)	126
12	Normalized Radiated Power History	130
13	Thermal Yield as a Function of Time	131
14	Spectral Power vs. Time for Two Bands (500 Tons HE)	134
15	Mean Cloud Temperature Vs. Scaled Time	135
16	Cloud Temperature Differential vs. Time for 155 mm Shell, Background Temperature = 1°C	136

FIGURES (Cont.)

NO.		PAGE
17	Main Cloud Parameters Vs. Time	139
18	Stem Height Vs. Time	141
19	Cloud History for Middle Gust III; (100 T), HOB = 1	144
20	Cloud Height as a Function of Time	150
21	Concentration, Transmission Vs. Time for One 155-mm Shell	151
22	Cloud Height History in Silicon and 8-12 um Region	153
23	Cloud Width History in Silicon and Thermal Region Measurements	155
24	Comparison of Measured Relative Transmission and Calculated Values	156
25	Layout of SWII-29 Event	157
26	Comparison of Measured and Calculated C · L Histories at Three Lines	158
27	Comparison of Measured and Calculated C · L History	159
28	Comparison of Calculated and Measured Cloud Height and Width vs. Time	161
29	Comparison of Calculated and Measured C · L History	162
30	Main Cloud Parameters vs. Time	166
31	Stem Height vs. Time	167
	PART 3 - VEHICULAR OBSCURANT MODEL	
1	Visibility Zones as a Function of Concentration and ρ	179
	APPENDIX C - PLUME HEIGHT	
C.1	Plume Parameters at Low Wind Speeds	196

FIGURES (Cont.)

NO.		PAGE
	APPENDIX D - ADDITIONAL CRATERING DATA	
D.1	Nomograph for Crater Depth and Radius	200
D.2	Nomograph for Crater Depth and Radius	201
D.3	Mixed Company Series	204
D.4	Middlegust Series	205

TABLES

NO.		PAGE
	PART 1 - SMOKES AND OBSCURING AEROSOL MODEL	
1	Submunition Burn Time	21
2	Burn Time for Foreign Rounds	21
3	Extinction Coefficients (m^2/g) and Ratios at Various Wavelengths	29
4	Bulk Phosphorus Smoke Particle Size Distribution Parameters	30
5	Pasquill Stability Categories	40
6	Key Used to Estimate the Continuous Stability Classification	42
7	Diurnal Variation of Atmospheric Stability, Great Plains, Nebraska	44
8	Profile Parameters of Some Crops and Buildup Areas	46
9	Cloud Size Parameters for Non-Exothermic Munitions	47
10	Gustiness Intensities for Different Stability Conditions	49
11	Wind Fluctuation Parameters from Fast Response Data	50
12	Pasquill Stability Categories	73
	PART 2 - EXPLOSIVE DUST OBSCURATION MODEL	
1	Soil Material Density	92
2	Subsurface Soil Analysis of Fort Polk, Louisiana	93
3	Classification of Comparative Soil by Weight	95
4	Standard Soil Classification	98
5	US Geographical Variation of Particle Size (Wt. %)	99f
6	Percentage of Surface Soil Particles Below 74 μm	101
7	Particle Size Distribution in Main Cloud (100 Ton HE, Colorado)	103

TABLES (Cont.)

NO.		PAGE
8	Spectral Extinction Coefficients for Dust	1.9
9	Wavelength Variation of Refractive Index	110
10	Spectral Extinction Coefficient	111
11	Explosive Types and Properties	112
12	Apparent Crater Dimensions	120
13	Estimated Parameters for Shells and Mortars	127
14	Spatial Distribution of Shock-Heated Air for Atmospheric Detonation	128
15	Cloud Dimensions for HOB = 0, 1	142
16	Estimated Parameters for Shells and Mortars	164
	PART 3 - VEHICULAR DUST OBSCURANT MODEL	
1	Extinction Coefficient as a Function p	178
	APPENDIX A - MUNITIONS CHARACTERISTICS	
A.1	Types of Fill and Fill Weights for Smoke Munitions	184ff
A.2	Some Smoke Generators and Pots	189
A.3	UK Grenades	189
	APPENDIX B - A STABILITY CLASSIFICATION BASED ON HOURLY AIRPORT OBSERVATIONS	
B.1	Stability Class as a Function of Net Radiation and Wind Speed	194
B.2	Insolation as a Function of Solar Altitude	194
	APPENDIX D - ADDITIONAL CRATERING DATA	
D.1	Crater Data	199
D.2	Middle Goat 1000 lb Cratering Data	202
D.3	Mixed Company 1000 lb Cratering Data	203

INTRODUCTION

1.1 BACKGROUND

This is a final report on the General Research Corporation (GRC) effort dealing with the formulation of a model to describe obscurants and their behavior in a military environment. The effort, during the past two years, has been sponsored by the Night Vision & Electrooptics Laboratory under Contract DAAK02-74-C-0366, and ably monitored by L. Obert.

The model initially addressed the dispersion of smokes and other obscuring aerosols.[1] Emphasis was given to a model that can readily be used in combat simulation models; however, the physical aspects of the model were sufficiently broad and accurate that it could be used for a variety of applications. Subsequently the model has been extended to include explosive and vehicle-generated dust.

The explosive dust model has two stages. The initial dust cloud is determined by the hydrodynamics of the explosion (high-explosive) process, and the dispersion of this cloud is described by the smoke dispersion model. Hence, the overall utility of the model becomes broader. It should be noted that the explosively dispersed bulk white phosphorus shell (155 mm) can, if desired, be modeled like explosive dust.

During the past several years the US Army has conducted extensive field test programs. Data derived from these efforts have been employed here to some extent to assist in validating the concepts used. However, full access and use could have furthered the formulation of a more thorough, flexible model. The reasons for this statement are as follows:

1. The field test data represent a large body of unique data on the generation and turbulent dispersion of various aerosol generators, particularly quasi-instantaneous types.

---

[1] Zirkind, R., An Obscuring Aerosol Dispersion Model, GRC Report 231, Vols. I and II, December 1978.

2. Verification of the laboratory experiments and theoretical results would have been possible.

Unfortunately, the data have been "shoehorned" in a preconceived dispersion model. Hence new model development by the US Army is a remote possibility and many important questions may remain unanswered.

1.2 APPROACH

The objective of the sponsored effort has been the development of a model that can readily predict the properties of a dispersing aerosol cloud produced by military munitions and smoke generators. To meet this objective a semi-empirical approach was adopted to be consistent with conventional military procedures, field conditions, and physical phenomena. Specifically, the chemical officer has a limited set of data for planning purposes and therefore the inputs should be consistent with this fact.

Of greater importance is the fact that existing representations of diffusion based upon Gaussian distribution functions appear too inadequate for aerosol releases at or near ground level where the entire dispersal process occurs within, at most, a several minute period. Examination of gust data for 1-sec sampling and 5-min and 10-min averaging periods exhibit large differences.[2] This implies that a very large sample of instantaneous concentration values would be required to approach a Gaussian distribution and obtain the mean value. On the other hand, the fluctuations per se are of equal import since periods of low concentration along the line of sight of a sensor, comparable to acquisition time, would defeat the usage of the obscurant. Further the several obscurants used are initially buoyant plumes; i.e., they release significant thermal energy, and therefore a fraction of their temporal behavior is dominated by heat exchange and not momentum exchange.

For the above reasons, the approach taken was to establish the mean concentrations on the basis of experimental data using Pasquill stability

[2] "Exploring the Atmosphere's First Mile," (H. H. Lettau and D. Davidson, eds.), Vol. II, Pergamon Press 1957. (Proceedings of the Great Plains Turbulence Field Program.)

parameters and establish the variations therefrom, again from experimental observations.

In the main text we will provide the background material to justify the various rules adopted for the proposed models and the models proper.

Although we have discussed the obscuring aerosol, the remarks are equally applicable to explosive dust; that is, we have developed a semi-empirical model to describe the cratering phenomena and subsequent dispersion of the dust cloud. Once this cloud is "stabilized," its dispersion is handled like that of any aerosol cloud.

The report is divided into three parts: Part 1 - Smokes and Obscuring Aerosol Model; Part 2 - Explosive Dust Obscuring Model; and Part 3 - Vehicular Dust Obscuring Model. Collectively, the three models constitute a "dirty" battlefield atmospheric model.

This writer recognizes that improvements can be made in these models; however, additional experiments and analyses are required to establish the bases for the improvements.

PART I

SMOKES AND OBSCURING AEROSOL MODEL

1 MODEL DEVELOPMENT SYNOPSIS

1.1 INTRODUCTION

In Ref. 1 we presented a semi-empirical model that can predict the spatial-temporal characteristics of the aerosol cloud produced by smoke and other obscuring aerosol sources (artillery shells, mortars, smoke pots, and aerosol generators). These characteristics are: (1) mean concentration, (2) path length, and (3) radiation transfer. In addition, Ref. 1 provided several validations of the proposed model where the detonated munitions were either bulk white phosphorus (WP) or phosphorus submunitions (WP wicks).

Ref. 1 addressed the following topics: source size data; fluctuations effects; and the model structure for quasi-exothermic and non-exothermic obscurant sources. However, topics not discussed therein:

(a) A treatment of the still air case (mean wind speed, $\bar{u} = 0$)

(b) Field test data

(c) Extinction coefficient data

are treated in this report; we extend here the model presented in Ref. 1. In the remainder of this section we summarize the discussion; and in Sec. 2 (2.1 to 2.5) the reader will find a complete discussion and several additional validations.

1.2 MODEL EXTENSION AND MODIFICATION

1.2.1 Concentration Fluctuations

The experimental concentration data exhibit small and large scale fluctuations about a mean value. In Ref. 1 we indicated that horizontal wind-speed variations can account for the overall concentration fluctuations; however, the available sampling data could, at best, provide an estimate of the standard deviation.

---

[1] Zirkind, R., An Obscuring Aerosol Dispersion Model, GRC Report 231, Vols. I and II, December 1978.

Since the atmospheric stability descriptor used in our model is the Pasquill Category (Ref. 1), we have selected fluctuation data that have been correlated with Pasquill Category; see values given below.

Pasquill Category	A	B	C	D	E	F	G
$\sigma(u)$	1.13	1.2	1.6	1.33	1.08	0.89	0.51
$u'_{RMS}/\bar{u}$	0.2	0.18	0.20	0.2	0.18	0.17	0.14

where u'_{RMS} is the root mean square of the horizontal wind-speed fluctuation u', and $\sigma(u)$ is the standard deviation of u. For use in the model, the u'_{RMS} value should be used to obtain an estimate of the small-scale fluctuations.

The larger scale fluctuations of interest here occur with a period on the order of 40 to 60 sec; however, data available from field tests have not been analyzed. These fluctuations are responsible for the phenomenon known as intermittency (when the concentration approaches a near-zero value for a period of about 40 to 60 sec). The available data indicate that the effect occurs at random times and, therefore, a statistical model is required if the impact on sensors is to be treated accurately.

1.2.2 Aerosol Dispersion

The basic algorithms to find the cloud growth for $\bar{u} > 0$ have remained unchanged; however, the rise of the buoyant cloud has been clarified and updated. For example, when the atmospheric stability is unstable or neutral then the final rise, ΔH_{max} is

$$\Delta H \simeq 1.6F^{1/2}(3.5x_*)^{2/3} \div \bar{u}$$

where $x_* = 14F^{5/8}$ for $F \leq 55\ m^4/sec^3$

$x_* = 34F^{0.4}$ for $F > 55\ m^4/sec^3$

in which x_* = transition distance and $F = 3.6 \times 10^{-5}$ (heat release/sec)

Similarly, the values of $\bar{y}$ and $\bar{z}$, the lateral and vertical coordinates respectively, have been given as continuous functions for unstable to stable atmospheric conditions; see Appendix C.

Lastly, we suggest the following rules be used for still air, $\bar{u} = 0$:

(1) For an instantaneous source the maximum rise is

$$H_{max} = 1.89Q^{0.25} \quad (m)$$

(2) For a maintained source

$$H = 5F^{0.25}/\bar{s}^{3/8}$$

Where $\bar{s} = g[(\Delta T/\Delta Z) + \Gamma] \div T$

The definitions of the above are as follows:

g = gravitation acceleration (m/sec)

Γ = adiabatic lapse rate

$\Delta T/\Delta Z$ = actual lapse rate

T = ambient absolute temperature (°K)

The shape of the aerosol cloud is assumed to be a right circular cone with a vertex angle of 52°.

In Ref. 1 we omitted the effect of a ground or elevated inversion layer on the growth of the aerosol cloud. In Sec. 2 the rules are provided for various atmospheric stability conditions and are incorporated into the model structure, Sec. 3.

1.2.3 Model Issues

We will now discuss several topics that require further clarification and probably additional research and development.

Source Size

The experimental data defining the initial cloud size generated by munitions filled with bulk phosphorus are limited. These data would indicate that the initial cloud dimensions are large; e.g., the 1σ value of the radius and height for an artillery-delivered 155-mm shell are ~8 m and 3 m, respectively; and within several seconds the downwind dimension, x, can be an order of magnitude greater than the calculated value, where x = wind-speed × time. The importance of this parameter* is twofold: (1) it gives us the distribution of the source material for buoyancy calculations; and (2) it is the mathematical representation of the source, i.e., whether the source is a quasi-point or a distributed type. If the bulk material is spread over a large area then the buoyancy will be less than if, as assumed in the model, the material is released within a small area. With respect to the dispersion modeling, if we assume a distributed source, then the cloud development would be similar to the treatment used for submunitions like the white phosphorus wicks. Since the model reproduces the observed cloud geometry quite accurately from statically fired munitions, we assert that the bulk material is concentrated in the vicinity of the detonation. Also, the observed cloud at early times ($\lesssim$ several seconds) is a visible phenomenon generated by small quantities of the total fill weight and the coupling of the high-explosive burster with the WP. This topic is discussed in greater detail in Sec. 3.

This issue and the burn time require additional experimentation and research to provide a more solid base to this and other models.

For the white phosphorus submunitions, the situation is similar, particularly the ground dispersion pattern of the wicks or wedges for live firings. Although the proposed dispersion pattern simulation, three linear arrays in our model, yields good agreement with experiments, we strongly recommend extensive further experimentation to obtain statistical data of the ground dispersion pattern and additional burn time and rate data.

*For the Smoke Obscuration Model this parameter is important since the distribution for the source is assumed to be Gaussian and is an initial condition for the diffusion equation.

Efficiency

The literature specifies the fill weight of the active basic chemicals; however, the percentage of conversion to smoke factor, efficiency is not available except in a qualitative sense. For example, we find such statements as "any material entering a pool of water is not converted to smoke" or "fragments will be buried in soft dirt". Evidently, this should be quantified by experimentation. In the interim we have assumed that the efficiency for hard dirt is 100%; however, in soft dirt or "muck" the values are 85% and 50% respectively.

Extinction Coefficient

The spectral extinction coefficient is a critical parameter to establish the optical properties of the obscuring cloud; however, the values for the different obscurants are not firmly established. For example, the values are dependent on the particle size distributions. Field data indicate that the size distribution varies during the lifetime of the obscuring cloud, and that the distribution descriptors, mass mean diameter (MMD) and geometric standard deviation (σ_g), differ from the values used in laboratory experiments to obtain the spectral extinction coefficients. It should be noted that these and related topics are discussed in Sec. 2.

Hence an in-depth analysis of the field test data is necessary to establish the spectral extinction coefficient; that is, correlate the laboratory data, independent concentration and particle size data, and transmissometer data.

Lastly, we strongly recommend that an analytical and measurement program be conducted to establish the intermittency properties of military smoke clouds. The intermittency is important to reliably establish electro-optical sensor performance, especially laser systems.

2 BASIC CONCEPTS

2.1 GENERAL

The basic objective of the obscurant model is to determine, to some degree of accuracy, sensor performance when an obscurant cloud exists in the field of view of the sensor. This may imply the temporal history of the path transmission, cloud radiance (self or reflected), or other parameters that affect sensor performance.* To calculate these parameters for different obscurant sources several factors are required, and these are as follows:

1. Source characteristics
2. Description of the aerosols produced by the source
3. Spatial-temporal history of obscurant aerosol concentration
4. Environmental interaction with the aerosol cloud production and development

With the exception of the first, the remaining factors are characterized by the turbulent diffusion of source material in the environment. In the next several sections we present a discussion of each factor.

2.2 SOURCE CHARACTERISTICS

The nomenclature, fill weight, burst radius, and other technical data for inventory munitions are given in US Army publications (FM9-137, 38, etc.). Several of these data sheets are given in Appendix A. Recent developmental items include submunitions such as white phosphorus wedges and wicks.

Hence we now have a spectrum of sources varying from near instantaneous point types to linear, continuous arrays. The importance of this lies in the variety of mathematical descriptions needed to describe the dispersion history. This is considered in Sec. 2.5.

*The radiation transfer methodology is omitted here; the reader is referred to Ref. 1.

2.2.1 Source Size

The character os the smoke obscurant is of interest to the cloud dispersion. We consider smoke pots and fog oil generators as point emitters. Until further data are available, we consider that munitions filled with wedges, wicks, or plasticized phosphorus produce ground patterns that can be simulated as linear arrays. This gap in our knowledge needs to be filled by further explicit tests.

In our model, we assume that artillery shells and mortars delivering the bulk white phosphorus are quasi-point sources; the source is invariant with the shell and mortar size. Since this material is a major smoke cloud generator, we will consider it here in greater detail than in Ref. 1 and include the initial cloud development.

Dolce and Metz[3] have attempted to characterize the smoke cloud formation and development for static firings and artillery-delivered bulk white phosphorus. We will first examine the source size data. Figure 1 presents the Dolce and Metz data along with older data, the half-width of the source radius, σ_{YS}, and the source height, σ_{ZS}. It should be noted that these values refer to the cloud dimensions and not the ground mass distribution. Several additional values are added from the Fall 1977 Dugway tests.

The artillery curve is higher than the mortar curve. We will now attempt to explain this and other data.

In Fig. 2 we have plotted the initial and subsequent cloud rise for a 60-mm mortar and a 155-mm artillery shell. We observe that the plume centroid has a different time history than the initial cloud rise and subsequent "source" height. In Ref. 3 the authors identify a "weapon phase" time (t_w). This time corresponds to the time interval from initial detonation of the high explosive to the time the cloud becomes white, i.e., loses

[3] Dolce, T. J., and D. F. Metz, An Analysis of the Smoke Cloud Data from August 1975 Jefferson Proving Ground Smoke Test, AMSAA Technical Report 301, September 1977.

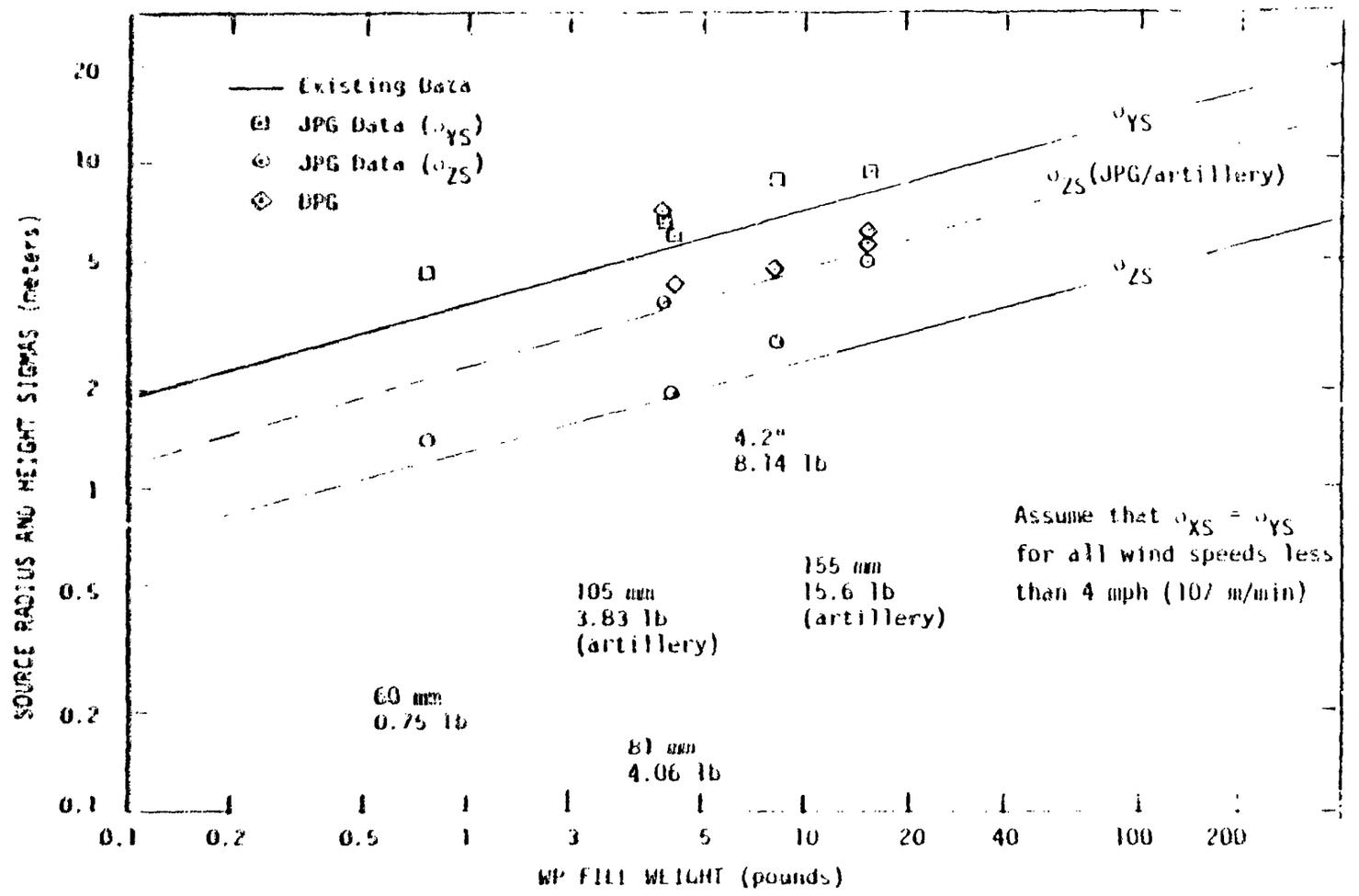

Figure 1. Source Sigmas vs. WP Fill Weights

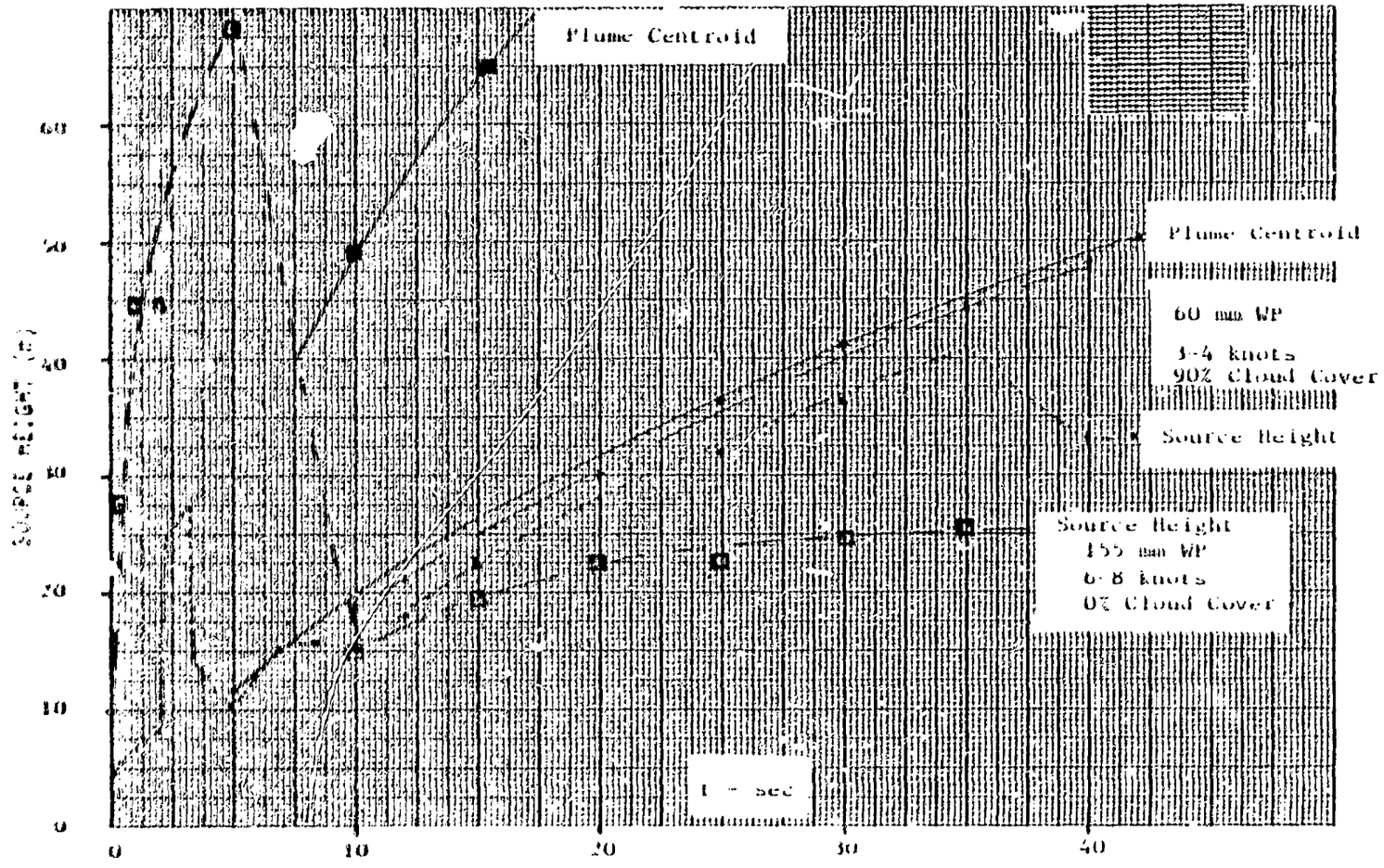

Figure 2. Cloud Rise History (60mm ●— — , o—— ; 155 mm (— — , —●—)

its orange glow. The mean values of the weapon phase time for several munitions are given below, along with the weights of high explosives used to disperse the white phosphorus. An examination of the times clearly

Munition	HE (lb)	WP (lb)	t_w (sec)
60 mm	0.025	0.75	0.44
81 mm	0.08	4.0 (1.75)	0.56
4.2 in	0.73	0.75	0.87
105 mm	0.51	3.83	~0.6
155 mm	0.83	15.6	1.1

indicates that they correlate with the mass of HE; that is, the mean cloud temperatures would be at mean ambient for times equivalent to t_w (see Part 2). Further, the power released by the HE is approximately 100 times greater than that from the oxidation of the white phosphorus within the initial 25 msec. At later times (~ 1 sec intervals), the WP material, with the exception of the rare large piece, will be oxidized and converted to phosphoric acid.

Hence, the initial rapid rise for $t \lesssim 5$ sec is primarily due to the HE detonation and some entrained phosphorus particles; however, the effect on the vertical cloud rise behavior at later times is negligible. This may be justified on energetic considerations: the heat release/unit weight is approximately the same for HE and WP, whereas the ratio WP/HE varies from 8:1 to 30:1; therefore, the total impact on overall buoyancy is small. However, the turbulent flow generated by the HE fireball may be responsible for the early history of a WP smoke cloud.

The effect of the large difference between the quantity of WP and HE in the two weapons is now clear. For 60-mm, the small quantity of HE, the effect is small and the centroid is not different than the "source"; however, for the 155-mm the explosive effect and certainly the quantity of WP is larger. The latter is responsible for the significant centroid rise.

In Ref. 3, the initial dispersion of cloud in the downwind direction (x-axis) is not addressed except that $\sigma_{XS} = \sigma_{YS}$ for wind speeds ≤ 4 mps (see Fig. 1). The latter statement is inconsequential since the data indicate that the cloud length at the end of the weapon phase may be in excess of 100 m; see Fig. 3. Beyond this time the axial growth is characteristic of mean wind-speed magnitude; i.e., $x = \bar{u} \times t$. These results are not dissimilar for static and dynamic detonations; e.g., a static firing of a 105-mm had a ground dispersion of ~ 61 m. If a significant amount of bulk phosphorus is dispersed, these data are difficult to understand.

A simple explanation is possible of the overall dispersion observations discussed in Ref. 3 and similar tests; that is, a small quantity of material can generate a cloud "apparent" to the observer or camera. Actually, this cloud has a low concentration but with sufficient glare to be interpreted as a significant cloud.

If the phosphorus is dispersed over a large area, then the engulfed air volume would quickly reduce the buoyancy since the volume increase $\propto$ surface area $\equiv$ (dispersion width)^2. Hence there should be a marked effect on plume rise; however, the plume rise data agree with experimental and analytical models of quasi-point buoyant plumes to be described later and therefore the quantity of dispersed material is assumed to be small.

In view of the limited data in Ref. 1, e.g., extremely unstable conditions for the static firings and other similar uncertainties in other test results on cloud geometry and dispersion, we cannot resolve the above problem. A definitive experiment is required.*

2.2.2 Burn Time

Salomon and Peterson[4] reported their findings on burn rate and time for several types of smoke munitions. The burn rates for HC and WP (wick/

*It should be noted that the validations performed here show excellent agreement with single and multiple rounds that explicit, valid data are required prior to making major model modification.

[4]Salomon, L. L., and E. Peterson, Testing of Smoke Munitions and Submunitions, Paper H, Proceedings of the Smoke Symposium II, April 1978, DRCPM-SMK-T-003-787, June 1978.

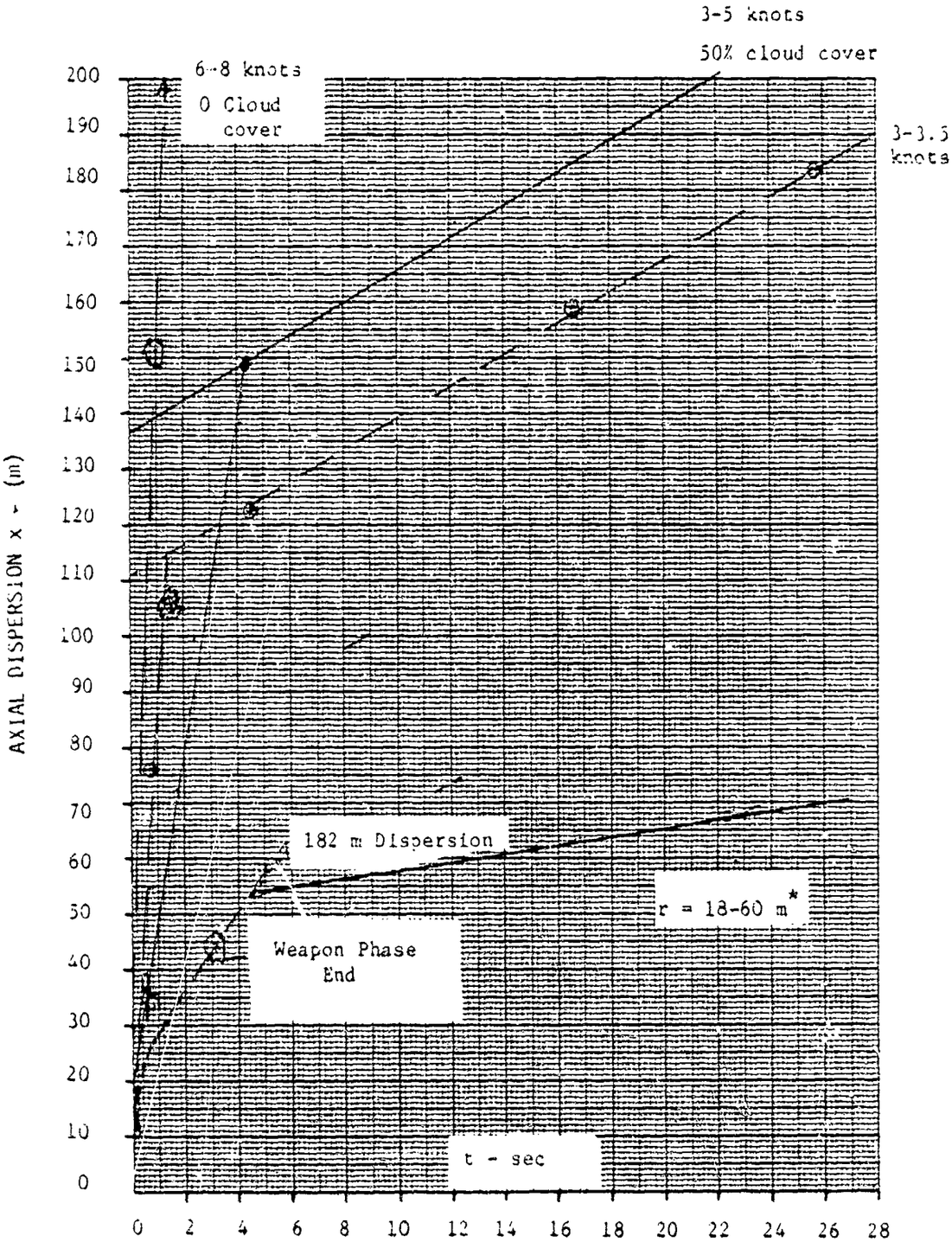

Figure 3. Axial Dispersion of Bulk WP. Dispersion radius, r (r* value in US Army FM9-13).

wedge) are shown in Figs. 4 and 5. We observe that the rates are relatively uniform for HC and WP (wick) but nonuniform for the RP wedge, Fig. 6. Since the sample is small, a single characteristic may be appropriate for phosphorus. We assume linear burning for WP and the rate for HC as given in Fig. 4.

The burn times for the various submunitions as reported by Salomon and Peterson[4] are given in Table 1. It should be noted that (1) the RP munitions are wedges or wicks and (2) the second 155M1 should read 155M2.

TABLE 1

SUBMUNITION BURN TIME

Munition	Type	Time (min)
155M1	HC	2.3
155M1	HC	1.3
105 mm	HC	2.0
6" Wick	WP	6.5
3" Wick	WP	7.8
2.75" Wick	WP	4.3
81 mm (Navy)	RP	4.3
81 mm (German)	RP	3.6
155 mm (Navy)	RP	6.4

The burn time for several foreign rounds are given in Table 2.

TABLE 2

BURN TIME FOR FOREIGN ROUNDS

Type	Time (min)
82 mm Mortar	0.33
120 mm Mortar	4.75
122 mm Artillery	>9.0
130 mm Artillery	>5.0

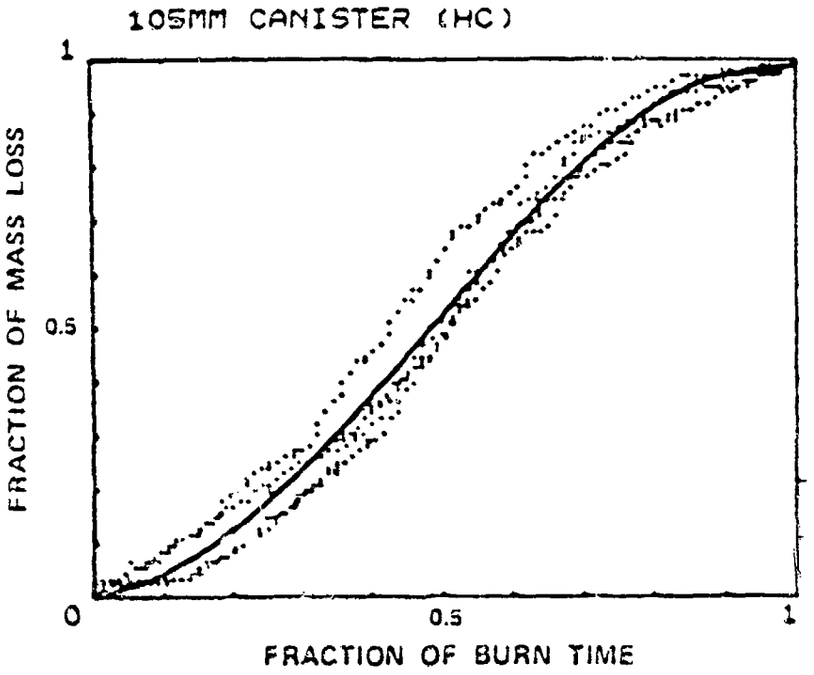

Figure 4. Submunition Burn Rate, 105 mm Canister (HC)[4]

[4] Salomon and Peterson, op. cit.

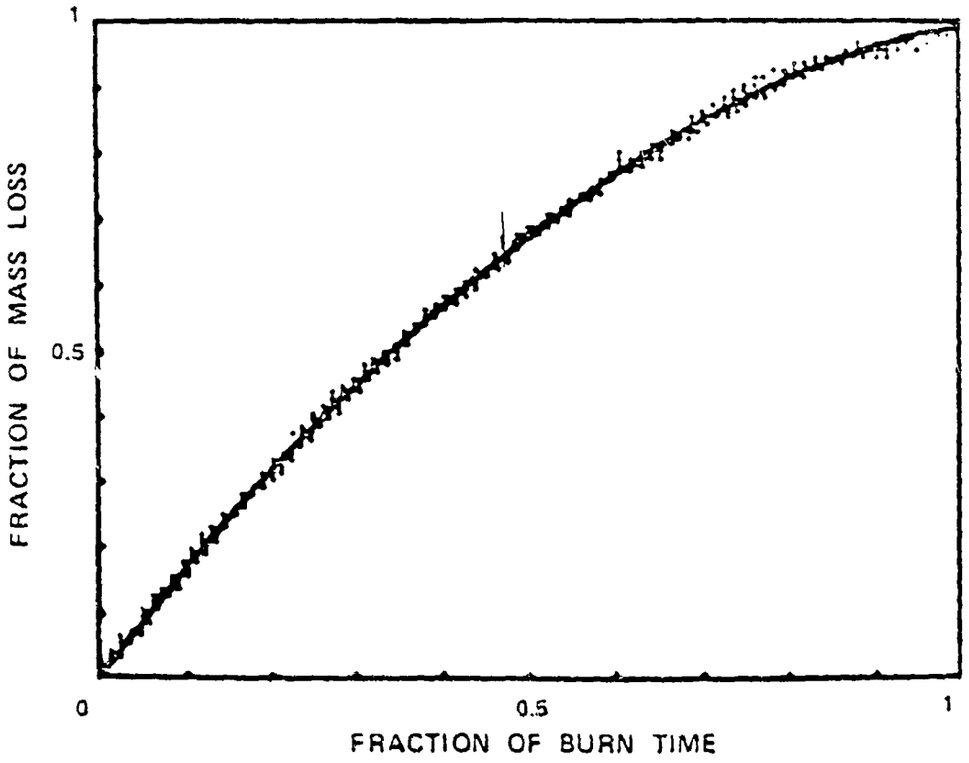

Figure 5. Submunition Burn Rate, 6" Wick (WP)[4]

[4]Salomon and Peterson, op. cit.

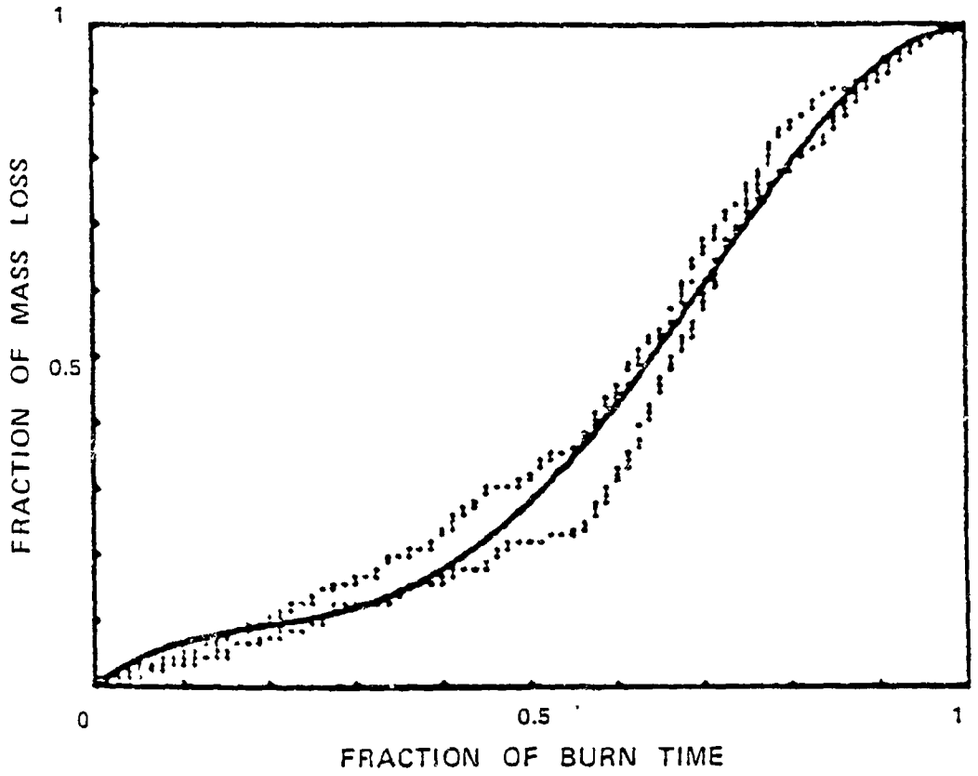

Figure 6. Submunition Burn Rate, Navy 155 mm Wedge (RP) [4]

[4] Salomon and Peterson, op. cit.

First, if the burn times in Table 2 are for bulk white phosphorus (WP) and not plasticized white phosphorus (PWP) then they are not in agreement with the foreign literature. Second, the weight of WP is relatively low to burn for such long periods; that is, on the basis of firing replacement rates the estimate burn times are extremely long. The results for the 82-mm mortar are longer than for the US 81-mm mortar where 80% is oxidized in ≤ 2 sec and the balance in ≤ 10 sec.[5]

Lastly, the experimental data on concentration histories do not agree with Salomon and Peterson's data.

In the Dugway tests held in the fall of 1977, where inventory smoke munitions were tested, the 4.2" WP mortar like the 81 mm is primarily oxidized rapidly (≤ 2 sec). To support this we note that the concentration is ~ 0.8 g/m^3 at 1 sec, 55 m from the origin; within 10 sec the entire quantity is oxidized.

The impact of the explosive-generated thermal environment on the kinetics of bulk phosphorus does not appear in the literature.

With respect to HC canisters the following burn time data were provided by the Program Manager (PM)/smoke-obscurants:

Munition	Burn Time
155 mm M1	120-240 sec
155 mm M2	60-240 sec
105 mm M1	180 sec

It should be noted that the M2 has $\sim 50\%$ the fill weight of the M1. The above do not differ from the earlier results, but the obscuration of smoke pot emission is simple compared to that of an explosive munitions like a mortar or artillery round.

[5]Private communication, CSL Edgewood Arsenal, 1 December 1978.

The estimates made by Salomon and Peterson are qualified by them and relate to mass loss. In the next paragraph we discuss the burn time.

The fill weight specified in a standard munitions manual gives the basic weight of basic chemicals that can generate an obscuring aerosol cloud. For munitions delivered by artillery, mortars, or rockets, the fuze altitude (or type) is important since for a near or on-ground burst the ground hardness plays a role in conversion efficiency. If the ground is soft or adjacent to water then part of the fill material may be embedded in the subsurface material and not available to the aerosol production process. Also an efficiency factor appears to exist for smoke pots; that is, the entire material is not converted into an obscuring aerosol cloud.

Soviet pots appear to have efficiencies as low as 40%, a low value. Observations by US sources are unknown to this writer; however, highly efficient smoke pots should not be difficult to produce.

Thus we assume that for phosphorus munitions the fill efficiency is $\simeq 1$ for hard pack dirt, 85% for loose dirt, e.g., plowed field, and $\leq 30\%$ for "muck." For smoke pots, it is again assumed that if the pot ignites with the outlets exposed to the atmosphere then the efficiency $\simeq 1$; actually, the value, on the average, is less. Further, the percentage of upright canisters is <100%; the exact number is not available.

2.2.3 Yield

The yield factor is defined as the final mass to the initial mass available for smoke generation. Johnson and Forney[6] published yield results for various smoke materials. These are summarized in algebraic form, where RH = relative humidity:

$$Y(WP) = 3.8 + 0.003\ (RH\% - 10)^{1.67}$$

$$Y(ZnCl_2) = 1 + 0.051\ (RH\% - 5)^{0.85}$$

$$Y(AlCl_3/H_2SO_4) = 2.8 + 0.016\ (RH\% - 20)^{1.25}$$

$$Y(Fog\ Oil) = 1$$

[6] Johnson, M. C. and P. D. Forney, The Effectiveness of Obscuring Smokes, ORG Edgewood Arsenal, 1972 (unpublished).

Recently Rubel[7] published theoretical yield results for white phosphorus which agree with the Johnson and Forney theoretical results. On the other hand, field measurements of concentrations would indicate that lower values give better agreement: $Y(WP) = 2.9 + 0.003\ (RH\% - 40)^{1.67}$. At 40% relative humidity the difference is ~1.74, a major difference that could not be accounted for in observed and calculated values of aerosol concentration unless several factors compensate for the difference.

For completeness, we cite two recent studies that consider the physico-chemical problem of phosphorus/phosphoric acid[8,9], where the former considers particle size and kinetic times.

With respect to kinetic times, the various stages are modeled with the exception of the oxidation (combustion process), which is responsible for the heat release and subsequent conversion to phosphoric acid. Clearly, the large variations in burning times should have an effect upon the overall particle size distribution, etc. Further, the environment created by the high-explosive bursters should alter the initial amount of oxygen and moisture available for chemical reactions and the state variable of pressure and temperature.

2.3 DATA PROBLEMS

2.3.1 Extinction Coefficients

One of the agonizing problems for the modeler (and analyst) is the magnitude of the spectral extinction coefficients (absorption and scattering)

---

[7] Rubel, G. O., Predicting the Droplet Size and Yield Factors of a Phosphorus Smoke as a Function of Droplet Composition and Ambient Relative Humidity under Tactical Conditions, ARCSL-TR-78057, Chemical Systems Laboratory, APG, November 1978.

[8] Rubel, G. O., An Aerosol Kinetic Model for the Condensational Growth of a Phosphorus Smoke, Proc. of Smoke Symposium III, 1979.

[9] Frickel, R. H., G. O. Rubel, and E. W. Stuebing, Relative Humidity Dependence of the Infrared Extinction by Aerosol Clouds of Phosphoric Acid, Proc. of Smoke Symposium III, 1979.

for the different obscuring aerosols. For example Milham[10] gives the extinction coefficient at 1.06 μm for HC/RP as 1.5 m^2/g, whereas derived values from the field data are 0.98 (HC) and 0.59 (WP); see Table 3. The differences between laboratory and field trial data are difficult to rationalize for several reasons:

1. The concentration history at the transmissometer is different than the values at the sampler, therefore, correlation is not probable.

2. The particle size distribution in the field changes with time, and, therefore, the distributions characteristic of the extinction coefficient are unknown.

3. Broadband devices are utilized; e.g., the 9.75-μm transmissometer actually covers from ~9 to 11 μm; see Table 3. Now the integrated extinction coefficient is a function of the detector spectral response and the spectral extinction coefficient so that the "effective" extinction coefficient depends on the C · L value. Hence, the suggested field values for "x" is not obvious.

Conversely the ability to validate the transmissometer measurements from a predicted C · L vs. time curve will be difficult due to the repeated deviations in the experimentally determined extinction coefficients.

We will now examine the laboratory and field data, and the impact of particle size on the accuracy of spectral extinction coefficients when a transmissometer is used.

Rubel (Ref. 7) reports that at 36% relative humidity he found for the phosphorus particles that the mass median diameter = 1.24 μm and geometric standard deviation, σ_g = 1.34, where the particle size is

[10] Milham, M., A Catalog of Optical Extinction Data for Various Aerosols/Smokes, Edgewood Arsenal Report ED-SP-77002, June 1976.

TABLE 3

EXTINCTION COEFFICIENTS (m^2/g) AND RATIOS AT VARIOUS WAVELENGTHS

Trial No.	Type of Smoke	α(1.06 μm) (m^2/g)	α(3.4 μm) / α(1.06 μm)	α(0.4-0.7 μm) / α(1.06 μm)	α(3.4 μm) / α(9.75 μm)	α(9.75 μm)
R1	HC	0.86		3.1		
2	HC	0.62	0.12		1.8	0.067
3	HC		0.11	4.1	2.3	0.048
5	WP	0.63	0.20		1.0	0.2
6	WP	0.71	0.32		0.98	0.326
7	WP	0.61	0.20		0.96	0.208
9	WP	0.65				
10	WP	0.43	0.16		0.80	0.2
14	WP	0.42	0.18	3.6	0.73	0.246
15	WP		0.19		0.72	0.263
17	WP		0.35			
18	WP	0.69	0.29		0.69	0.32
19	WP	0.60	0.21		0.92	0.23
21	WP	0.76	0.21		0.76	0.274
22	WP	0.49	0.23		0.93	0.247
23	WP	0.48				
25	HC	1.1	0.10	3.5	2.1	0.476
26	HC		0.89		3.0	0.296
27	HC	0.89	0.074	3.0	3.2	0.023
29R2	HC	1.5		3.2		
31	HC	0.91	0.14	3.4	2.4	0.058

Summary

λ (μm)	HC α(m^2/g)	WP α(m^2/g)
0.4-0.7	3.3	2.1
1.06	0.98	0.59
3.4	0.11	0.23
9.75	0.044	0.27

defined by a log-normal distribution. An analysis of several Dugway trials was performed here for particle size characteristics where the relative humidity varied between 32% and 36%. The results are given in Table 4 for the average values. Clearly the spread is greater than can be attributed

TABLE 4

BULK PHOSPHORUS SMOKE PARTICLE SIZE DISTRIBUTION PARAMETERS

Test	Munition	MMD (μm)	σ_g	RH (%)
DPI-002-T34	155 mm	3.39	2.13	35.0
DPI-002-T16	4.2"	1.14	1.76	34.2
DPI-005-T16	130 mm	3.38	2.0	32.6
DPI-002-T24	155 mm	2.65	2.08	36.2
DPI-005-T12	122 mm	1.795	1.83	31.8

to statistical variation. Further, the observed field data show time dependence on size distribution where settling or coagulation processes are insignificant if not nonexistent; see Fig. 7.

Hence, if the aerosol distributions for WP are time dependent and munition related, then the use of transmissometers to establish concentration histories is subject to further validation. We now discuss this important topic.

The determination of the aerosol concentration in an obscurant cloud has been made by aerosol (photometric) samplers and transmissometers. There is an extensive literature on sampling techniques and their limitations and, therefore, samplers are not discussed here except to note that the system noise spectrum for the devices used in the field by test personnel would be extremely valuable. The reason is the desirability of separating the

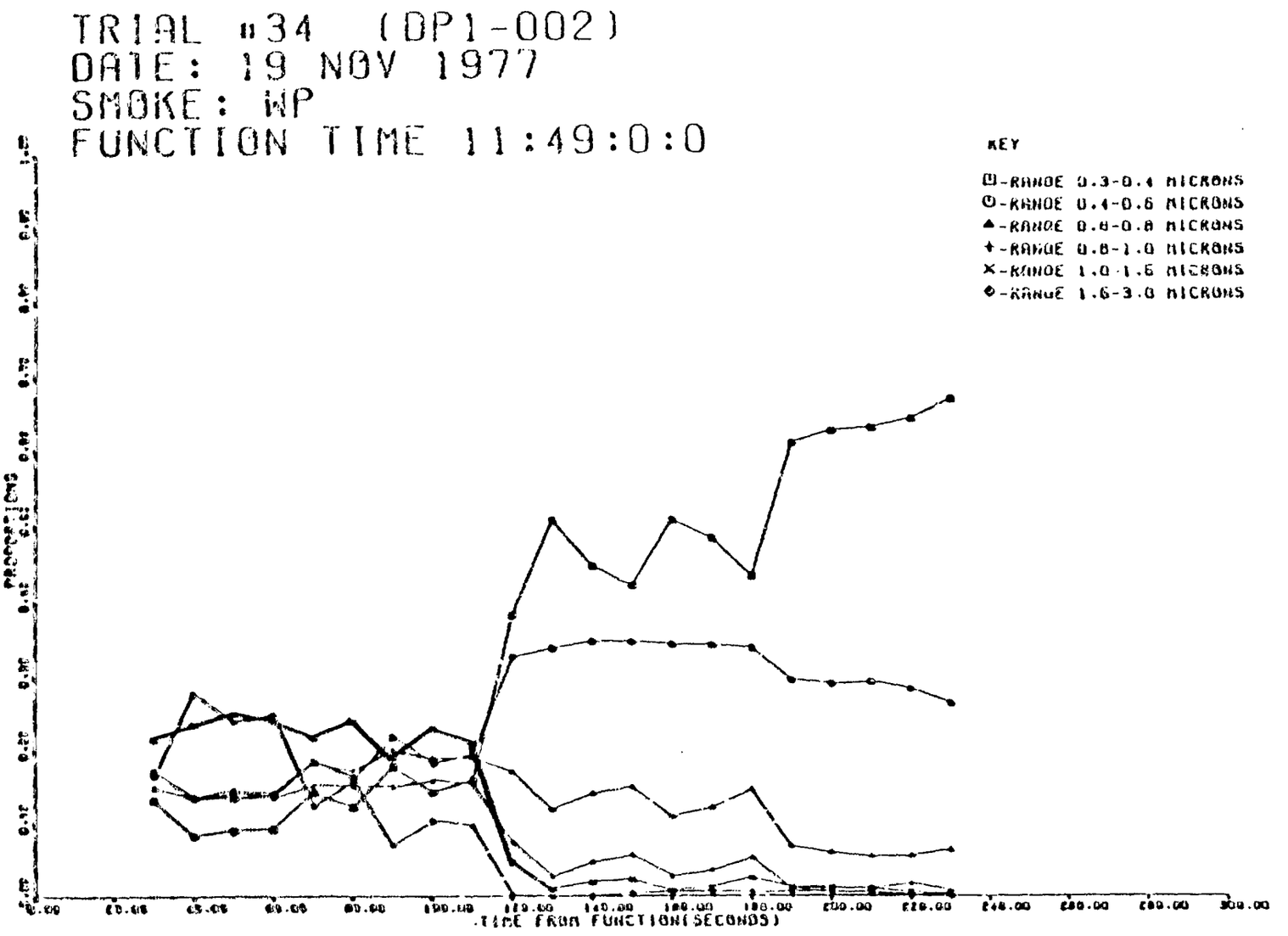

Figure 7. Proportion of Particles in Various Ranges (see Key) as a Function of Time Based on Number (private communication from NVL and ECOM Laboratory)

contribution of atmospheric fluctuations in the temporal variation of the C · L curve from system noise, where C = concentration (g/m^2) and L = path length in cloud (m). This separation is required, as the data clearly indicate noise fluctuations. The use of transmission measurements in order to derive particle concentration requires some discussion.

First, there is a question about the current value of the spectral extinction coefficient. The parameter C · L (g/m^2) is found from the relation

$$C \cdot L = \ln T/\alpha_\lambda \tag{1}$$

where α_λ = spectral mass extinction coefficent

T = fractional transmission through the cloud

The standard procedure is to utilize laboratory measurements. These may not simulate free space conditions as discussed earlier. We will now attempt to show that this may not be serious at some wavelengths. For this we will follow the treatment of Chylek.[11]

A relation between the volume extinction coefficient, k, and the mass concentration, M, can be written as

$$M = \frac{4\rho}{3}\left[\frac{\int r^3 \cdot n(r)\, dr}{\int r^2 Q_{ext}(m,\ r,\ \lambda) n(r)\, dr}\right] k(\lambda) \tag{2}$$

where ρ = bulk density

r = particle radius

n(r) = number of concentrations per unit radius change

Q_{ext} = extinction efficiency factor

[11] Chylek, P., et al., "Infrared Extinction and the Mass Concentration of Atmospheric Aerosols," Atmospheric Environment, 13, 1979, pp. 169-173.

Since ρ and m (the refractive index) are not significantly different in time and position, the relation (Eq. 2) strongly depends on n(r). On the other hand, if the bracketed expression is equal to a constant, h, for a specified n(r) then it follows that

$$M = k(\lambda)4\rho/3h \tag{3}$$

A sufficient condition for this situation is

$$Q_{ext}(r, \lambda) = hr \tag{4}$$

or, the extinction efficiency factor is proportional to particle size. Let $x = 2\pi r/\lambda$ be the size parameter; then

$$Q_{ext} = h \cdot \frac{\lambda}{2\pi} \cdot x = c \cdot x \tag{5}$$

and, therefore,

$$M = k(\lambda) \cdot \frac{2\rho\lambda}{3\pi c} \tag{6}$$

where c is the slope of Q_{ext} vs. x. Clearly if c is a constant or slowly varying for a given range of particle sizes, then the mass concentration is a constant if $k(\lambda) \propto \lambda^{-1}$. The latter occurs for moderate-size particles, $\lesssim 1.0$ μm. In Ref. 11, Mie calculations for a realistic particle show that Q vs. r (μm) is linear at $\lambda = 0.55$ μm for particle radii $\lesssim 0.5$ μm and for $r \lesssim 5$ μm at $\lambda = 11$ μm.

The range of applicability is defined by the ratio

$$R(r_a, \sigma) = 3\int_0^\infty r^2 Qn(r)\, dr / 4\int_0^\infty r^3 n(r)\, dr \tag{7}$$

where r_a is the geometric mean radius and σ is the geometric standard deviation; that is, if R = constant for a range of r_a, then $k(\lambda)$ and mass concentration are independent of size distribution. (Note for a fixed λ, $R = 3\ c/2 \equiv$ constant.)

For particle distributions of interest (smoke, aerosols) where r_a is of the order of 0.2 μm, then at λ = 11 μm, R = constant; however, for λ = 0.55 μm, the variation in R is $\sim$100, hence, mass concentration at λ = 11 μm is known to high accuracy whereas, in the visible and near infrared ($\lambda \leq 2$ μm) the error may be as large as a factor $\sim$100. It should be noted that for particle radii $\lesssim 3$ μm, the error at $\lambda \simeq 4$ μm is similar to λ = 11 μm, that is, relatively small.

In view of the above, the use of transmission measurements to establish mass concentration must be exercised with caution if accurate values are to be derived; that is, the size distribution must be known and the appropriate wavelength used for the transmissometer.

With the above background and data, let us examine the differences that may exist between the field test derived extinction coefficients and the laboratory values.

In Table 4 we indicate estimates of the MMD and σ_g for several events where bulk WP was used. The variation in MMD was from 1.14 to 3.39 and correspondingly 1.7 to 2.13 for the value of σ_g. Milham et al.[12] examined the variation in the spectral extinction coefficient for O-phosphoric acid for two values of MMD and σ_g, and their results are shown in Fig. 8 along with the value for WP smoke (35% relative humidity) in the 7-14 μm band. For the 3-5 μm band they conclude that WP smoke is no different than O-phosphoric acid and, therefore, we can conclude that size distribution properties can have a significant effect on the integrated or spectral

[12] Milham, M. E., et al., New Findings on the Nature of WP/RP Smokes, CSL, ARMCOM Report ARCSL-TR-77067, July 1977.

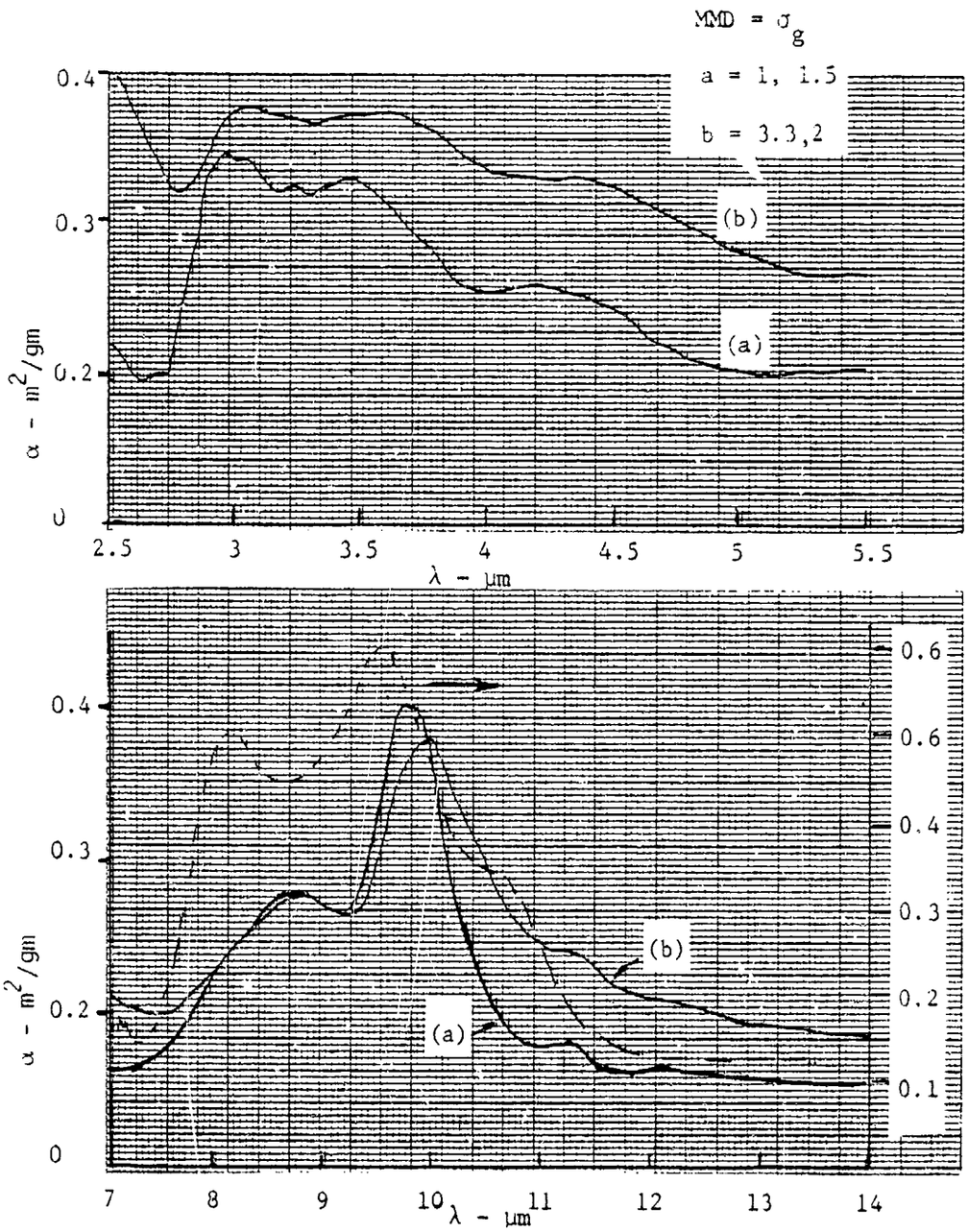

Figure 8. Extinction Coefficient vs. Wavelength (— — bulk WP): (a) MMD = 1 μm, σ_g = 1.5; (b) MMD = 3.3, 2 μm, σ_g = 2 (Milham, M. E., et al., New Findings on the Nature of WP/RP Smokes, CSL, ARMCOM Report ARCSL-TR-77067, July 1977.)

extinction coefficient. The field value at 3.4 μm is given as 0.22 ± 0.04 (1σ) (m^2/g), which does not agree with Fig. 8 in absolute value or variance. At 9.75 μm the field trial result is ~0.32 m^2/g, or 0.27 m^2/g, which again is lower than the laboratory values. The effect of size distribution on O-phosphoric acid, which should be a good approximation to WP in the 9-11 μm band, shows a marked difference in the 9-11 μm spectral region.

There is a real need to reduce the field data on a systematic basis; that is, to calculate the effective extinction coefficient as a function of time using the time variation in particle size distribution properties and C · L and then compare the results with laboratory observations.

2.3.2 Field Data

There are many problems related to the published data and are best illustrated by the differences between Trials 9 and 10 of the Dugway tests[13] called Inventory Smoke Munition Test (Phase IIa). These are tests of the 4.2" WP mortar.

In Trial DPI-002-T-9 a single 4.2" mortar was detonated at 76 m from the aerosol sampling line* under the following conditions:

$\bar{u}$ (m/sec) = 3.8

Azimuth wind angle, γ = 21.6°

Pasquill Category = C

The published cloud dimensions as a function of time are given as follows

[13] US Army D.P.G., Inventory Smoke Munition Test (Phase IIa), Final Test Report, Report DPG-TP-77-315, June 1978.

*One should note that locations of the detonation lines from the sampler line are uncertain for some tests in spite of the fact that the test array is a fixed geometry.

t (sec)	Length (m)	Width (m)		Height (m)	
		Measured	Calculated	Measured	Calculated
0	8	9	--	5	--
10	17	28	--	30	--
20	23	33	27	58	43
30	27	43	37	87	80
40	Plume aloft				

The fact that the samplers registered an initial value of $C \cdot L = 0.8\ g/m^2$ at $\simeq 50$ sec does not agree with the length or the "plume was aloft" after 40 sec. Similarly, the dosage curve indicates a width of 100 m. The height values agree reasonably with the calculated values.

If the reported azimuthal variation is superimposed on the expected value of the cloud width at the sampling line, i.e., at 76 m, then the "sampler width" would indeed be 100 m. We observe a cloud that is meandering rather strongly in the azimuth direction, and, therefore, some delay to reach the sampling line.

In Fig. 9 we present the C • L history. The calculated values prior to 50 sec are greater since the estimated mean arrival time = 76/3.8 = 20 sec. The possible explanation is that the cloud did rise and then fall after 40 sec; however, the plume would have to have been significantly longer than the reported observations. On the other hand, Trial 10 is relatively well behaved and agrees with calculations.

The non-zero values prior to 50 sec and beyond ~ 150 sec are to be considered as either noise or other contamination such as dust.

Finally, it should be noted that the C • L results derived from the transmissometer measurements are not meaningful, particularly in light of agreement between sampler observations and model estimates shown in Fig. 9.

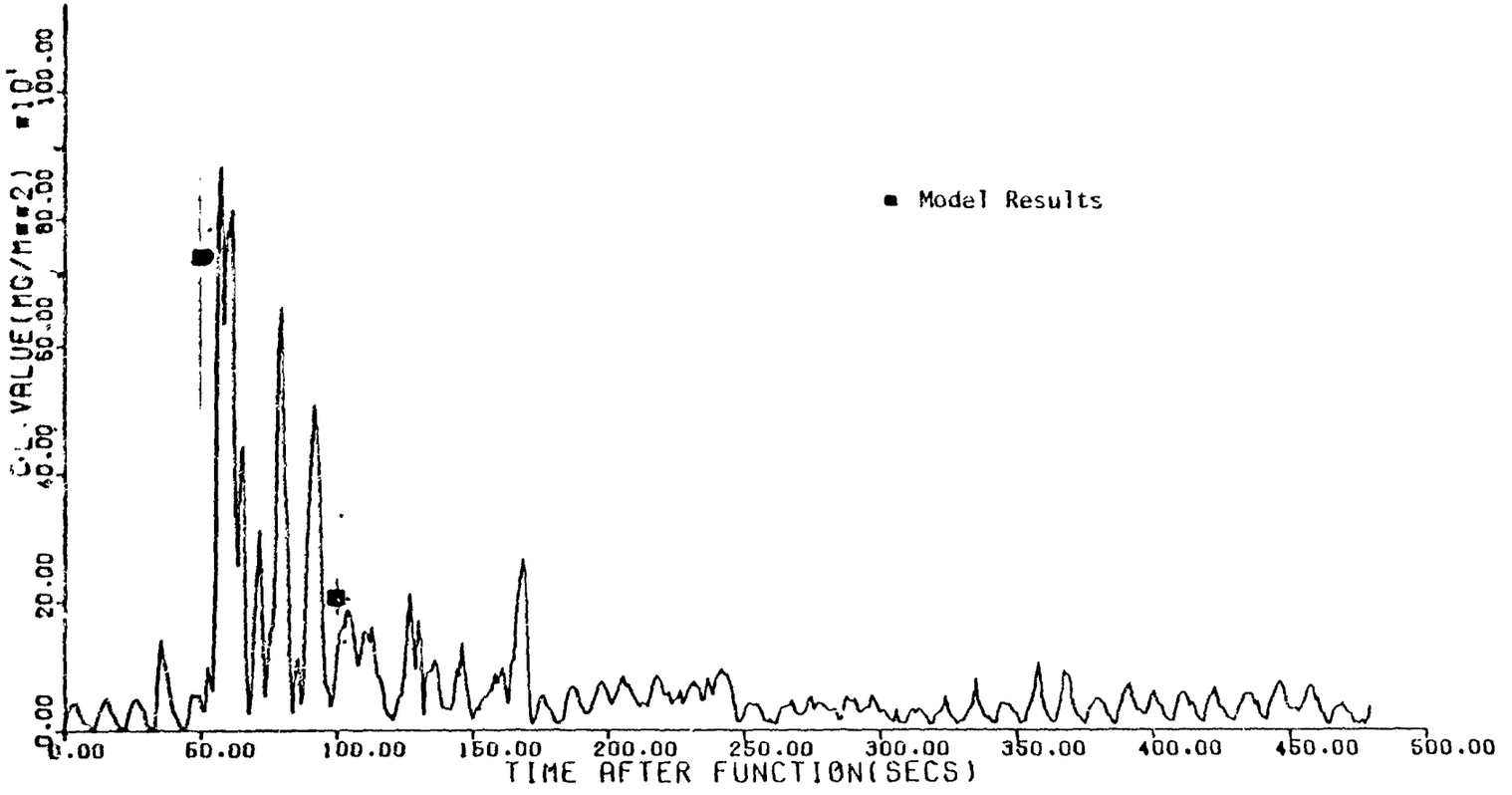

Figure 9. Trial 9 (DP-1-002), 23 September 1977, 13:03:00, WP Smoke. C • L values computed from aerosol samplers.

2.4 AEROSOL DIFFUSION

The diffusion of the aerosol cloud is of primary concern here since it determines the spatial-temporal history of the airborne material. Extensive study of this subject, theoretical and experimental, has been in progress for the past fifty years.[14,15] Our basic interest here is to adequately describe the obscurant aerosol generated by a smoke munition, high explosive, or smoke generator. With the exception of fog oil, the other sources release large quantities of thermal energy which dominate the early history of the diffusion process; that is, we are interested in both buoyant plumes (clouds) and turbulent (momentum exchange) diffused clouds.

The general behavior of the clouds depends upon the atmospheric environment (temperature gradient, wind velocities and gradient, surface roughness, etc.), or the stability of the atmosphere. Characterization of the atmospheric stability has been studied by many investigators and for use here we adopt the Pasquill stability definitions. The reason is that it depends primarily upon insolation and mean wind speed at 10 m. However, it suffers from a deficiency, i.e., absence of surface roughness. We will first give the general definitions and then correct for surface roughness.

The three basic stability classes are (1) unstable - Pasquill Categories A, B, and C; (2) neutral - Pasquill Category D; and (3) stable - Pasquill Categories E, F, and G, where G is the extremely stable situation. A simple summary is given in Table 5, and a more precise method to determine the class is given in Appendix B.

---

[14] Morton, B. D., et al., "Turbulent Gravitational Convection from Maintained and Instantaneous Sources," Proc. Royal Soc., Series A, 234, June 1956, pp. 1-23.

[15] Sutton, O. G., Atmospheric Turbulence, Methuen & Co., London, 1949.

TABLE 5

PASQUILL STABILITY CATEGORIES

Surface wind speed at 10 m ($m\ sec^{-1}$)	Insolation			Night	
	Strong	Moderate	Slight	Thinly overcast or ≥4/8 low cloud	≤3/8 cloud
<2	A	A-B	B	--	--
2-3	A-B	B	C	E	F
3-5	B	B-C	C	D	E
5-6	C	C-D	D	D	D
6	C	D	D	D	D

Classically the stability definitions are given by the environmental lapse rate, unstable ≡ lapse, neutral ≡ neutral, and stable ≡ inversion; that is, if θ_z is defined as the potential temperature and Γ the adiabatic lapse rate (0.098°C/10 m), then

$$\theta_z = \frac{\partial \theta}{\partial z} = \frac{\partial T}{\partial z} + \Gamma \tag{8}$$

where $\partial T/\partial z = T\ (10\ m) - T\ (0.5\ m)$. Hence, if $\theta_z < 0$ we have an unstable condition. Similarly, $\theta_z = 0, >0$ we have a neutral or inversion condition.

For convenience, we introduce here a parameter needed later, the stability parameter, s, where

$$s = \frac{g}{T} \frac{\partial \theta}{\partial z} \tag{9}$$

where g and T are gravity acceleration and ambient ground temperature (K), respectively. The parameter can be interpreted as the restoring acceleration per unit vertical displacement for adiabatic motion in a stratified atmosphere.

A somewhat more elaborate scheme of Pasquill categories is reproduced[16] in Table 6, where negative values are equivalent to instability, etc.

In Fig. 10, the seasonal variations of the Pasquill categories for the Netherlands are depicted, and one observes that Category A does not occur frequently.

To show the diurnal variation of the atmospheric stability, we present in Table 7 data from the Great Plains, Nebraska, reported in Ref. 2. We note that the frequency of Category A is low and, in general, unstable conditions occur primarily during the day.

The stability definition of Pasquill (see Appendix B) depends, as stated earlier, on wind speed and insolation and is independent of surface roughness and ground cover height. This can be accomplished by introducing the Monin-Obukhov "mixing" length, L (m), defined as

$$L = \frac{u_*^3}{k(g/T_0)(q/c_p\rho)} = \frac{u_*^3\, \partial\bar{u}/\partial z}{g/T_0 \cdot \partial\bar{T}/\partial z} \qquad (10)$$

where u_* = friction velocity (m/sec)

g = acceleration of gravity (m/sec^2)

T_0 = standard temperature

k = Karman constant

$\bar{u}$ = mean wind speed

$\bar{T}$ = mean temperature

q = vertical turbulent heat current

$c_p\rho$ = air specific heat capacity, density

[16] Shir, C. C., and L. F. Shieh, Journal Applied Met., March 1974, p. 189.

TABLE 6

KEY USED TO ESTIMATE THE CONTINUOUS STABILITY CLASSIFICATION

Mean wind speed ($m\ sec^{-1}$)	Day			Transient period		Night	
	Incoming solar radiation					Thinly overcast or 4/8 low cloud	3/8 Cloud
	Strong	Moderate	Slight	Day	Night		
<2	-3.5 ~ -3.0	-3.0 -2.2	-2.5 ~ -2.0	-1.5 ~ -0.5	0.5 ~ 1.5	1.5	2.5
2 - 3	-3.0 ~ -2.2	-2.2 -2.0	-2.0 ~ -1.0	-1.0 ~ -0.3	0.5 ~ 1.0	1.5 ~ 0.6	2.5 ~ 1.6
3 - 5	-2.2 ~ -1.5	-2.0 ~ -1.0	-1.0 -0.5	-1.0 ~ -0.3	0.3 ~ 0.5	0.6 ~ 0.3	1.6 ~ 0.5
5 ~ 6	-1.5 ~ -1.0	-10. ~ -0.3	-0.5 ~ -0.2	-0.4 ~ -0.2	0.2 ~ 0.4	0.3 ~ 0.1	0.5 ~ 0.3
6 ~ 8	-1.0 ~ -0.3	-0.3 ~ -0.1	-0.2 ~ 0	-0.3 ~ -0.1	0.1 ~ 0.2	0.1 ~ 0	0.3 ~ 0.1
>8	-0.3	-0.1	0	0		0	0

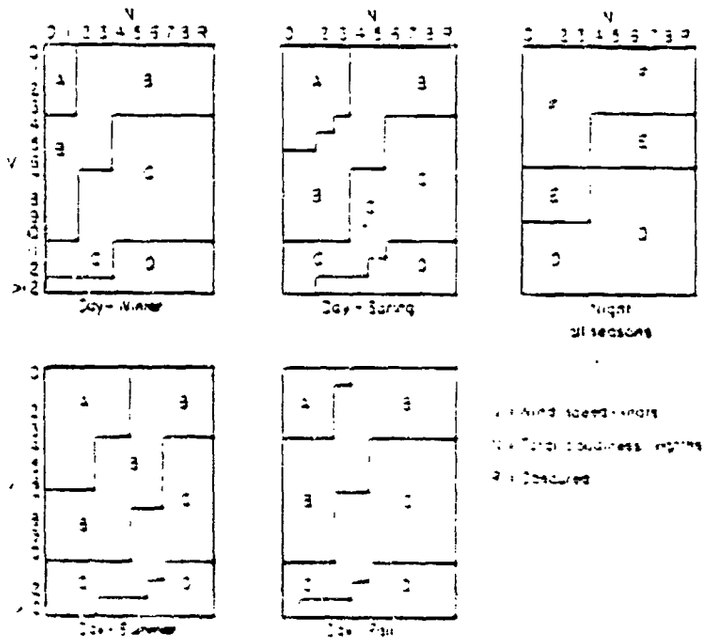

Figure 10. Prevalence of Pasquill Stability Categories Over the Netherlands*

*Reproduced from J. H. Strom, "Atmospheric Dispersion of Stack Effluents," p. 257, Air Pollution (A. C. Stern, Ed.) 2nd Ed. Academic Press, 1968.

TABLE 7

DIURNAL VARIATION OF ATMOSPHERIC STABILITY
GREAT PLAINS, NEBRASKA*

Month & Day	Hour of Mean Local Time											
	00	02	04	06	08	10	12	14	16	18	20	22
8 Aug										D	H	G
9 Aug	G	F	E	D	D	C	C	C	D	E	F	-
13 Aug	-	-	F	E	D	B	B	A	D	G	H	G
14 Aug	H	G	-	-								
18 Aug	-	-	-	-	-	-	-	-	-	H	H	H
19 Aug	H	H	G	G	A	A	A	A	B	H	H	H
22 Aug	-	-	G	E	G	A	A	B	-	-	-	-
24 Aug	-	-	-	-	-	-	B	C	D	F	F	D
25 Aug	E	D	D	D	D	C	C	C	D	E	G	-
31 Aug	-	-	E	D	C	A	A	B	C	D	F	E
1 Sept	F	F	E	D	B	-	-	-	-	-	-	-
7 Sept	-	-	H	G	B	B	B	B	C	E	E	F
8 Sept	F	G	G	F	A	A	A	-	-	-	-	-

*Source: Lettau and Davidson, Ref. 2.

The value of L is characteristic of the "dynamic" layer; that is, if q = 0, T(z) = constant, we have neutral stratification L = ∞; and if q < 0, > 0, we have L > 0, < 0, respectively. One can show that the rise, $\Delta z/\Delta x$, of a smoke cloud is ~L; that is, the ratio of the standard deviations of vertical and horizontal wind speed fluctuations σ_w and σ_y respectively, is ~ $\phi(z/L)$. Hence, this quantity has significance; however, the reader is referred to Csanady[17] for a complete discussion.

Golder[18] established a relation between the Monin-Obukov length, L, and Pasquill stability:

$$1/L = \pm[d \ln (1.2 + 10/z_0)]^{\frac{1}{c}} 10^{f(s)} \qquad (11)$$

and

$$f(s) = -a/(1 + b|s|^c)$$

where s = stability class defined in Table 6

a = 4, b = 1.3, c = 0.85, d = 0.21659

z_0 = the surface roughness in meters

The surface roughness, z_0, varies from $\sim 10^{-3}$ m (sand) to ~0.10 m (tall vegetation). Kung and Lettau have found an empirical relation between z_0 and plant height, h_e:

$$\log z_0 = -1.14 + 1.19 \log h_e \qquad (12)$$

Several values of z_0, h_e are given in Table 6.

The effect of surface roughness is to increase or reduce in some instances the stability class; see Fig. 11.

---

[17] Csanady, G. T., Turbulent Diffusion in the Environment, D. Reidel Pub. Co., 1973.

[18] Golder, D., "Relations Among Stability Parameters in the Surface Layer," Boundary Layer Meteorology 3 (1972), p. 47.

TABLE 8

PROFILE PARAMETERS OF SOME CROPS AND BUILDUP AREAS

Crop	z_0 (m)	h_c (m)
Snow covered	0.0049	0.03
Grassy surface	0.0173	0.10
Low grass	0.032	0.20
High grass	0.039	0.30
Wheat	0.04	1.3
Suburban area	0.4	
Urban	6.0	24.0

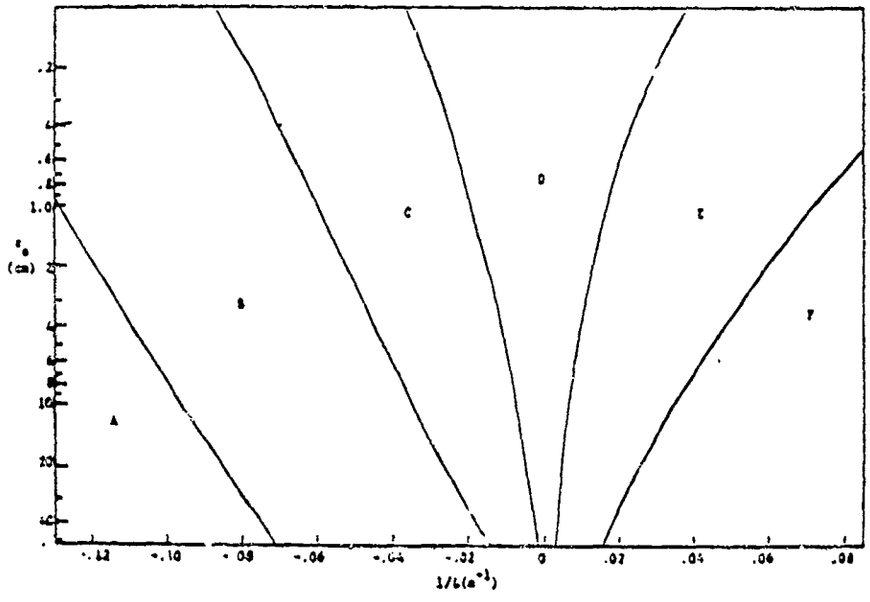

Figure 11. 1/L as a Function of Pasquill Classes and z_0.

2.5 CLOUD HISTORY

The clouds formed from various sources rise because of their buoyancy and/or by momentum exchange. Since our initial work, numerous validations have provided confidence in the basic formulations for thermal sources (e.g., WP) and nonthermal sources (fog oil). Hence, we will discuss these formulations and some modifications; we first consider the nonthermal.

2.5.1 Non-Exothermic Munitions

Although the number of pure non-exothermic munitions, e.g., fog oil, are few, an HC mixture with Zn or ZnO is a quasi-exothermic material because of its long burning time and, therefore, the cloud rise behavior after the short buoyancy phase is described as momentum exchange. Also, the lateral diffusion appears to be unaffected by any thermal effects.

The cloud size parameters determined from experimental observations are given in Table 9.

TABLE 9

CLOUD SIZE PARAMETERS FOR NON-EXOTHERMIC MUNITIONS

Stability Category				
Pasquill	Turner	Width, $\bar{y}$ (m)	Height, $\bar{z}$ (m)	Remarks
A	-3	9.1 + 0.419x	2.73 + 0.137x	Sunny day
B	-2	9.1 + 0.328x	2.73 + 0.11x	Day, broken cloud
C	-1	9.1 + 0.238x	2.73 + 0.073x	Overcast day/night
D	0	9.1 + 0.20x	2.73 + 0.06x	Neutral
E	1	9.1 + 0.18x	2.73 + 0.055x	Evening/early am
F	2	9.1 + 0.146x	2.73 + 0.046x	Evening/early am

The general shape of the cloud is a semi-cone, and the slope is given by $\bar{z}/\bar{x}$. Soviet measurements for a smoke pot ($\Delta T \simeq 2°C$), terrain roughness

z_0 equal to 0.4 cm, gave the following cloud slopes in terms of the Monin-Obukov length:

$$\begin{aligned} \tan \alpha &= -0.85/L + 0.07 \quad \text{(unstable)} \\ &= 0.07 \quad\quad\quad\quad\quad\quad \text{(neutral/stable)} \end{aligned} \tag{13}$$

When z_0 = 0.4 cm and the Pasquill stability is A - B, the value of $L^{-1} \leq -0.07$ (m^{-1}) and the cloud slope $\simeq 0.11$. Since the z_0 from Table 8 may differ somewhat, the value of 0.11 is a good average value (0.09-0.17) for Category B. This indicates a good correlation between the Pasquill Turner and Monin-Obukov stability parameters.

One should recognize that the discrete values given in Table 10 for the constants multiplying "x" are continuous for $0.5 \leq \bar{u} \leq 5$ m/sec; see Appendix C. The low-speed values are omitted since the behavior at or near $\bar{u} = 0$ should be defined by a different model, i.e., for still air.[19]

Let us examine the expressions in Table 10. Since $x = \bar{u}t$, then for $t = 0$, $\bar{y} = 9.1$ m and $\bar{z} = 2.73$ m. This implies that the source is defined by a radius of ~4.5 and height 2.73 m values not inconsistent with observations (Fig. 1). In Ref. 17, the standard deviations, σ_y and σ_z, are represented by the linear expressions

$$\begin{aligned} \sigma_y &= i_y x \\ \sigma_z &= i_z x \end{aligned} \tag{14}$$

where $i_{y,z}$ are the gustiness intensities, in which i_y is the ratio of the RMS lateral speed fluctuations to mean time lateral speed; similarly for i_z. The experimental values for i_y and i_z are given in Table 10.

[19] Keil, R. W., A Description of Buoyant Plumes in a Still Atmosphere, Ph.D Thesis, University of California, Davis Campus, 1974.

TABLE 10

GUSTINESS INTENSITIES FOR DIFFERENT STABILITY CONDITIONS

	i_y	i_z
Extremely Unstable	0.40-0.55	0.15-0.55
Moderately Unstable	0.25-0.40	0.10-0.15
Near Neutral	0.10-0.25	0.05-0.08
Moderately Stable	0.08-0.25	0.03-0.07
Extremely Stable	0.03-0.25	0.00-0.03

We note that the constants in Table 10 fall within the range given in Table 9 and, therefore, since we use the mean speed to define x, we assert that the factors $\bar{x}$ and $\bar{y}$ and $\bar{z}$ of Table 9 are the mean values, and the derived volume and concentration are the mean values of these parameters.

Above in defining the Pasquill stability categories and other concepts, we have used mean values. Clearly, fluctuations of wind components play an important role in any spatial-temporal history; e.g., the horizontal fluctuations will affect the concentration and plume rise. The ability to relate the fluctuations to the Pasquill category would provide a potential means to find the bounds of the mean value. However, the data are limited. We present some data in Table 11 from Ref. 2, where $\sigma(u)$ is the standard deviation of u, the wind speed component in the direction of the wind, w, and the vertical wind speed, $\bar{u}$ and u' are the mean value and fluctuations of u, and $\left(\overline{u'^2}\right)^{1/2}/\bar{u}$ is called gustiness. We note the following facts:

1. The standard deviation $\sigma(u)$ decreases in magnitude with increasing stability since $\bar{u}$ increases from stability category A to H.

2. The ratio $\sigma(w)/\sigma(u) \simeq$ constant.

TABLE 11

WIND FLUCTUATION PARAMETERS
FROM FAST RESPONSE DATA

Stability Class	A	B	C	D	E	F	G	H
$\sigma(u)$ m/sec	1.13	1.20	1.61	1.33	1.08	0.89	0.51	0.30
$\sigma(w)/\sigma(u)$	0.38	0.40	0.37	0.36	0.41	0.41	0.45	0.32
$\sqrt{\overline{u'^2}}/\bar{u}$ @ Z = 1.5 m	0.214	0.204	0.220	0.219	0.199	0.198	0.163	0.155
@ Z = 3.0 m	0.198	0.184	0.200	0.198	0.179	0.174	0.136	0.106
$\sqrt{\overline{w'^2}}/\bar{u}$ @ Z = 1.5 m	0.071	0.074	0.085	0.079	0.079	0.080	0.061	0.035
@ Z = 3.0 m	0.069	0.068	0.065	0.065	0.067	0.065	0.06	0.029

3. The horizontal gustiness decreases with altitude.

For our purposes we may utilize the gustiness value for "u component" at ~3 m to establish limits.

From observations of the time history of the concentration at a point we find that the concentration varies from near zero values to peak values far in excess of the mean; see sketch. These observations are made perpendicular or approximately so to $\bar{u}$. This effect of intermittency has

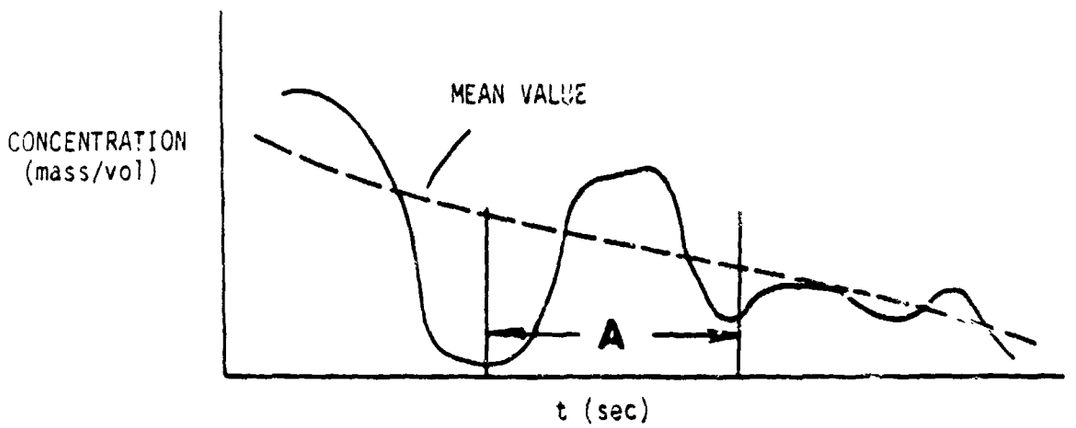

practical import since it is the period of time there is a near-zero concentration in direction of $\bar{u}$ and this may be as low as 35% of the time even at the center of the cloud. Although we can specify that length of time "A" is about 20-40 sec, corresponding to the period of gustiness, we cannot, at the present, precisely define this effect in the lateral (y) direction. Therefore, the actual concentration as a function of time along the line of sight is not defined beyond the mean value and standard deviation.* This is a serious practical shortcoming. Csanady (Ref. 17) defines, on the basis of a theoretical development, the ratio of $\sqrt{N'^2}/\bar{N}$ as $\sqrt{\exp(\sigma_1^2) - 1}$, where σ_1 is the standard deviation of the concentration, N. The parameter σ_1 has the values of 0.2 (stable, smooth terrain), 0.35 (neutral, smooth terrain), and 0.70 (rough). The peak value of the concentration can be defined by the following expression:

$$\frac{N_p}{\bar{N}} = \exp\left[\sigma_1(2.326 - 0.5\sigma_1)\right] \tag{15}$$

or

$$\frac{N_p}{N_{RMS}} = \exp\left[\sigma_1(2.326 - 0.5\sigma_1)\right] / \sqrt{\exp(\sigma_1^2) - 1} \tag{16}$$

For an average condition, $\sigma_1 = 0.5$, $N_p = 2.8 \times N_{RMS}$, which appears to agree with reported data.

Before we present the overall diffusion model we must discuss the buoyant plume.

2.5.2 The Buoyant Plume

We consider here the buoyant plume which is formed as a result of exothermic chemical reactions, i.e., oxidation, deliquesence. The

*A series of experiments is needed where samples and transmissometers are placed at several angles with $\bar{u}$. One of the parameters should be Pasquill category.

excess temperature reduces the density below ambient, resulting in a rising buoyant volume.

Generally speaking, the sequence of events for WP munitions appears to be as follows: (1) the creation of a hot volume due to the detonation and initial phosphorus oxidation; (2) an obscuring cloud in the vertical for still air or a bent cloud due to atmospheric winds, and (3) the turbulent diffusion of the cloud downwind.

From limited thermal imagery the spread of bulk material in the earth-plane does not appear to be extensive and probably depends on the shell trajectory. Hence, we assume the source to be limited and be approximated by a quasi-point source for artillery and mortars. When wicks or wedges are used the source is normally a continuous linear source. We now present the general behavior of buoyant plumes.

To estimate the effect of the initial vertical momentum which occurs within a fraction of a second, we utilize a result from Briggs:[20] the vertical momentum is less important than buoyancy at a distance x_1 downwind;

$$x_1 = \bar{u} W_g / g(\Delta T_g / T_0) \tag{17}$$

where W_g = initial vertical velocity (m/sec)

ΔT_g = initial temperature excess

T_0 = ambient temperature (K)

g = gravitational acceleration (m/sec^2)

Assume $\bar{u}$ = 3 m/sec, $\bar{W}_g$ = 20 m/sec, and ΔT = 500 and substitute into Eq. 17. We obtain for x_1

[20] Briggs, G. A., Plume Rise, ESSA, Oak Ridge, Tennessee, 1969 (TID-25075).

$$x_1 = 5.20/9.8\ (500/300) = 6.4\ \text{m}$$

or, a very short distance from the origin. For still or near still air ($\bar{u} < 0.5$ m/sec) the initial momentum should be treated as part of the overall cloud rise.

In Ref. 1, we adapted the recommended formulations of Briggs (Ref. 20) for plume rise; that is, for unstable and neutral we have

$$\Delta h = \frac{1.6F^{1/3}x^{2/3}}{\bar{u}}\ (F^{1/6}) \tag{18}$$

$$\Delta h = \frac{1.6F^{1/2}x^{2/3}}{\bar{u}}\left\{0.4 + 0.64\,\frac{x}{x_*} + 2.2\,\frac{x}{x_*}\right\}^2\left[1 + 0.8\,\frac{x}{x_*}\right]^{-2} \tag{19}$$

respectively, where F = buoyancy flux (m^4/sec^3) = 3.7×10^{-5} (cal ÷ burn time), and x_* = transition value for $x = 0.52F^{0.4}$ (English units). It should be noted that the addition of $F^{1/6}$ is to correct for cloud top instead of centroid. The appropriate values for the heat release is given in the model structures.

Venter[21] refining Briggs' work, reports that Eq. 18 represents the initial rise until $x = x_*$ and Eq. 19 represents the trajectory after x_*, where

$$x_* = 14F^{5/8} \quad \text{for } F < 55\ m^4/s^3$$
$$x_* = 34F^{0.4} \quad \text{for } F > 55\ m^4/s^3 \tag{20}$$

[21] Venter, G. P. N., "A Comparison of Observed Plume Trajectories with Those Predicted by Two Models," Atmospheric Environment, 11, 1977, pp. 421-426.

where s = stability parameter and the final rise is given approximately by

$$\Delta h \simeq 1.6F^{1/2} \ (3.5x_*)^{2/3}/\bar{u} \tag{21}$$

for $x > 3.5x_*$.

The constant (1.6) appearing in the above equations can be shown to be related to the entrainment factor β with a value of 0.6. β represents the cloud growth rate with vertical rise; that is, $\beta \simeq$ cloud radius/$\bar{z}$.

For stable plume rise, Ref. 1 shows that Eq. 18 describes the rise until $x = 2.4\bar{u}/s^{1/2}$. The maximum rise was given as

$$\Delta h_{max} = 2.9 \ (F/\bar{u}s)^{1/3} \tag{22}$$

where again the constant 2.9 relates to an entrainment factor = 0.5. Venter gives an alternative form by Briggs for the complete rise as

$$\Delta h = 2.9 \ (F/\bar{u}s)^{1/3}[1 - \cos \ (xs^{.5}/\bar{u})]^{1/3} \tag{23}$$

which has a maximum at $x = \pi u/s^{.5}$ and is equal to Eq. 22.*

The different values for entrainment factor are not unusual since the magnitude is one of the major uncertainties in analytical treatments and the entrainment value is established when the predicted results are compared to experimental results. Shwartz and Tulin[22] state that β can vary between 0.3 and 1.0 and for their work the values ranged between 0.42 and 0.60.

---

*From experimental results one can estimate for the non-buoyant plume that the maximum rise at x = 100, 500, 1000 m under neutral and stable conditions is $60/\bar{u}$, $105/\bar{u}$, and $150/\bar{u}$, respectively.

[22]Shwartz, I. and M. P. Tulin, "Chimney Plumes in Neutral and Stable Surroundings," Atmospheric Environment, 1972, pp. 19-35. (An interesting paper on the vortex formation of the plume in a stable atmosphere.)

Equations (22) and (23) apply $\bar{u} > 0$, i.e., the bent plume or cloud, or $x = \bar{u}t > 0$. When $\bar{u} = 0$, i.e., for still air, Morton et al. (Ref. 14), in their classic paper give the maximum rise of a buoyant plume in the following expressions for the instantaneous and maintained sources. The expressions are given below:

Instantaneous

$$H_{max} = 1.87Q^{0.25} \quad (m) \tag{24}$$

Q = energy release (joules). For example, a cloud produced by 100 lb of TNT will reach a height 230 m.

Maintained

$$H_{max} = 31 \frac{Q^{0.25}}{(1 + n)^{3/8}} \quad (m) \tag{25}$$

where Q = energy/unit time (kilowatts), and n = ratio of (actual lapse/adiabatic lapse).

In conjunction with the above, we assume an entrainment factor of 0.5 so that the cloud radius is $\simeq 0.5z$. Hence, we can define the approximate maximum diameter of the plume; that is, the diameter = H_{max}. The diameter at any other height $\sim 2z$ or the plume half-angle is 26°.

Briggs indicates that for stable, calm conditions the maximum rise is given accurately by

$$\Delta h = 5.0F^{0.25}/\bar{s}^{3/8} \tag{26}$$

where $\bar{s}$ is the average potential temperature gradient traversed by the cloud. (Note the analogous forms of Eqs. 22 and 26.)

When a ground inversion exists then the cloud will penetrate the inversion if $(\Delta h)_{max}$ defined by Eqs. 22 or 26 exceeds the height of the inversion. When the inversion layer is elevated, i.e., begins at $Z > 0$, then the plume will penetrate if the inversion top $z_i \leq 4F^{0.4}/b_i^{0.6}$ for calm conditions ($u = 0$) and $z_i \leq 2\,(F/ub_i)$ for $u > 0$. The parameter b_i is defined by the expression

$$b_i = g\Delta T_i/T \tag{27}$$

where ΔT_i = temperature difference of the inversion layer

T = absolute ambient temperature (°K)

g = gravitational acceleration (m/sec^2)

Alternatively, if the plume characteristic temperature excess exceeds the inversion temperature ΔT_i then the plume will penetrate; that is

$$(\Delta T)_{plume} \simeq \frac{T \cdot F}{\beta^2 g \bar{u} z^2} > \Delta T_i \tag{28}$$

Briggs (Ref. 19) suggests that $\beta = 0.5$ when the plume is rising through neutral air (category D).

In Ref. 1, we developed an expression for plume (ΔT) as function of concentration and relative humidity was developed. The result is given in Fig. 12.

We now return to the exothermic chemical munition and determine the dimensions of the resultant aerosol cloud. The overall cloud rise, z, is given by the expression

$$z = \bar{z} + \Delta h \tag{29}$$

where $\bar{z}$ = momentum rise (see Table 10)

Δh = rise due to heat addition

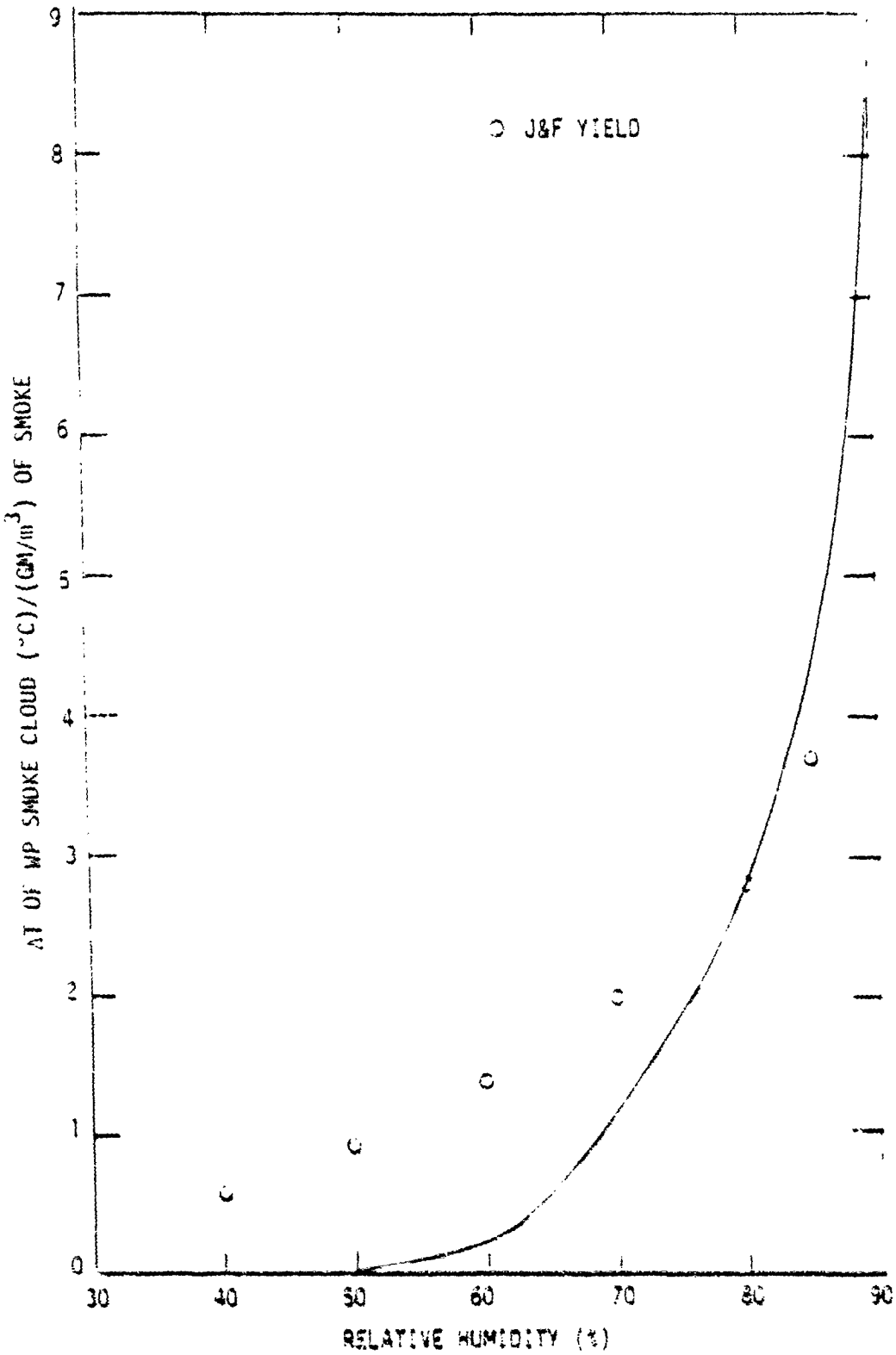

Figure 11. Cloud ΔT as a Function of Relative Humidity
(O - Values. Ref. 6)

These parameters have been defined above. The value of the lateral spread, $\bar{y}$, is given in Table 9. Since $Z > \bar{y}$ the aerosol cloud shape is assumed to be defined as a quarter of an ellipsoid, i.e., the volume for a point source is given by

$$V(t) = \bar{x}\bar{y}Z/6 \tag{30}$$

2.6 MULTIPLE AND ARRAY SOURCES

For a linear array equally spaced instantaneous point sources, e.g., n-munitions spaced "d" meters apart where $d > y$ ($t = 5$) they can be treated as individual sources; see Fig. 13. From Fig. 13 we note the overlap occurs at time $t = (d - 9.1)/A\bar{u}$ where A is the constant given in Table 9. $y = 9.1 + Ax$. Beyond this, the lateral path length for $n = 2$ will decrease by the amount.

$$\Delta = d \cdot (x_2 - x_1)/x_1 \tag{31}$$

where x_1 is the value of x at time of intersection and x_2 the value of x at the point of interest. For n munitions we can write immediately

$$\Delta = (n - 1)(d)(x_2 - x_1)/x_1 \tag{32}$$

When the wind speed is at an angle, θ, appropriate adjustment is required.

The overlap zones are significant for radiation transport (optical properties) laser propagation and some cases of backscatter. However, for $C \cdot L$ computation one may treat the sources as additives, $\sum_i C_i L_i$.

For a linear continuous source of length, ℓ, where Q grams of smoke material of yield Y are released, the quantity of smoke produced per unit length per sec is $(Q \cdot Y)/(\ell \cdot t)$ gms/msec.

The concentration to a first approximation is defined by the relation

$$C(x,y,z,t) = \frac{Q \cdot Y}{t \cdot \ell} \frac{2}{\frac{\pi}{6}\bar{u} \cdot \bar{z}(x,t)(1 + k)} \quad (g/m^3) \tag{33}$$

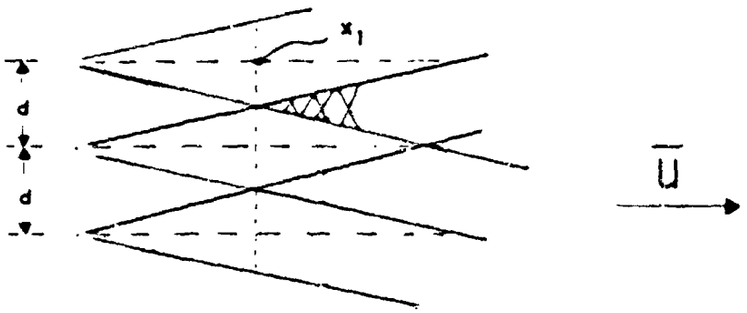

Figure 13. Multi-Position Schematic

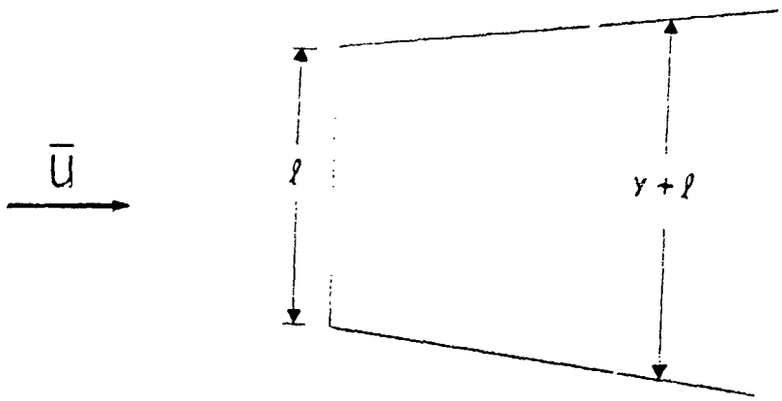

where $\bar{u}$ = mean speed (m/sec)

Z = smoke cloud height @ "x" ($\bar{z}$ or Z)

k = incremental length of smoke width @ "x"

For the case when wind speed is normal to the smoke line, $k = \bar{y}/\ell$, and when $\bar{u}$ is at angle, ϑ, to the smoke $k = y \sin \vartheta/\ell$. The non-uniform spatial distributions in the x and z may have a form similar to Eqs. 3.18 and 3.19.

For a distributed source, a combination of point and/or linear arrays may be applied with appropriate accounting of the time coordinates; that is, if we have linear arrays at x_i, x_j and x_k then any x is $(x - x_i)$, $(x - x_j)$ and $(x - x_k)$ and the relative time is $t_1 = (x - x_i)/\bar{u}$, etc. A program for distributed steady sources like smoke pots and generators is given in Appendix D, Ref. 1.

When a moving ground generator is utilized a vectorial representation is applied; that is, the generator velocity, v, is added vectorially to the wind velocity, u, hence for a headwind, a line source is produced with a resultant mean wind speed of $\bar{u} + \bar{v}$. The value of x is found by

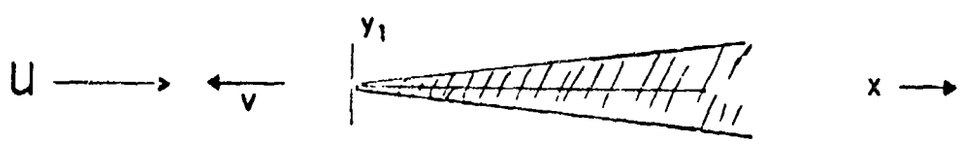

applying the expression, $x = [|\vec{u}| + |\vec{v}|]t$. The expansion in y and z directions are defined by Table 9.

When the generator moves at an angle to the mean wind then the resultant speed would be found again by vector addition.

2.7 VALIDATION TESTS

In Ref. 1 we present numerous examples of the model's capability to predict a priori the mean concentration, C, and concentration × path length (C · L). Here we will again illustrate the validity of the proposed smoke-obscurant aerosol model and discuss any deviations.

1. Test DP1-002-T-4 (HC Smoke)

The initial conditions provided by the test organization are as follows:

$\bar{u}$, mean wind speed - 4.0 m/sec
Pasquill Category - C
Relative Humidity - 36%
Munitions - 36, M84A1 canisters
Array - linear

With these data the resultant calculated and measured values are shown in Fig. 14. Although the general agreement is good, better agreement could have been achieved if the non-linear burning time had been applied, particularly in the 60-100 sec time period.

2. Trial 2 (DP1-002) (HC Smoke)

The initial data provided by the test organization are as follows:

$\bar{u}$ - 8.8 m/sec
Pasquill Category - D
Relative Humidity - 25%
Munitions - 8, M84A1 canisters

With these data the resultant calculated values were compared to both the aerosol photometer results (see Fig. 15) and the C · L derived by the

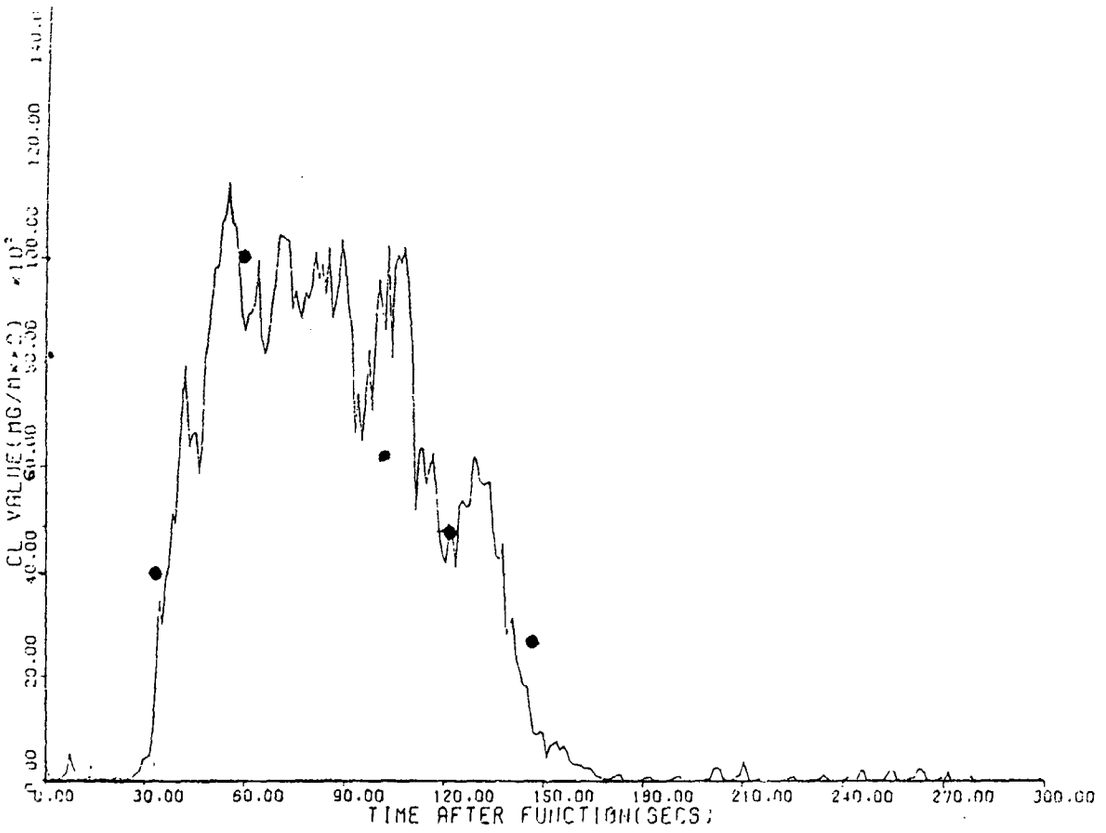

Figure 14. Trial 4 (DP1-002), 19 November 1977, 12:58:00, HC Smoke (—— C · L Values Computed from Aerosol Photometers; ● Model Calculations)

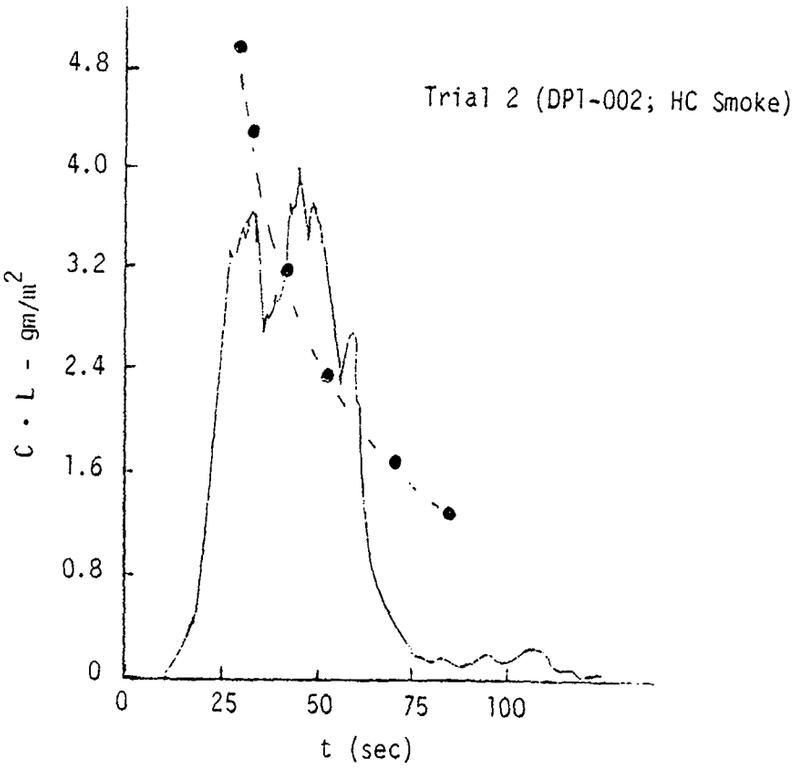

Figure 15. C · L History Determined by Aerosol Photometers
(●——● Model Results)

adjacent transmissometers (see Fig. 16). First we note the difference in the two C · L plots, particularly at times greater than 60 sec. Second, the absolute magnitudes differ. Hence, correlation would be difficult between the two results except for the fact that they are not collocated; that is, the transmissometers are displaced 10 m and this can account for differences as noted in Sec. 2.3.

The agreement of the calculated points is better for the transmissometer with the following exceptions: (1) at early times the nonlinear burning would reduce the first point to about the correct value and also raise the second; and (2) the observed dip at about 80 sec is due to atmospheric fluctuations.

3. Trial 17 (DPI-002) - WP Smoke

The initial conditions are as follows:

$\bar{u}$	- 3.7 m/sec
Pasquill Category	- C
Relative Humidity	- 36%
Munition	- 1, 81-mm mortar

The comparative results are shown in Fig. 17 where the photometer C · L curve is used. The initial difference between the two is probably due to atmospheric fluctuations.

In Fig. 18 we have plotted the C · L values (the outside one applies to "1") for the three transmissometer lines which are spaced 60 m apart, i.e., ±60 m on either side of the one near the sampler line. We note that the single mortar behaves more like a puff than a quasi-point source, i.e., like multi-mortar arrays or artillery shells.

Lastly, the small C · L values or the "flare-up" of (3) at late times are not afterburning but concentration fluctuations due to atmospheric instabilities.

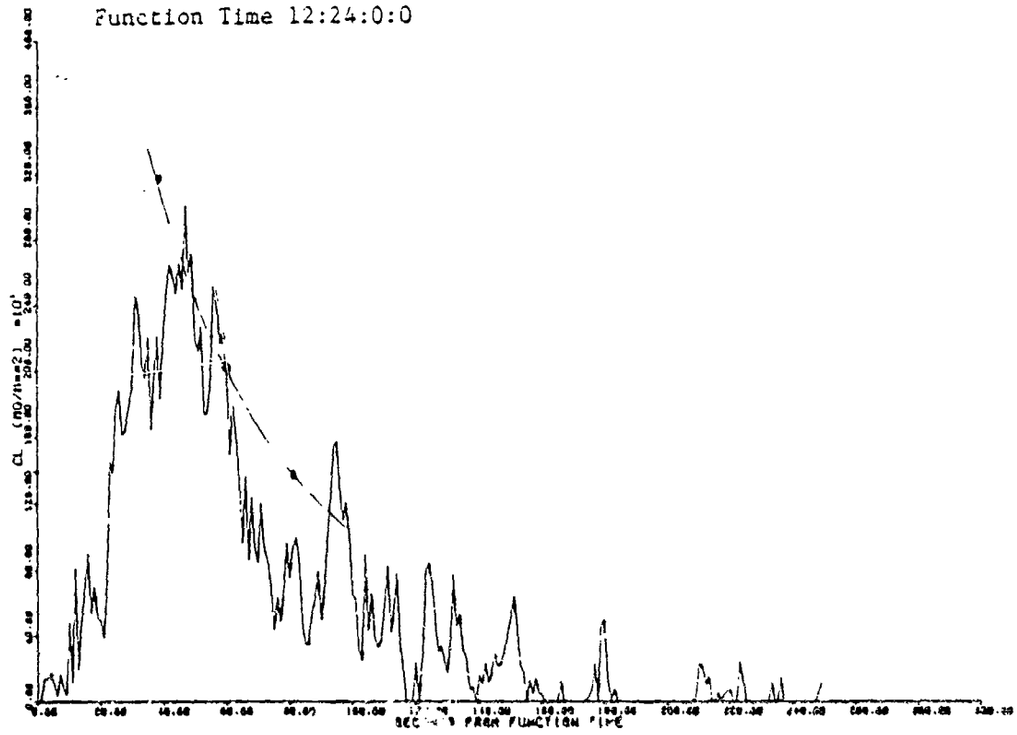

Figure 16. C · L Values Versus Time for Row 0 (—— Calculated Using Transmittance and Extinction Coefficient, ●——● Model Results)

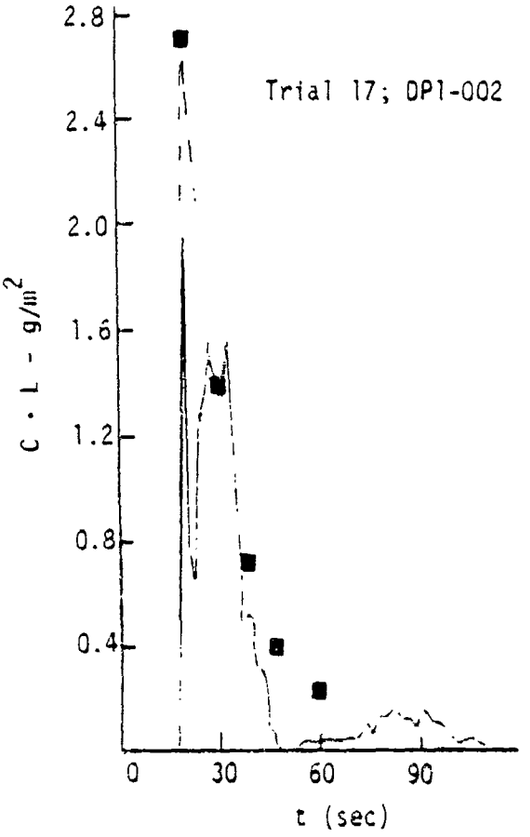

Figure 17. C · L History from Aerosol Samplers (■ Model Predictions)

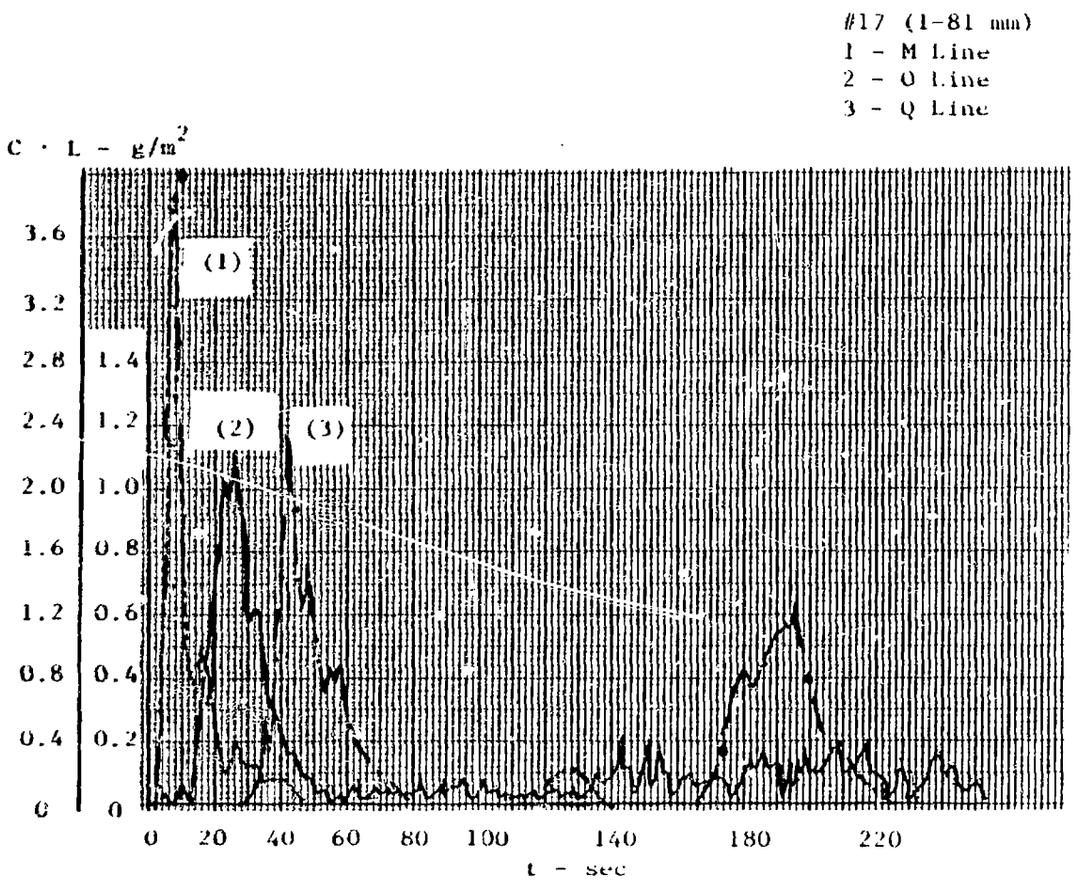

Figure 18. C · L History Calculated from Transmissometers

4. Trial 10, DP1-002; WP Smoke

Input data:

$\bar{u}$ - 7.9 m/sec

Pasquill Category - D

Relative Humidity - 52%

Munition - 4, 4.2" mortars

The comparative results are shown in Fig. 19, and the agreement is excellent.

5. Trial 21, DP1-002, WP Smoke

Input data:

$\bar{u}$ - 4.6 m/sec

Pasquill Category - C

Relative Humidity - 25%

Munition - 1, 155-mm shell

The comparative results are shown in Fig. 20, and the agreement is excellent. Here the effect of fluctuation at different values are evident and the model predicts adequately the tail particularly when the fluctuations are considered.

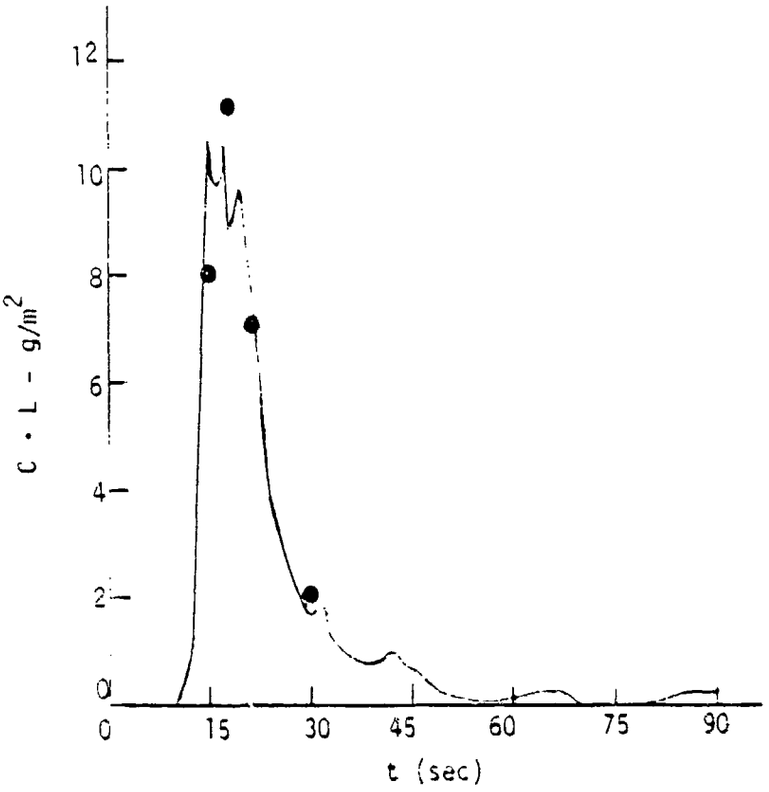

Figure 19. C • L Time History; Trial 10, DP1-002, 4-42" Mortars (● Model Predictions)

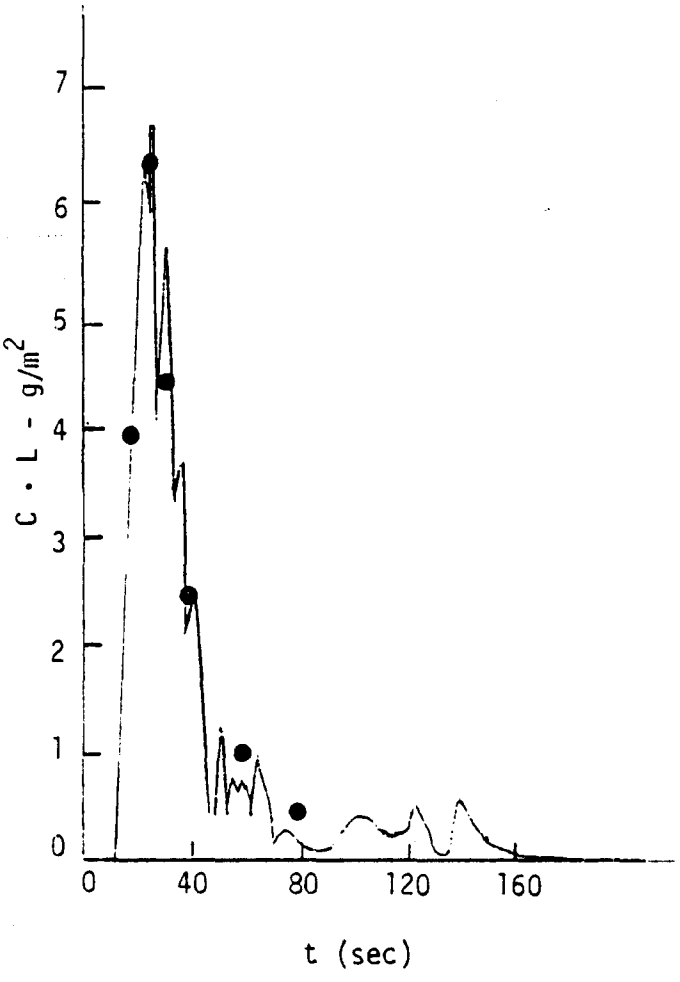

Figure 20. C · L Time History; Trial DP1-002, 1-155 mm WP (● Model Predictions)

3 MODEL STRUCTURE

The models described here are written in a self-contained format for each type of smoke and obscuring aerosol. Hence, there is considerable repetition of expressions that could be compiled in several subroutines if a general computer program were generated.

3.1 COMPUTATION SCHEME FOR CLOUD CONCENTRATION OF SMOKES OBSCURING AEROSOLS

In this section, a procedure is outlined to permit the determination of the concentration, C (g/m^3), path length in the cloud, L (m), and, the important parameter, C · L (g/m^2). The units used here are defined; however, we utilize primarily grams, meters, and seconds. We initiate the discussion with the requisite input data and then proceed to the procedure proper.

3.1.1 Input Data

A. Scenario

Local target and observer locations
Munition deployment plan
Munition rate
Sensor type and operational wavelength band

B. Smoke Munitions

Type (Mk No., Caliber, etc.)
Fill weight (g)
Fill material (WP, RP, HC, Oil, etc.)
Burn time and rate

C. Meteorological Conditions

Time of day, Cloud cover } To establish stability category

Mean wind speed (m/sec) - surface to 10 m

Temperature, T (°C) - @ 10 m and 0.5 m above ground level

Wind direction

Relative humidity (RH %)

Elevated Inversion; specify height above ground level and temperature gradient

D. Optical Properties

Scattering, absorption, and extinction coefficients

Visibility, if Eq. 28 and Tables 9 and 10 of Ref. 1 are used.

3.1.2 Determine Concentration for Single or Separate Bulk WP Munitions

3.1.2.1 Basic Concentration Equations

$\bar{u} \neq 0$

$$C(x,\bar{y},\bar{Z},t) = (W \cdot \eta \cdot Y) \div (\pi x \cdot \bar{y} \cdot \bar{Z}/6)$$

$\bar{u} = 0$

$$C(x,\bar{y},\bar{Z},t) = (W \cdot \eta \cdot Y) \div (\pi \bar{Z}^3/12)$$

(Note: Cloud shape is a cone with apex ~d m below the ground level.)

where W = fill weight (g)

η = fill efficiency

Y = yield

x = length in direction of $\bar{u}$ (m)

$\bar{y}$ = lateral spread ⊥ to x (m)

$\bar{Z}$ = buoyant rise (Δh) + momentum rise ($\bar{z}$) - m

$\bar{u}$ = mean time wind speed (m/sec)

3.1.2.1 Mass Calculation

$$M = W \cdot \eta \cdot Y$$

W = fill weight is specified for given munition

= 1.0 for ordinary terrain surfaces

= 0.85 for soft, plowed field surfaces

= 0.50 for muddy terrain

$Y = 2.9 + 0.003\ (RH - 40\%)^{1.67}$

3.1.2.3 Calculation for x, $\bar{y}$, $\bar{z}$, and h; $\bar{u} < 0$

(a) Establish Stability Category

$\Delta T = T(10\ m) - T(0.5)$

$\theta_z = \Delta T + 0.098$

if $\theta_z < 0$, unstable

$= 0$, neutral

> 0, stable

> 0.1, retain value for ground inversion height

(b) Establish $\bar{u}$ at 10 m, time of day and cloud cover enter Table 12 and find specific Pasquill Category, $\theta_z = 0$, sufficient for CAT D.

TABLE 12

PASQUILL STABILITY CATEGORIES

Surface Wind Speed at 10 m (m/sec^{-1})	Insolation			Night	
	Strong	Moderate	Slight	Thinly Overcast or ≥ 4/8 Low Cloud	≤ 3/8 Cloud
<2	A	A-B	B	--	--
2-3	A-B	B	C	E	F
3-5	B	B-C	C	D	E
5-6	C	C-D	D	D	D
>6	C	D	D	D	D

(c) Cloud Dimensions

1. $x = \bar{u}t$

2. Given Pasquill Category, find $\bar{y}$ in table below.

$\bar{y} = 9.1 + 0.419x$	Pasquill Category - A
$= 9.1 + 0.328x$	Pasquill Category - B
$= 9.1 + 0.238x$	Pasquill Category - C
$= 9.1 + 0.20x$	Pasquill Category - D
$= 9.1 + 0.18x$	Pasquill Category - E
$= 9.1 + 0.146x$	Pasquill Category - F
$= 9.1 + 0.$	Pasquill Category - G

---

3. Given Pasquill Category, find $\bar{z}$ in table below.

Note: This $\bar{z}$ value represents momentum exchange; see use when $Z = \Delta h + \bar{z}$ is presented.

$\bar{z}(x) = 2.73 + 0.39x$	$\bar{u} = 0.5$ m/sec	Cat - A
$= 2.73 + 0.25x$	$= 1.0$ m/sec	Cat - A
$= 2.73 + 0.18x$	$= 1.5$ m/sec	Cat - A
$= 2.73 + 0.15x$	$= 2.0$ m/sec	Cat - A
$= 2.73 + 0.137x$	2.0 m/sec	Cat - A
$= 2.73 + 0.11x$		Cat - B
$= 2.73 + 0.073x$		Cat - C
$= 2.73 + 0.06x$		Cat - D
$= 2.73 + 0.055x$		Cat - E
$= 2.73 + 0.046x$		Cat - F
$= 2.73 + 0.03x$		Cat - G

4. Buoyant Plume Rise, Δh

(a) Compute $F = 3.7 \times 10^{-5}$ [800 • η • W ÷ burntime] (m^4/sec^3) using values from Sec. 3.1.2.2 and a burntime of 1 sec for artillery and 1.5 sec for mortars.

(b) For Unstable and Neutral, CAT - A, B, C, and D,

$$\Delta h(t) = 1.6F^{1/2}x^{2/3} \div \bar{u}, \quad \text{CAT A, B, and C}$$

$$= 1.6F^{1/2}x^{2/3}[0.4 + 0.64x/x_* + 2.2(x/x_*)^2] \div \bar{u}\,[1 + 0.8(x/x_*)]^2$$

where $x_* = 14F^{5/8}$ $\quad F < 55\ m^4/sec^3$

$= 34F^{0.4}$ $\quad F > 55\ m^4/sec^3$

Maximum Buoyant Rise (Cloud Top)

$$(\Delta h)_{max} = 1.6F^{1/2}\ (3.5x_*)^{2/3} \div \bar{u}$$

Alternative Rule

$(\Delta h)_{max}$ @ x when concentration = $0.1 g/m^3$ or exact expression for $\overline{\Delta T}$ in Fig. 12.

WARNING: Check for elevated inversion; if none,

$Z = \Delta h + \bar{z}$, otherwise follow the steps below.

1. Determine height of inversion and $\Delta T_i = T(Z_2) - T(Z_1)$
2. Calculate $b_i = g\Delta T_i/T$ (see Eq. 27, Part 1)
3. If inversion top defined by Z_i, then plume penetrates if $Z_i \leq 2\ (F/ub_i)^{0.5}$
4. Clearly if $(\Delta T)_{plume} > (\Delta T_i)$ the cloud will penetrate

(c) For Stable Conditions: CAT E, F, etc.

Compute $s = (g/T)\,\partial_z$ (see Sec. 3.1.2.3)

Determine $x_1 = 2.4\ \bar{u}/s^{0.5}$

$\Delta h = 1.6F^{1/2}x^{2/3} \div \bar{u}$ for $x \leq x_1$

$(\Delta h)_{max} = 2.9\ (F/\bar{u}s)^{1/3}$

Note: If $\Delta h_{max} > H_i$, ground inversion height, plume will penetrate.

$(\Delta h) \leq H_i$, then H_i is maximum

$\dot{Z} = \bar{z} + \Delta h$

The substitutionof x, $\bar{y}$, and $\bar{Z}$ into volume expression gives the concentration when $\bar{u} > 0$.

3.1.2.4 Still Air, $\bar{u} = 0$

Concentration = $(W \cdot \eta \cdot Y) \div$ Volume

$(W \cdot \eta \cdot Y)$ defined in Sec. 3.1.2.1.

$\bar{Z} \equiv (\Delta h)_{max} = 5.0F^{0.25}/s^{3/8}$

F, s defined above

Volume = $(\pi/3)\bar{Z}^3 \cdot \beta^2$, $\beta = 0.5$

if inversion top $z_i < Z$, the cloud will penetrate or,

$$z_i \leq 4F^{0.4}\ b_i^{-0.6}$$

Note: Plume is a cone with apex ~8 m below ground level.

$$\beta = r/Z = (x^2 + y^2)^{1/2} \div Z$$

$$t(Z_{max}) = (4Z/g)^{1/2}$$

3.2 METHOD FOR WR/RP - WICKS, WEDGES, PLASTICIZED MATERIAL

Munitions Characteristics	Burntime (min)
2.75" - Wick, Wedge	4.3
3" - Wick, Wedge	7.8
6" - Wick, Wedge	6.5
Navy, 81 mm - Wedge (RP)	4.3
Navy, 155 mm - Wedge (RP)	6.4
PWP/PRP	2.0

We assume that the source is a linear-array, continuous emitter. The material is dispersed in a radius of ~25 m, and we treat the source as three lines 25 m apart where the center line contains 50% munitions weight and the other two 25% each.

1. Basic Equation for Concentration

$$C(x, \bar{y}, Z, t) = \left[(Q \cdot Y \cdot \eta)/(t \cdot \ell)\right]\left[12/\pi\bar{u} \cdot Z(x,t)(1 + k)\right] \quad (g/m^3)$$

2. For each line, Eq. 1 applies; however, we have at each value of t the values of x are $(\bar{u}t \pm 25)$. Hence, at the position x the cloud arrives at times, $t = x/\bar{u} \pm 25/\bar{u}$.

where
- Q = fill weight
- Y = yield for WP/RP
- η = efficiency factor of fill
- t = burntime (sec)
- ℓ = length of array (m)
- $k = \bar{y}(x)/\ell$ when $\bar{u} \perp \lambda$
- $\bar{u}$ = mean wind speed (m)
- $\bar{y}$ = mean cloud width at x
- Z = cloud height, $\bar{z} + \Delta h$ at x
- $x = \bar{u} \cdot t$

If $\bar{u}$ is at an angle θ to ℓ, then $k = \bar{y}(x) \sin \theta/\ell$

$$Y = 2.9 + 0.003 \text{ (RH \% - 50\%)}^{1.67}$$

where $\bar{\eta}$ = 0.5 for muddy terrain

η = 0.85 for soft, plowed terrain

η = 1 for general conditions

ℓ = determine from operational plan

t = burntime look-up value

3. From input data, determine Pasquill Category

PASQUILL STABILITY CATEGORIES

Surface Wind Speed at 10 m (m/sec^{-1})	Insolation			Night	
	Strong	Moderate	Slight	Thinly Overcast or ≥4/8 Low Cloud	≤3/8 Cloud
2	A	A-B	B	--	--
2-3	A-B	B	C	E	F
3-5	B	B-C	C	D	E
5-6	C	C-D	D	D	D
>6	C	D	D	D	D

4. Expression for $\bar{y}$

$\bar{y} = 9.1 + 0.419x$	Pasquill Category - A
$= 9.1 + 0.328x$	Pasquill Category - B
$= 9.1 + 0.238x$	Pasquill Category - C
$= 9.1 + 0.20x$	Pasquill Category - D
$= 9.1 + 0.18x$	Pasquill Category - E
$= 9.1 + 0.146x$	Pasquill Category - F

5. Calculate $k = \bar{y}(x)/\ell$ and $(1 + k)$

6. Procedure for $Z = \bar{z}(x) + \Delta h$

(a) For Cat A, B, and C

$$\Delta h = 1.6F^{1/2}x^{2/3} \div \bar{u}$$

$$F = 3.6 \cdot 10^{-5}[800 \cdot \eta \cdot \text{Fill Weight (g)} \div \text{burntime (sec)}]$$

(b) For Cat D

$$\Delta h = 1.6F^{1/2}x^{2/3}\,[0.4 + 0.64\,x/x_* + 2.2(x/x_*)^2] \div \bar{u}[1 + 0.8\,x/x_*]^2$$

(c) $(\Delta h)_{max}$ for Cat A, B, C, and D

$$(\Delta h)_{max} = 1.6F^{1/2}(3.5x_*)^{2/3} \div \bar{u}$$

where $x_* = 14\,F^{5/8}$ $\quad F < 55\ m^4/sec^2$

$= 34\,F^{0.4}$ $\quad F \geq 55\ m^4/sec^2$

The values for $\bar{z}$ for different categories are given below.

$\bar{z}(x) = 2.73 + 0.39x$	$\bar{u} = 0.5$ m/sec	Cat - A
$= 2.73 + 0.25x$	$= 1.0$ m/sec	Cat - A
$= 2.73 + 0.18x$	$= 1.5$ m/sec	Cat - A
$= 2.73 + 0.15x$	$= 2.0$ m/sec	Cat - A
$= 2.73 + 0.137x$	2.0 m/sec	Cat - A
$= 2.73 + 0.11x$		Cat - B
$= 2.73 + 0.073x$		Cat - C
$= 2.73 + 0.06x$		Cat - D
$= 2.73 + 0.055x$		Cat - E
$= 2.73 + 0.046x$		Cat - F

(See notes for Bulk WP on inversion procedure.)

(d) Cat E, F, and G

Compute $s = (g/T)\partial_z$

$$x_1 = 2.4\bar{u} \div s^{1/2}$$

$$\Delta h = 1.6F^{1/2}x^{2/3} \div \bar{u} \quad \text{for } x \leq x_1$$

$$(\Delta h)_{max} = 2.9(F/\bar{u}s)^{1/3}$$

If $(\Delta h)_{max} > H$, ground inversion height will penetrate, $(\Delta h)_{max} < H$, $Z_{max} = H$.

(e) Calculate $\bar{z}$ for specific Pasquill Category

$\bar{z}(x) = 2.73 + 0.39x$	$\bar{u} = 0.5$ m/sec	Cat - A
$= 2.73 + 0.25x$	$= 1.0$ m/sec	Cat - A
$= 2.73 + 0.18x$	$= 1.5$ m/sec	Cat - A
$= 2.73 + 0.15x$	$= 2.0$ m/sec	Cat - A
$= 2.73 + 0.137x$	2.0 m/sec	Cat - A
$= 2.73 + 0.11x$		Cat - B
$= 2.73 + 0.073x$		Cat - C
$= 2.73 + 0.06x$		Cat - D
$= 2.73 + 0.055x$		Cat - E
$= 2.73 + 0.046x$		Cat - F

(f) Calculate $Z = \bar{z} + \Delta h$

7. Calculate concentration

Substitute values for Q, y, ℓ, t, $\bar{u}$, Z, and k, compute C(x, y, z, t) for each line, and add value at each x or time, t, as needed.

8. Find L, the path length through the cloud, and then compute C · L.

9. For $\bar{u} = 0$, use algorithms described for bulk WP in Sec. 3.2.

3.3 METHOD FOR HC SMOKE CONCENTRATION TIME HISTORY

3.3.1 Munitions Characteristics

105mm M1 Canister; Fill Wt = 1.65 lb; Burntime = 180 sec ; M84 shell

155mm *M1 Canister; Fill Wt = 5.8 lb ; Burntime = 120-140 sec; M116B1 (3/shell)

*M2 Canister; Fill Wt = 3.0 lb ; Burntime = 60-240 sec; Ogive (1/shell)

Basic Equation for Concentration

$$C(x, y, z, t) = \left[\frac{Q \cdot Y}{t \cdot \ell}\right] \frac{12}{\pi \cdot \bar{u} \cdot Z(x, t)(1 + k)} \quad (g/m^3)$$

Q = quantity of fill (g)

Y = yield of HC

t = burntime (sec)

ℓ = length of canister array (m)

$k = \bar{y}(x)/\ell$ when $\bar{u}$ is $\perp$ to ℓ

$\bar{u}$ = time mean wind speed (m)

$\bar{y}$ = cloud width increase at x

*New fill weights are 5.46 and 2.69 lb, respectively.

Note: (1) We assume a near-linear array for the artillery delivered canisters; i.e., the starting point ($x = 0$, $t = 0$) will be the mean distance.

(2) If $\bar{u}$ is at θ to ℓ, $k = \bar{y}(x) \sin \theta/\ell$

(1) $Y = 1 + 0.051(RH\% - 5)^{0.85}$

(2) $\bar{y} = 9.1 + 0.419x$ Pasquill Category - A

$= 9.1 + 0.328x$ Pasquill Category - B

$= 9.1 + 0.238x$ Pasquill Category - C

$= 9.1 + 0.20x$ Pasquill Category - D

$= 9.1 + 0.18x$ Pasquill Category - E

$= 9.1 + 0.146x$ Pasquill Category - F

(3) $\bar{Z} = \bar{z}(x) + \Delta h$

Δh = correction for exothermic effect

(4) For Cat A, B, C

$$\Delta h = \frac{1.6F^{1/2}x^{2/3}}{\bar{u}} \quad \text{or} \quad \frac{1.6F^{1/2}t^{2/3}}{\bar{u}^{1/3}}$$

(5) $F = 3.7 \cdot 10^{-5}$ [500 cal/g · Fill Wt (g)/Burntime (sec)]

$t \leq 10$sec

(6) For Cat D

$$\Delta h = \frac{1.6F^{1/2}x^{2/3}}{\bar{u}} [0.4 + 0.64\ (x/x_*) + 2.2\ (x/x_*)^2] \div [1 + 0.8\ (x/x_*)]^2$$

$$(\Delta h)_{max} = 1.6F^{1/2}(3.5\ x_*)^{2/3} \div \bar{u}$$

$x_* = 14\ F^{5/8}$ $\quad F < 55\ m^4/s^3$

$x_* = 34\ F^{0.4}$ $\quad F \geq 55\ m^4/s^3$

(7) For Cat E, F, etc.

$$\Delta h = 1.6\, F^{1/2} x^{2/3} \div \bar{u} \quad \text{for } u \leq x_1 \quad (x_1 = 2.4\bar{u} \div s^{1/2})$$

$$(\Delta h)_{max} = 2.9\, (F/\bar{u}\bar{s})^{1/3}$$

$$\bar{s} = \frac{g}{T}\, \partial_z$$

θ = Potential Temp (z = 10 m, z = 0.5 m)

If $(\Delta h)_{max} > H$, ground inversion height will penetrate $(\Delta h)_{max}$ and, if $<H$, $z_{max} = H$.

(8)

$\bar{z}(x) = 2.73 + 0.39x$	$\bar{u} = 0.5$ m/sec	Cat - A
$= 2.73 + 0.25x$	$= 1.0$ m/sec	Cat - A
$= 2.73 + 0.18x$	$= 1.5$ m/sec	Cat - A
$= 2.73 + 0.15x$	$= 2.0$ m/sec	Cat - A
$= 2.73 + 0.137x$	> 2.0 m/sec	Cat - A
$= 2.73 + 0.11x$		Cat - B
$= 2.73 + 0.073x$		Cat - C
$= 2.73 + 0.06x$		Cat - D
$= 2.73 + 0.055x$		Cat - E
$= 2.73 + 0.046x$		Cat - F

For $\bar{u} = 0$ and inversion layer conditions, see algorithms in bulk WP Sec. 3.1.

3.3.2 Inputs

T (0.5 m)	Munition Type - 105 mm or 155 m
T (10 m)	Munition Quantity - M1 and M2
$\bar{u}$	Length of Array
Pasquill Category	Relative Humidity

A. Define Q, Burntime

B. Compute Yield use Eq. 1 using input relative humidity.

C. Compute Δh

(1) Stipulate Pasquill Category

(2) Calculate F, x_*, or $\bar{s}$

(3) Unstable - use Eq. 4

Neutral - use Eq. 6

Stable - use Eq. 7

D. Compile $Z(t) = \bar{z}(t) + \Delta h$

For given Pasquill Category and $\bar{u}$, select appropriate $\bar{z}(t)$ from Eq. 8 and appropriate Δh Eqs. 4, 6, or 7. Calculate Z(t).

E. Compile $\bar{y}(t)$

For given Pasquill Category, select appropriate $\bar{y}(t)$ from Eq. 2. Calculate $\bar{y}(t)$.

F. Calculate "k" and (1 + k)

G. Compute C(x, y, z, t)

Input A, B, D, and F, $\bar{u}$, and t as defined under munitions into Eq. 1. This is mean, homogeneous concentration.

H. To find C · L

Multiply appropriate C(t) value by line-of-sight path length, L, in meters.

I. Cloud Width at $x = \bar{y}(x) + \lambda$

Note: The persistence of the screen is terminated at the end of burntime. For $\bar{u} = 0$, use algorithms described for bulk WP (Sec. 3.1).

3.4 METHOD FOR FOG OIL GENERATOR

3.4.1 General Considerations

The M3 fog oil generator[1] is a pulse jet that vaporizes 25 to 50 gal/hr of oil. The weight is 3.36 kg/gal. In addition, the engine consumes 3 gal of gasoline/hr and exhausts the combustion products. For the present, we neglect the latter although it may have a near field effect on infrared transmission.

There is a thermo-mechanical effect in the near field of the generator; that is, the oil vapor is hot and leaves the nozzle at near local sonic speed. It is estimated that about 5 kcal/sec is released due to condensation and cooling. Also, the jet would come to near ambient air speed at ~3 m from the nozzle exit plane. Again these effects are omitted; however, the source is now located ~3 m from the generator.

Hence, the source is defined as a static, non-exothermic, point-emitting Q grams of oil droplets per second.

We assume the smoke cloud to be defined by a semi-cone resting on the ground; that is, the x, y axes are in the ground plane and the z axis is _ to the (x, y) plane.

3.4.2 Cloud Dimension

3.4.2.1 Cloud Length

$$\bar{x} = \bar{u}t \quad (x \text{ is in direction of } \bar{u})$$

where $\bar{u}$ = time mean wind speed at 2-m height

t = time (sec)

[1] When the air temperature is < 30°F, the cloud dissipates rapidly.

3.4.2.2 Cloud Width, $\bar{y}$

$\bar{y}(x) = 9.1 + 0.419x$ Pasquill Category = A

$= 9.1 + 0.328x$ Pasquill Category = B

$= 9.1 + 0.238x$ Pasquill Category = C

$= 9.1 + 0.20x$ Pasquill Category = D

$= 9.1 + 0.18x$ Pasquill Category = E

$= 9.1 + 0.146x$ Pasquill Category = F

3.4.2.3 Cloud Height, $\bar{z}$

$\bar{z}(x) = 2.73 + 0.39x$		$\bar{u} = 0.5$ m/sec
$= 2.73 + 0.25x$		$= 1.0$ m/sec
$= 2.73 + 0.18x$	Category A	$= 1.5$ m/sec
$= 2.73 + 0.15x$		$= 2.0$ m/sec
$= 2.73 + 0.137x$		> 2.0 m/sec
$= 2.73 + 0.11x$	Category B	
$= 2.73 + 0.073x$	Category C	
$= 2.73 + 0.066x$	Category D	
$= 2.73 + 0.055x$	Category E	
$= 2.73 + 0.046x$	Category F	

3.4.3 Concentration

To find the concentration during the emission phase, we assume a series of discrete instantaneous sources where the concentration for an instantaneous source is given by

$$C = \frac{Q}{\sqrt{\pi}\,\bar{x}\cdot\bar{y}^2} \quad (g/m^3) \tag{31}$$

where Q = grams released in 1 sec and $\bar{x}$ and $\bar{y}$ as defined in Secs. 3.4.2.1 and 3.4.2.2 respectively.

The conversion from gal/hr to g/sec is 0.93.

Equation (31) can now be written as a function of time since $\bar{u}$ = constant,

$$C(t) = \frac{0.930}{\frac{\pi}{24}\bar{u}} \frac{1}{t[9.1 + (A\bar{u}) \cdot t]^2} = \frac{7.130}{\bar{u}} \frac{1}{t(9.1 + A\bar{u} \cdot t)^2} \qquad (32)$$

where A is a constant defined by the specific Pasquill Category and Q is in gal/hr.

For 1-sec intervals, we have a series of equations such as

$$C(1) = \frac{7.130}{\bar{u}}\left[\frac{1}{1(9.1 + A\bar{u})^2}\right]$$

$$C(2) = \frac{7.130}{\bar{u}}\left[\frac{1}{2(9.1 + A \cdot u \cdot 2)^2}\right]$$

$$\vdots$$

$$C(n) = \frac{7.130}{\bar{u}}\left[\frac{1}{n(9.1 + A \cdot \bar{u} \cdot n)^2}\right]$$

where n = burntime in seconds, t_b

Now since $\bar{x}$ is an implicit function of t, we have at $x = \bar{u}$ (or at time = 1 sec), etc.:

$$C[x(1)] = \frac{7.130}{\bar{u}} \sum_{t=1}^{n'=t_b}\left[\frac{1}{t(9.1 + A\bar{u} \cdot t)^2}\right]$$

$$C[x(2)] = \frac{7.130}{\bar{u}} \sum_{t=2}^{n'}\left[\frac{1}{t(9.1 + A\bar{u} \cdot t)^2}\right]$$

For $t = t_b$, then $x = \bar{u}t_b$, and

$$C[x(t_b)] = \frac{7.13Q}{\bar{u}} \left[\frac{1}{t_b(9.1 + A\bar{u}t_b)^2} \right]$$

Note: The above simple procedure is suggested for ease of computation. Also, the concentration will fall rapidly and, therefore, the concentration calculation will be terminated at x values $<< x = \bar{u}t_b$.

For $t > t_b$, it is suggested as preliminary estimate to find the mass near the origin and treat as a new instantaneous source, at $x = 0$, retaining the initial concentration arrival. Hence,

$$M = \sum_{i=1}^{5} C_i \cdot V_j = C(1) \cdot \prod \bar{u} \cdot (9.1 + A\bar{u})^2$$

$$+ C(5) \cdot \prod \bar{u} \cdot 5(9.1 + A\bar{u}5)^2$$

$$C(t) = \frac{24M}{\bar{u} \cdot t(9.1 + A\bar{u}t)^2}$$

3.4.4 C · L Parameter

With the C given above and the specified line of sight, find C · L (see Appendix F of CR-231, Ref. 1). It should be noted that, near the source, the cloud is highly non-uniform.

PART 2
EXPLOSIVE DUST OBSCURATION MODEL

1 INTRODUCTION

In this part of the report we consider an explosive-generated dust model. The basic data are examined. The early work that pertains to the subsurface events (performed by the PM/Smoke-Obscurants during Smoke Week I and at other field trials) is described. In addition, several validations of the live and static firings performed at Smoke Week I, Fort Sill, and Grafenwohr II are presented.

As will become evident, there are difficulties associated here with the validations. The number of single events are few, and multi-events are extremely complex phenomena. Also, the available data on the initial conditions are limited; that is, the soil properties are not defined adequately, the extinction coefficients appear variable, cloud geometries are semi-quantitative, and/or meteorological data are limited. Nevertheless, the geometrical histories of the dust clouds may be calculated; however, the ability to calculate the transmission may be limited by the aforementioned shortcomings.

2 BASIC CONSIDERATIONS

2.1 THE SOIL MEDIUM

Since we are interested in the dust clouds generated by munitions exploded near the earth's surface (under or on), the soil characteristics of the first meter or so of the earth's crust are important. This includes the physical and mechanical characteristics and the constituents for different degrees of saturation where the latter is due to precipitation.* To avoid some of the difficulties such as mechanical properties, we will depend upon experimental cratering results whenever available for the different soils.

Table 1 lists the densities of several soil types. Note the profound effects of vegetation and moisture on the density. These variations affect the mass of dust injected into the atmosphere as a result of an explosion. In the literature we find an occasional loose statement that the average soil density is 2.5 g/cc.

TABLE 1
SOIL MATERIAL DENSITY

Material	Density	
Type	g/cc	lb/ft^3
Quartz	2.67	167
Clay	2	124.8
Loose loam, dry	1	62.4
Loam, wet	1.8	112.3
Loam, sandy	1.5	93.6
Fine sand, loose	0.7	44
Compact sand, wet	1.8	112
Light soil-grass roots	0.3-0.5	<31
Rock materials	~2.4	150

*Or water table level.

At Grafenwohr the results of soil analysis show, primarily after the explosion, that near the surface (0-5 cm), the density was 0.95 g/cc, which included ~28% vegetation; the moisture content was 28%. In another location the value was ~1.13 g/cc, and the moisture content was 27%.

In general, the soil type up to depth of ~0.35 m was loamy sand or sandy loam with an occasional gravelly loamy sand. The moisture content in Zone 4 was typically ~21%-27% and the specific gravity ~2.62 (163 lb/ft^3).

Hence, the surface layer will have a low density; however, the predominant crater material will have a near average value of specific gravity for a wet sandy soil.

The depth of the vegetated soil (sod) is important since the density is lower than the subsoil, and the likelihood that the sod does not participate in the airborne dust cloud due to the weight of the clumps.

An analysis of the subsurface soil at Fort Polk, Louisiana, a siltstone, is listed in Table 2. Note that the depth is in feet.

TABLE 2

SUBSURFACE SOIL ANALYSIS OF FORT POLK, LOUISIANA

Depth (ft)	Moisture Content (%)	Degree of Saturation (%)	Wet Density (lb/ft^3)	Dry Density (lb/ft^3)
2-3	21.1	42.6	85.7	70.8
3.3-4.3	23.0	50.2	91.2	74.4
4.5-5.3	20.2	36.8	80.0	66.9
2-3	24.2	84.8	113.1	91.2
3.3-4.3	24.0	80.2	111.9	90.0
4.5-5.3	22.4	94.7	121.9	100.0
2-3	25.5	79.5	112.5	91.2
3.3-4.3	30.0	80.1	106.9	81.9
4.5-5.3	24.9	70.8	106.2	85.0
2-3	29.0	100.0	127.8	107.5
3.3-4.3	26.4	96.5	126.2	105.0
4.5-5.3	25.3	100.0	106.2	98.1
2-3	29.2	100.0	131.9	94.1
3.3-4.3	24.0	100.0	125.0	100.6
4.5-5.3	29.2	89.8	113.1	87.6

We note that the moisture content does not correlate with degree of saturation or density at different locales in the same general vicinity; however, the percent of saturation correlates with the wet density. The dry density is obtained by dehydration of the wet (actual) density.

Alluvial moist sandy soil (sandstone subsoil) in Colorado has a density of about 120 lb/ft^3.

From Tables 1 and 2 we observe two interesting facts: (1) the quantity of silica, clay, and loam will determine the soil's basic density; and (2) in Table 2, sample 1 has a greater specific gravity and a lower dry density. For sample 1 there is probably somewhat more quartz than in the other samples. Further, at half the degree of saturation the percent weight increase is the same; that is, sample 1 is less compact as evident from the low dry density. At 100% saturation the wet weight would be comparable for all samples $\simeq 120$ lb/ft^3.

The chemical composition of soils depends on location and the nature of terrain (wooded, desert, etc.). In Ref. 1 data for several locales are given and are reproduced here in Table 3. One must recognize that soil composition is highly locale dependent; that is, to specify West Germany is not to imply that it is applicable to all of West Germany! Further, the existence of only 5% quartz in the Sinai is highly questionable. Samples from the periphery of the Sahara and other deserts were shown to have quartz as their major mineral constituent.

Flanigan and Delong[2] found from their sampling effort at several European locations that silica (quartz) concentrations were high and that little or no $CaCO_3$ was found in 68 different locations around the globe. The latter is common where shellfish are or were present.

---

[1] Cobla, C., Obscuration Due to Dust of a Laser Beam in a Gun Firing Environment, USARMCOM, Rock Island Arsenal, Report AC-TR-75003, October 1975.

[2] Flanigan and Delong, Spectral Absorption Characteristics of the Major Components of Dust Clouds, EATR4430, September 1970.

TABLE 3

CLASSIFICATION OF COMPARATIVE SOIL BY WEIGHT

Mineral	Chemical	Aberdeen	Mojave	Germany	Sinai
Montmor-illonite	$(Mg,Ca)0\text{-}Al_2O_3\ 5SiO_2 \cdot nH_2O$	35	25	45	25
Kaolonite	$Al_4Si_4O_{10}(OH)_8$	20	20	19	17
Illite	$K_1Al_4Si_7Al_1O_{20}(OH)_4$	20	20	10	20
Calcite	$CaCO_3$	15	15	20	20
Quartz	SiO_2	5	5	*	5
Hematite	Fe_2O_3	*	5	5	5
Corundum	Al_2O_3	*	5	*	2
Thenardite	$NaSO_4$	*	2	*	1
Halite	NaCl	*	2	*	1
Others	MnO, TiO, CaO MgO, K_2O, Na_2O, P_2O_5				

In the normal state these clay minerals are usually hydrated.

*Not measured.

Chemical analysis of dust aerosols over the Indian desert showed that on a percentage basis they fall into the following groups: quartz - 36%, mica - 20%, feldspar - 22% (includes the clay minerals), and carbonates (calcite, dolomite) - 22%. The existence of the carbonates is expected, as a high proportion of shellfish fragments are present in the southern part of the desert.

The important of soil chemistry is that the particulate scattering and absorption properties, particularly in the 7 to 14 μm region, are determined by the mineral type. Hence, to find the effective extinction coefficient integration of the complex band structure is required. More important, if a laser transmitter or transmissometer is used, significant differences will be obtained, and the resultant may not be representative of the integrated 8 to 13 μm bands. The latter may be a problem in some published dust data.

In Fig. 1, we show the spectral extinction coefficients, α_e, at 8 to 13 μm for Fort Benning and Fort McLellan, respectively. The silica content is low at Fort Benning and of medium value at Fort McClellan. The effect at 9.17 μm should be noted and also the difference in the absolute value of the extinction coefficient, namely, the Fort Benning values are 2× Fort McLellan. The minimum near 11.3 μm is real.

2.2 PARTICLE SIZE DISTRIBUTION

Another parameter of basic importance is particle size distribution since it enters into the determination of the dust's optical properties. Normally, the distributions found in the literature relate to surface conditions, whereas for near-surface explosions we are interested in the subsurface conditions. The former is germane to ambient aerosols, vehicular dust clouds, and airbursts without cratering. For complete coverage, we will consider both surface and subsurface detonations.

A standard soil classification that is not unreasonable is given in Table 3.

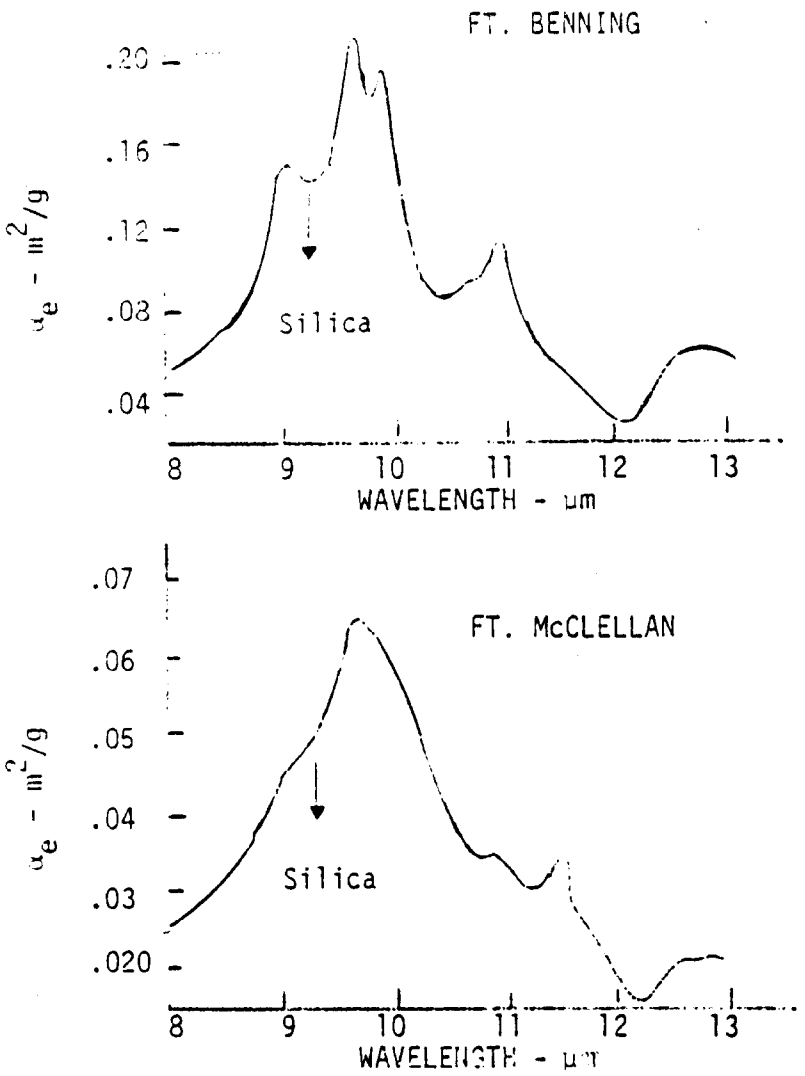

Figure 1. Extinction Coefficient for Ft. Benning and Ft. McClellan

TABLE 4
STANDARD SOIL CLASSIFICATION

Soil Class	Size (μm)	% by Weight
Clay	5	22
Silt	5-50	38
Sand, very fine	50-100	15
Sand, fine	100-250	14
Sand, medium	250-500	5
Sand, coarse	500-1000	4
Sand, very coarse	1000-2000	1
Fine Gravel	2000-10,000	1

In Table 5, we have listed the mass size distribution for various locations and soil types. Again the predominance of the mass fraction is in smaller particles; i.e., for a particle of similar density the mass of 50 μm particle is 10^3 greater than for a 5-μm particle or on a number density basis the distribution is predominantly of smaller size particles.

Observations of ambient dust may show few particles beyond 10 μm in size, whereas explosives may generate dust clouds with several orders of magnitude ($\sim 10^4$) of 100-μm particles or larger. For example, at Dugway Proving Ground, the surface soil mass median diameter (MMD) was 254 μm, whereas at 3-in depth the subsoil had an MMD = 354 μm. The Smoke Week I tests held at Dugway Proving Ground showed that only 0.33% of the particles were greater than 75 μm. On the other hand, at Fort Sill, Oklahoma, the particle sizes terminated at ≤10 μm.

In Ref. 3 measurements of the particle size lofted by a tank main gun muzzle blast at a dry lake bed, China Lake, showed that particles of radii ≤100 μm made up 50% of the dust cloud mass. This mass distribution

[3] Measurement of Laser Beam Transmission and FLIR Sight Obscuration in a Tank Gun Firing Environment, Ford-Aeronutronic Division, California, Report No. U-6362, March 1977.

TABLE 5

US GEOGRAPHICAL VARIATION OF PARTICLE SIZE
(Wt. %)

Particle Size (μm)	Anchorage Sandy Loam Silt	California Silty Clay-Clay	Georgia Sandy Loam	Hawaii Dark Clay	Hawaii Silty Clay	Illinois Mixed Clay, Silt	Mass. Gravel, Sand Loam
5	10	50	14	50	30	4	11
20	5	25	30	30	55	16	24
70	17	15	11	8	5	17	19
150	17	7	15	6	4	53	17
400	17	2	12	4	3	9	9
700	17	1	15	2	2	1	16
1500	17	0	3	0	1	0	4
5000	0	0	0	0	0	0	0

TABLE 5 (Cont.)

Particle Size (μm)	Berkshire Mass.	Miss. Silt Loam	Dunkirk Loam	Fine Sandy Loam	Alder Clay Loam	Louisiana Sharkey Clay	Memphis Silt Loam
5	6	15	19	10	29	38	23
20	24	-79-	-53-	10	-53-	-51-	-71-
70	22	3	14	20	8	7	2
150	25	1	6	30	4	2	1
400	6	1	3	10	1	1	1
700	13	1	4	10	2	1	1
1500	4	1	1	10	3	0	1
5000	0	0	0	0	0	0	0

Particle Size (μm)	Oklahoma Fine Sandy, Loam	Ohio Clay Loam	So. Dakota Silt Loam	No. Dakota Silt Loam
5	12	19	45	19
20	15	-54-	-17-	40
70	-37-	10	6	29
150	35	10	8	18
400	1	3	7	1
700	0	3	10	1
1500	0	1	7	0
5000	0	0	0	0

is characteristic of the surface layer. A similar mean mass diameter is found for the DIRT-I test area at the White Sands Missile Range; see Fig. 2. The additional data points are results from the Grafenwohr tests (November 1978): the dots are from a sandy clay loam; the lower points are from a sand soil; and the squares are the results for a soil like the one at WSMR. We observe that the MMD varies from 100 μm to ~ 2000 μm (coarse sand). Interestingly, the two silty sands are similar except for the variation in gravel content; however, the overall effect should be small.

In Table 6, we present the percentage of particles below 74 μm at several US military installations.

TABLE 6
PERCENTAGE OF SURFACE SOIL PARTICLES BELOW 74 μm

Location	Particle Percentage
Ft. Hood, Texas	16-38
Ft. Bliss, Texas	5-8
Ft. Bliss, Texas	24.4 (Field)
White Sands Missile Range, New Mexico	≥8.3
Ft. Huachua, Arizona	1.4-9.4
Yuma Proving Ground, Arizona	9.1-21.0
Yuma Proving Ground, Arizona	<45
Aberdeen Proving Ground, Maryland	7.6-30.4

Hence, we should anticipate large fractions of particles in excess of 75 μm. This statement therefore raises a question, "How valid are the Smoke Week and Ft. Sill sampler results?" What did the samplers actually intercept?

Although 100-ton detonations are not comparable to artillery-like detonations due to deeper craters and greater energy release, nevertheless

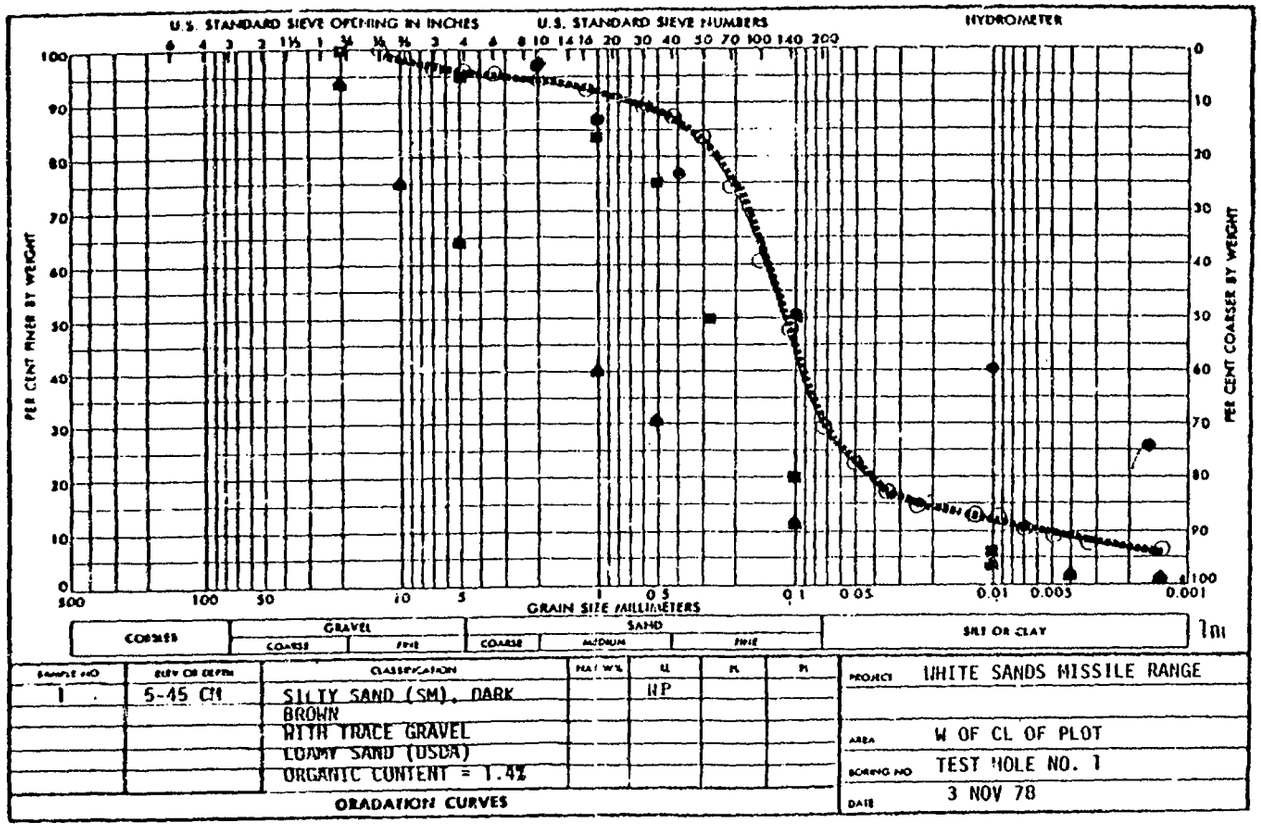

Figure 2. Typical Grain Size Distribution Curve for DIRT-I Test Area (Grafenwohr Data Supplied by Waterways Exp. Station, Department of Army)

their particle distributions have qualitative interest. Particle distributions following explosions of charges on the ground are presented below.

The in situ material (clay soil; water table 4 ft) prior to detonation has a distribution given by

$$\frac{dN}{dr} = \frac{5.6 \times 10^4}{r^{3.6}} \tag{1}$$

It should be noted that the primary emphasis was on the larger particles, radii >10 μm, and therefore, extrapolation to smaller radii are required. We assume the distribution is valid to ~1 μm. At 92 sec after the detonation the sampling of the rising main cloud showed the distribution in Table 7.

TABLE 7

PARTICLE SIZE DISTRIBUTION IN MAIN CLOUD
(100 TON HE, COLORADO)

D (μm)	dN/d (log D)
26	0.212
48	0.124
80	0.0606
112	0.035
160	0.021
224	0.011
320	5.5×10^{-3}
448	2.37×10^{-3}
640	1.19×10^{-3}
896	6.4×10^{-5}
1280	0

This distribution, like others, has a form given by the expression

$$\frac{dN}{d\ (\log D)} = \frac{A}{D^{n-1}} \tag{2}$$

where A is a "number density," or $dN/dr = A/r^n$. This form is approximately the same as the surface layer; however, the exponent was 3.3 for particles less than 500 μm.

At a later time, ~ 150 sec sampling of the cloud base and stem top showed an enrichment of large particles ≥200 μm due to settling; that is, the size distribution ~ $r^{-2.34}$ for the particles <500 μm. In the middle of the stem the slope is $r^{-3.75}$ and is compatible with the ejected distribution. Shortly thereafter, we established from the data a particle size distribution function near the cloud base/stem:

$$\frac{dN}{dr} = \frac{7.75 \times 10^5}{r^{3.69}} \tag{3}$$

The major difference is a variation in the number of particles >100 μm and their location. For particle sizes <60 μm the numbers remain approximately the same.

This sampling took place during high winds. When the winds were mild, the effect on the large particles results in earlier fallout.

In another test, the particle distribution near ground level was found to be

$$\frac{dN}{dr} = \frac{8.5 \times 10^5}{r^{3.6}} \tag{4}$$

With respect to particle size distribution from artillery and smaller changes, two particle distributions observed in DIRT-1, under mild wind conditions, have been reported in Ref. 4. The first was obtained at 120 sec after a barrage of 8-155 m projectiles where the sampler was at 10.6 m above

[4] Lindberg, J. D., A Preliminary Report on Dusty Infrared Test - 1 (DIRT-1), ASL-TR-0021, January 1979.

ground level. We note that the particle sizes/diameters varied from ~1 to 200 μm. At this time the cloud should be at ~40-50 m altitude and retain most of the lofted particles (no ballistic trajectories assumed); however, the large particles (≥100 μm) should have settled to the ~10-m level. The second event consisted of 15-lb bare charges totaling 140, detonated in a rectilinear array. Here the measurement was made at 150 sec after detonation and at an altitude of ~26.3 m above ground level. The number of small and large particles were both larger than in the above case. The greater number of small particles is understandable in view of the later time and sampling altitude. With respect to the larger number of large particles, this may be due to the charge array and the interacting effect of charges which may have lofted a larger fraction of loose surface dust to a higher altitude than normal.

A fit to the data gives the expression,

$$\frac{dN}{dD} = \frac{1.79 \times 10^{6}}{D^{2.65}} \; ; \quad (\text{liter}^{-1}, \mu\text{m}^{-1}) \tag{5}$$

or in units of (cm^{-3}, μm^{-1})

$$\frac{dN}{dr} = \frac{5.7 \times 10^{2}}{r^{2.65}} \tag{6}$$

The exponent (2.65) is characteristic of large particle enrichment as noted earlier.

We have assumed in our analysis that the particle size distribution is given by

$$\frac{dN}{dr} = \frac{8.5 \times 10^{3}}{r^{3.6}} \tag{7}$$

which is more characteristic of standard aerosol distributions and observed functions of airborne dust generated by explosives. Although there is a

difference between the two, the basic question is: What is the time-space-dependent particle size distribution? The optical properties will depend upon this question, particularly the particles with radii $\lesssim 5$ μm.

We will attempt to formulate the particle size distribution history.

First, we must establish the distribution of the soil type that will be lofted into the atmosphere. For this we assume that the distribution is given by

$$\frac{dN}{dr} = \frac{A}{r^{3.6}} \tag{8}$$

Obviously, the exponent will vary between ~3.3 and 3.7. Next we assume the important particle radii lie between ~1 and 200 μm. Now, the mass density (g/cc) of this function is

$$m = \left(\frac{4\pi}{3} \rho A \int_1^{200} r^{-0.6}\, dr\right) \times 10^{-12} \tag{9}$$

where ρ = density of material (g/cc).

If we assume $\bar{\rho} = 2$ then M can be obtained directly; that is

$$m(t) = 76.7 \times 10^{-12} A(t) \tag{10}$$

To find "A" we consider a time, $t' = 0.1W^{1/3}$, where W = lb of HE. Now we define a cratering efficiency, η(cc/lb HE). Then the ejected mass for W lb of HE is

$$M = \eta \cdot W \cdot \rho \quad \text{(grams)} \tag{11}$$

where ρ is the soil density. Since the entire mass is not lofted we introduce a fractional fallout mass, m_0, to represent the "instantaneous fallout." Hence, the airborne fraction is

$$M(t') = (1 - m_0) \cdot \eta \cdot W \cdot \rho \tag{12}$$

The factors m_0 and σ are functions of soil type and soil wetness and will be given later. Thus the factor A at t' for a cloud volume, V, is defined by

$$A(t') = \frac{(1 - m_0)\,\eta \cdot W \cdot \sigma}{76.7 \times 10^{-12} V(t')} \tag{13}$$

If the concentration were uniform then A(t) would decrease as V(t')/V(t) and similarly m(t). However, there is settling of the larger particles and, therefore, the vertical particle size distribution changes with time as well as the concentration. The latter depends upon wind speed and particle size.

To simplify the problem we note that electro-optical transmission is limited to less than 60 sec, probably ~30 sec. Within this time period the upper part of the cloud should be free of particles with radii ≥ 200 μm; however, these should have settled near the base of the main cloud. Further particles from the stem will be blown into the cloud base; however, only 10% of the entire lofted mass is in the stem.

Hence, we assume that the particle size distributions are given by the following expressions, when $\bar{u} > 0.3$ m/sec, $\bar{u} \leq 10$ m/sec.*

For $t \leq 5$ sec

$$\frac{dN}{dr} = \frac{A}{r^{3.6}} \tag{14a}$$

For $5 < t \leq 15$ sec

The cloud base ±3 m

$$\frac{dN}{dr} = \frac{A}{r^{2.5}} \tag{14b}$$

*See Part 1 for definition of $\bar{u}$.

The remainder, cloud and stem

$$\frac{dN}{dr} = \frac{A}{r^{3.7}} \tag{14c}$$

For $t > 15$ sec

$$\frac{dN}{dr} = \frac{A}{r^{3.7}} \tag{14d}$$

The values of A are found by the procedure described above with the auxiliary condition that the total mass for $t > 0.3W^{1/3}$ is distributed accordingly, 90% in the main cloud and 10% in the stem.

Additional discussion is given later when the concentration distribution is considered.

The above functions are needed to establish the Mie values for the extinction, scattering, and absorption; that is, the optical properties of the dust. We consider this topic in the next section.

2.3 DUST OPTICAL PROPERTIES

From the above discussion we observe that to specify the dust (explosive) optical properties is, to say the least, a difficult task. In Table 8 we have assembled several experimental values and a theoretical one.* The theoretical value for the photopic region (0.4 to 0.7 μm) is based on a water-like particle. We have omitted the effect of diffraction, which will increase the forward scattering and reduce the extinction coefficient.

*Patterson, E. M., "Extinction Between 0.55 μm and 10.6 μm due to Soil-Derived Aerosols," Applied Optics, 1977, pp. 2414-2418. In this reference Patterson reviews and discusses his results on the extinction coefficient induced by varying atmospheric dust aerosol size distributions. The variation due to size distribution is ~2 orders of magnitude. For each spectral distribution, the photopic value is ~2× the 10-11 μm value and the variation within the 3-5 μm region is small.

TABLE 8

SPECTRAL EXTINCTION COEFFICIENTS FOR DUST*

(m^2/g)

	Wavelength (μm)						
Dust Origin	.4-.74	.67	3-5	3.8	1.06	8-13	Source
Edgewood		.55	.4			.30.4	CSL
Fort Sill[2]	.06		.04		.05	.03	DPGFR-78-313
Fort Sill (Surface)	.24		.16		.19	.13	DPGFR-78-313
Dugway	.32		.27		.35	.21	Smoke Week I
Wyoming Clay[3]				.07-.125			Aerodyne Inc.
Theoretical	.4-.5					.13	
Eglin AFB	.27		.25		.26	.23	Smoke Week II

*See Part 3 for additional data on the values for the photopic region.

[2]A single major deviation is the Fort Sill photopic extinction coefficient; that is, the lowest value observed for field data.

[3]Crushed to optimize size to 4 μm particle diameter, i.e., comparable to surface. Also a minimum should exist at ~ 3.8 μm for the 3-5 μm band.

The variations in Table 8 are primarily related to composition and particle size distribution (location). To appreciate variation in absolute magnitude see also Fig. 1.

The theoretical calculation at the 8 to 13 μm region was performed by B. Frickel, CSL, and the input data were provided by this writer as representative of Grafenwohr (wet site). The inputs were mineral content, index of refraction and particle distribution. Our estimate for the mineral content of the soil is as follows: quartz (40%); feldspar (26%), mica (30%), and carbonates (2%). From this, the complex index of refraction was established with the effort focused on the 8-13 μm region; see Table 9. With these values and the particle size distribution $dN/dr = 8 \times 10^3/r^{3.6}$, the mass extinction coefficients were computed for spherical particles whose

TABLE 9

WAVELENGTH VARIATION OF REFRACTIVE INDEX

Wavelength (μm)	Real Index	Imaginary Index
8.2	1.130	.850
8.5	1.300	.141
8.7	1.400	.143
9.0	1.700	.197
9.5	1.730	.315
10.0	1.750	.300
11.0	1.620	.182
13.0	1.470	.142

upper and lower size limits were varied. Some results are given in Table 10, and a variation of the coefficient with particle size is shown in Fig. 3. For the present study we used a lower limit for r = 2 μm and an upper limit of 200 μm. From Fig. 3 we note that the important region for this wavelength band is r ≤ 10 μm. Hence, a good representation of the particle distribution is significant.* For shorter wavelengths the important region shifts inversely with wavelength since the particle size parameter, x, is defined by $x = r/\lambda$ and $x \leq 5$ is the significant range.

In the above discussion we did not examine an effect of the explosion; that is, the possible dehydration of some ejected mass (particularly the

*Although this statement is self-evident, we make this apparent from the analytical expression for the extinction coefficient,

$$\sigma_e\ (cm^{-1}) = \iint N(r_i)\pi r_i^2 Q_e(m, x_i, \lambda)\, dr\, d\lambda$$

$$= \frac{3}{4}\iint \frac{C_{ce}}{\rho_p r_i} \cdot Q_e(m, x_i, \lambda)\, dr\, d\lambda$$

where Q_e = efficiency factor extinction, C_{ce} = cloud concentration, and ρ_p = particle density.

TABLE 10

SPECTRAL EXTINCTION COEFFICIENT

λ (μm)	α (m^2/g)
8.2	.059
8.5	.089
8.7	.101
9.0	.128
9.5	.133
10.0	.140
11.0	.142
13.0	.138

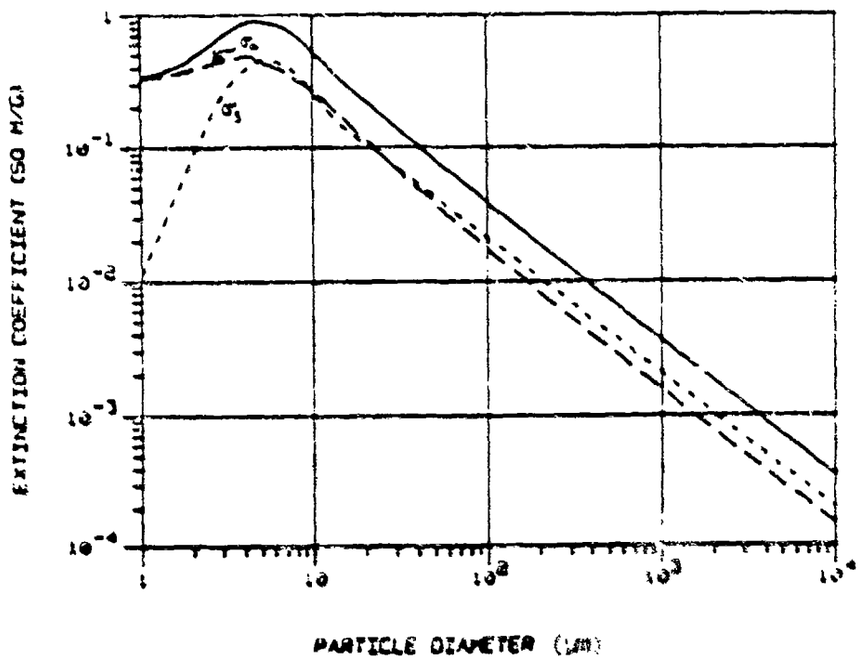

Figure 3. Extinction Coefficient as a Function of Particle Diameter (wavelength = 9.5 μm; refractive index: 1.730, 0.315)

minerals) since the fireball will be ≥600° K for 1 sec detonation. Also soil moisture is ~20% of the total mass ejected. The moisture should appear either in liquid or vapor phase.* A possibility is that the moisture recondenses on the particles in the dust cloud and therefore, the cloud particles are similar to the ejecta. For the present we neglect this effect; see brief dicussion in Sec. 3.8.1.

Also, there is produced about 0.2 g of carbon per gram of TNT. This aerosol should be included with the dust. A preliminary estimate of the effect would indicate that the transmission can vary by ~25%.*

Thus, we see that the optical properties are varied, and a quantitative understanding of the soil type, etc., is required to obtain a reasonable estimate of the transmittance.

2.4 EXPLOSIVE EFFECTS

The effects of explosive type can have some importance either for charge weight equivalent or possibly cratering phenomena. We follow convention and use TNT as the reference explosive in Table 11. The explosive

TABLE 11

EXPLOSIVE TYPES AND PROPERTIES

	cal/g	TNT Equivalent	Detonation Velocity (mm/μsec)
TNT	984	1.0	6.93
Comp B	1119	1.19	7.99
(RDX/TNT/WAX)	1083	1.19	--
Comp C4	1200	1.1	8.04
Explosive D	761	0.86	--

*This is not true of the Fort Sill data.

*Consider the crater efficiency of 1 ft^3/lb then the lofted material ~10 lb/lb of HE or, 50% the amount of carbon. If the mass extinction for carbon is 10^4 dust, then the contribution to attenuation is ~10%. The amount of carbon will depend upon the type of explosive used!

Comp B is also an RDX/TNT material. The ratio of RDX/TNT differs from the mixture listed directly below. With respect to cratering a lower detonation velocity explosive will be more effective. We assume the effect is linear with velocity.

Above we used the value of 984 cal/g for TNT, a quantity whose exact value is uncertain. Some investigators give a value of ~740 cal/g. Experiments performed on encased charges indicate that the effect of total shell weight should be included. The expression established experimentally is given as

$$\text{Heat Released (cal/g)} = 740\ (\text{total weight/HE weight})^{.2} \qquad (15)$$

Thus, for a 155-mm shell we would have ~1000 cal/g.

Since the high-explosive filler is not a sphere, the length/diameter ratio of the filler and initiator location should produce strong effects on cratering, etc. These effects are omitted at this time; however, they should be examined in an upgraded model. The reader is referred to Ref. 5.

To account for ambient conditions, i.e., pressure altitudes, we propose the use of the Sach's scaling law. Hence, the effective W of explosive is

$$W_{eff} = W\left(\frac{P_{\text{sea level}}}{P_{\text{altitude}}}\right) \qquad (16)$$

For later use, we include Fig. 4, which gives the significant blast parameters for an air blast in scaled form. These include pressure, arrival time of the shock wave, shock duration, and material velocity. For a surface burst the equivalent charge weight is ~2 and therefore at a given range the peak pressure will be equivalent to a range/$2^{1/3}$. For

[5] Wisotski, J., and W. H. Snyder, Characteristics of Blast Waves Obtained from Cylindrical HE Charges, Denver Research Institute, DRI1166, 1965.

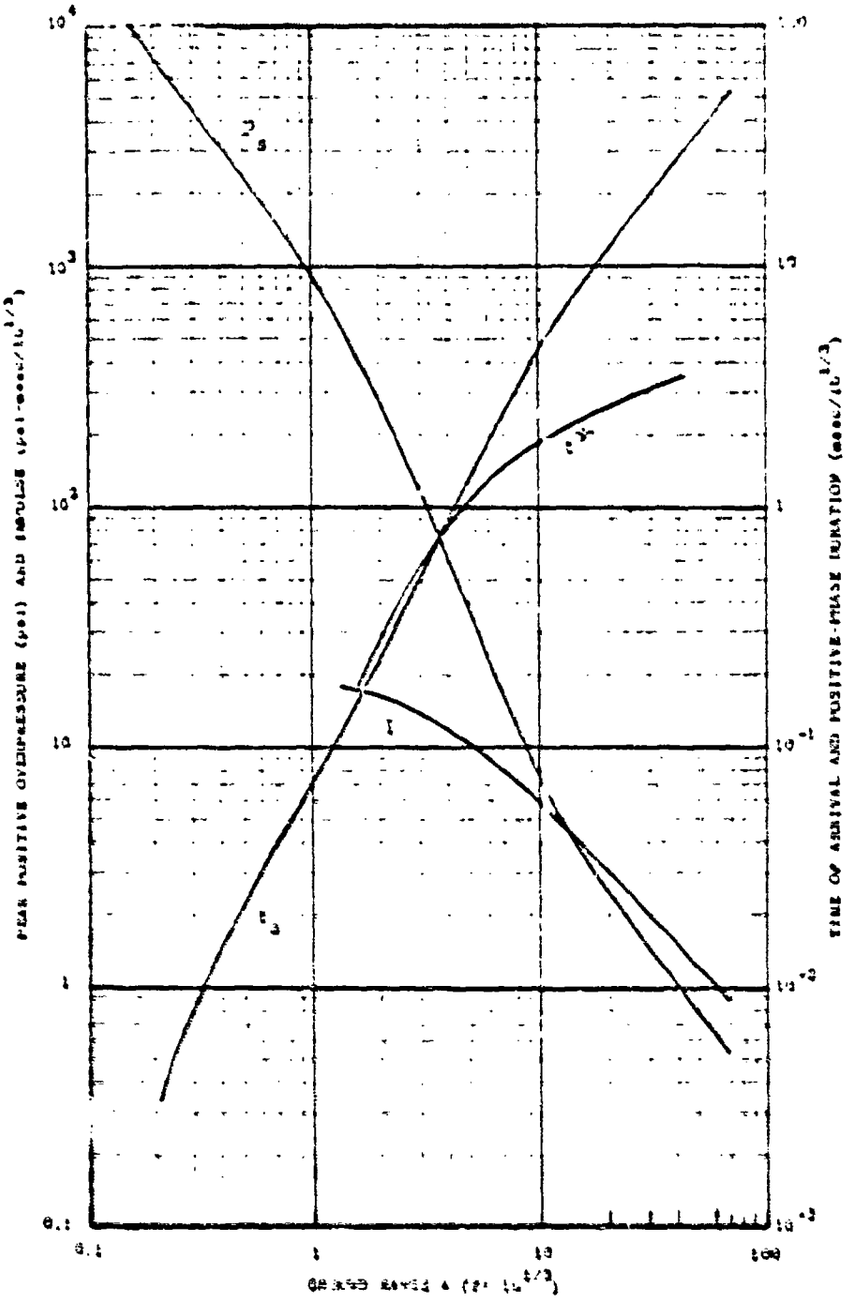

Figure 4. Significant Blast Parameters. Spherical TNT charges in free air at sea level conditions. Heat released = 740 cal/g (total weight/HE weight)**

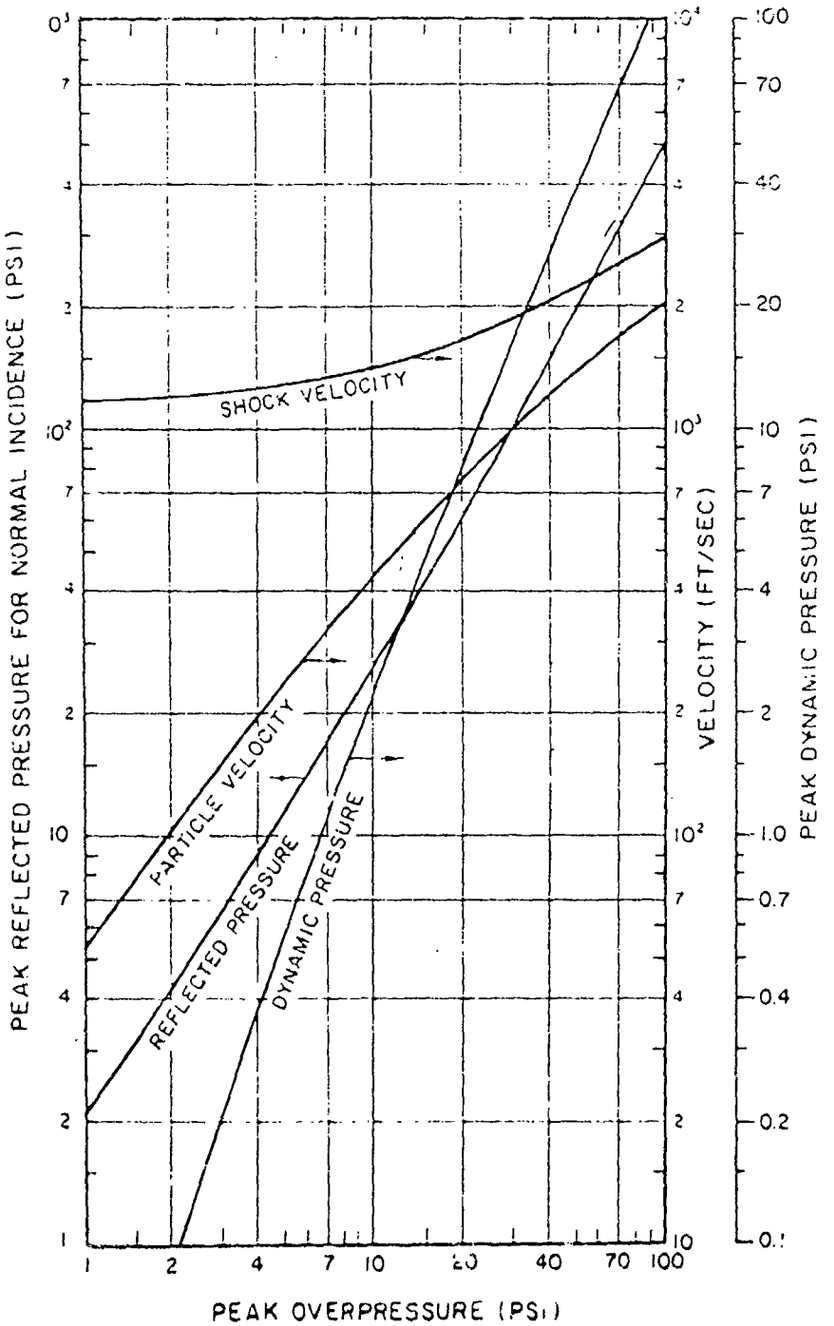

Figure 4 (Cont.). Significant Blast Parameters. Relation of ideal blast wave characteristics at the shock front to peak overpressure.

underground detonations, the equivalent free air charge weight is given by

$$W(\text{air}) = W(\text{ground}) \exp(-3\rho\lambda_d) \tag{17}$$

where ρ = soil specific gravity

λ_d = charge depth/$W^{1/3}$ (ft/lb$^{1/3}$)

The latter is valid for $\lambda_d \leq 2$, the range of interest here.

3 CLOUD DEVELOPMENT MODEL

Here we expand the model presented in Ref. 6 to include detonations occurring at various depths and heights relative to the surface, and an upgrade of the thermal effects. Although we discuss the cratering effects produced by spherical bare charges, we recognize that differences can exist with artillery shells and other munitions.

3.1 CRATERING EFFECTS

The explosive energy coupled into the ground to produce cratering is a function of burial depth. For a half buried charge, i.e., a surface burst with the charge center at surface, the coupling is about 20% and will rise to 100% when the depth (ft) = $0.6W^{1/3}$ where W is the charge weight (lb). For near-surface bursts, i.e., above ground level, the coupling drops rapidly. Hence, the fuzing effect can have a profound effect on the crater size.

Although the mechanical interaction between the coupling energy and terrain is significant, the topic is beyond the scope of this study. For our model, we will relay upon experimental data to formulate the cratering effects in different soils and conditions as a function of charge location relative to the ground surface.

We will now describe the results of several experiments performed under varying conditions for the express purpose of deriving a basis for scaling laws. Again, we note that we have adopted the established procedure of relating spatial coordinates and times to (charge weight)$^{1/3}$.

Since we are primarily interested in near-surface bursts, discussion will emphasize the range where the charge center location is ±1 charge radius above or below ground level (see Fig. 5) where ST and HB are used to denote surface tangent and half buried, respectively.

---

[6] Zirkind, R., A Preliminary Description of an Explosive Dust Cloud Model, General Research Corporation Report TM-235, 1978.

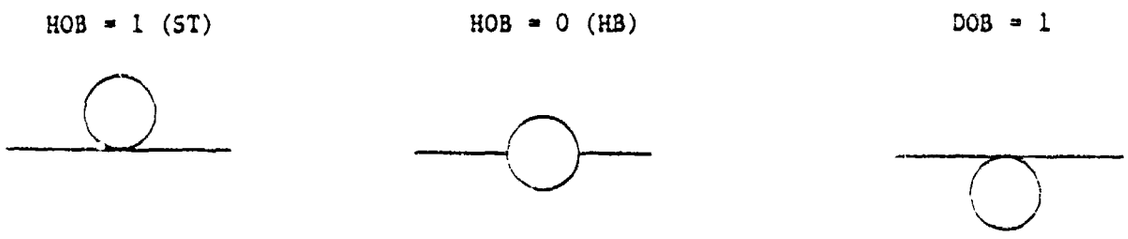

Figure 5. Definitions of Charge Placement

For clarification we note that a 1000-lb spherical TNT charge has a radius of 1.33 ft. Thus, at an HOB = 1 (geometrical height to charge radius ratio = 1) the center of the charge is located 1.33 ft above ground level. Similarly, for HOB = 2, the center of a 1000-lb charge is located 2.66 ft above the ground level. For a 1-lb charge the radius is 0.133 ft.

In each of these cases a crater will be formed whose size depends upon charge weight and soil conditions. In Fig. 6 we provide some definitions applicable to the crater where "apparent" means the created physical void. It is assumed here that the volume of the apparent crater, V_a, is initially discharged into the atmosphere and creates the primary and secondary dust clouds. The latter may be caused by stones, etc., (saltation process) but for the present is neglected. Our major interest will be on the following:

c_r or r_a = crater radius, apparent

c_d or d_a = crater depth, apparent

One should note that the lip contains some ejecta and compact soil upthrusted by the explosive force. The lip ejecta is fall-back material and is nontrivial. Let us now examine the test data and derive therefrom a suggested set of rules.

We initiate the discussion with a set of data obtained at Fort Polk, Lousiana: 1000-lb TNT spheres were detonated in or on silt stone. The

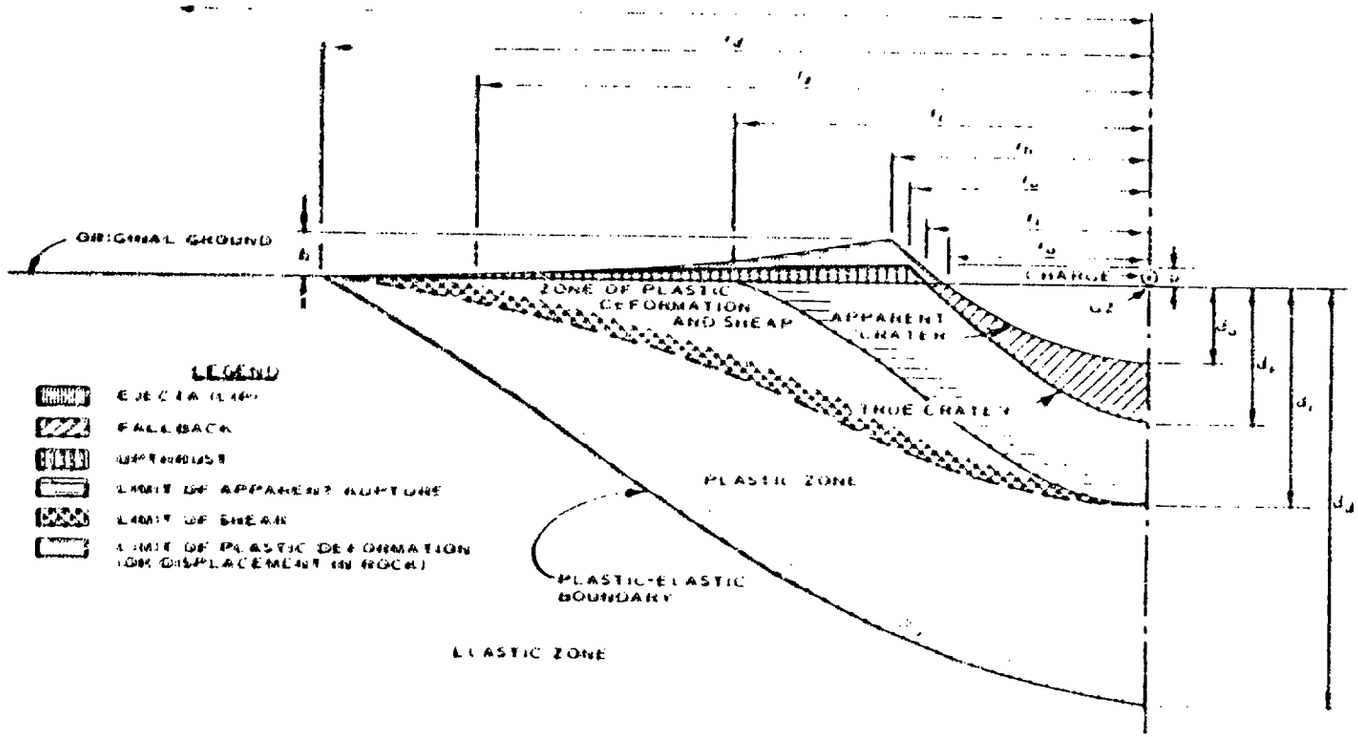

Figure 6. Typical Half-Crater Profile and Nomenclature for Near-Surface Burst

soil was wet (> 85% saturation) except for one event, #1, where the saturation was only about 50%. The pertinent results are given in Table 12.

TABLE 12
APPARENT CRATER DIMENSIONS*

Event No.	1	2	3	4	5
HOB (charge radius)	-1	0	+0.5	+1	-0.5
r_a(ft);($r_a/W^{1/3}$)	11.4 (1.14)	10.4 (1.04)	7.9 (.79)	6.9 (.69)	10.2 (1.02)
d_a(ft);($d/W^{1/3}$)	5.7 (.57)	4.3 (.43)	2.7 (.27)	3.0 (.30)	5.7 (.57)
V_a(ft^3) - parabolic	859.3	703.1	254.6	114.4	729.4
Soil density (#/ft^3)	85	112	108	120	120
Crater Efficiency (ft^3/ton)	1719	1406	509	229	1459
(ft^3/lb)	.86	.703	.255	.115	.73

*Harvey, W. T., et al., Near-Surface Cratering Experiments, Fort Polk, Louisiana, AFWL TR-74-351, November 1975.

We observe that the crater radius appears to increase with decreasing height of burst since the coupling energy into the ground increases.

In Fig. 7, we see the effect of some soil types on the crater radius and depth as a function of scaled burial depth. Clearly the two extremes, marine muck and basalt, behave as expected. Further, as the burial depth increases the crater depth increases initially and then decreases. Eventually no crater is formed. The data from Ft. Polk tests agree with the sandstone curve.

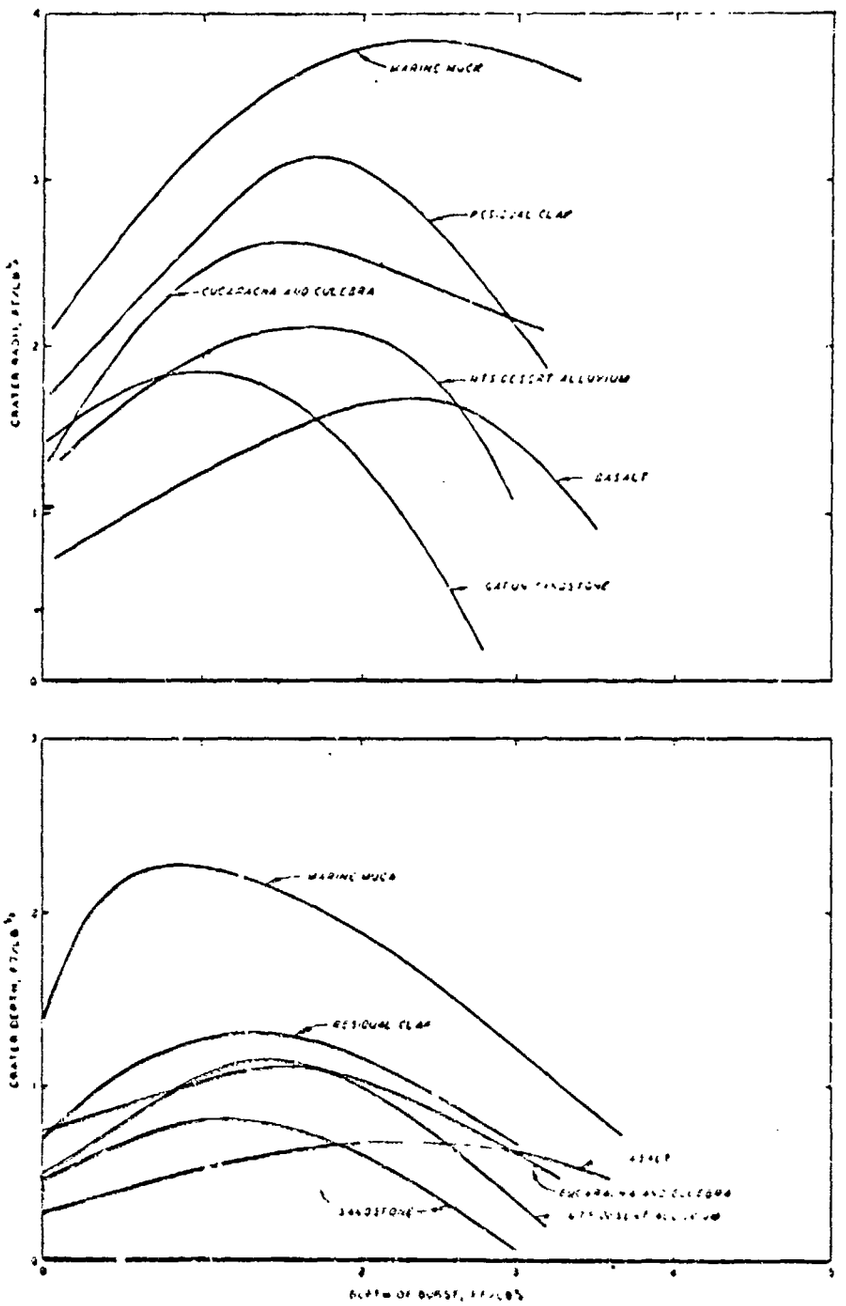

Figure 7. Crater Radii and Depth Versus Depth of Burst Relation for Various Earth Materials (Nordyke, 1961, taken from M.I.T. Final Report, No. 26, May 1970)

In Figs. 8 and 9 we present data on the cratering ability of $\geq$1000-lb and larger spherical charges in Colorado soils and different percentages of soil saturation. These were scaled-down versions of DNA tests, Middle Gusts, and Mixed Company. DRES is the Defence Research Establishment, Canada. The effects of wet and dry soil are evident. Additional specific data are given in Appendix D.

The shape factors for the various craters are shown in Fig. 10, where the crater shape is normally parabolic or ellipsoidal. For artillery shells, the elliptical crater has been suggested.

Since we are interested in cratering efficiency, we show this parameter as a function of burst height (in charge radii) in Fig. 11. Clearly, for most situations where artillery or mortars are used, the height of burst lies between 0 and 1, since the charge radii are only several inches. Since we are interested in scaling charge weights $\leq$100 lb then we should establish the range of validity for scaling. In Ref. 7, experiments were performed with 0.08 lb to 0.247 lb of HE in simulated alluvial soil. For HOB = 0, the scaled crater radius and depth are 0.69 and 0.62, respectively. This result agrees reasonably well with the data obtained with fraction to multi-ton explosive charges. Similarly, for other conditions we can assert the scaling is applicable.

In Table 13 we have estimated the parameters needed in this model for several soil types where Item 1 is the values used for the Grafenwohr tests in November 1978. The values for WSMR are limited since the moisture content is not available at this time. We caution the reader these are current values and additional data can modify them significantly.

---

[7] Seifert, K., et al., Experimental Report of Cratering Displacement and Ejecta Processes, Physics International Report DNA 4482T, August 1974.

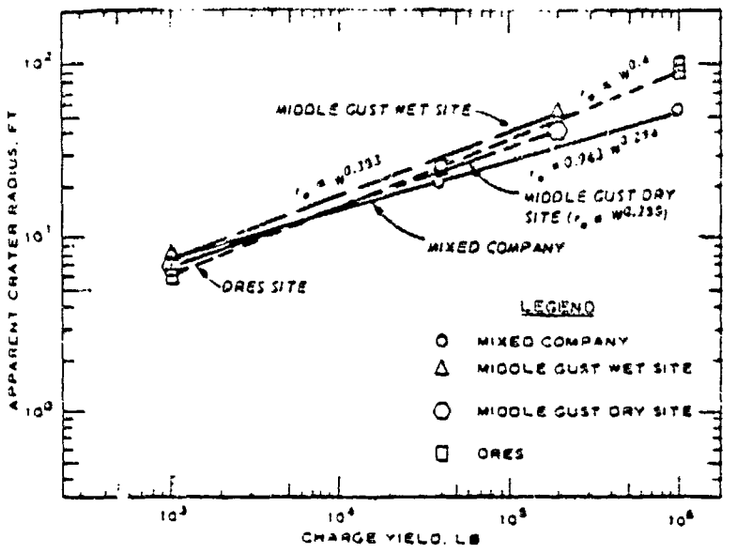

a. APPARENT CRATER RADIUS VERSUS CHARGE YIELD

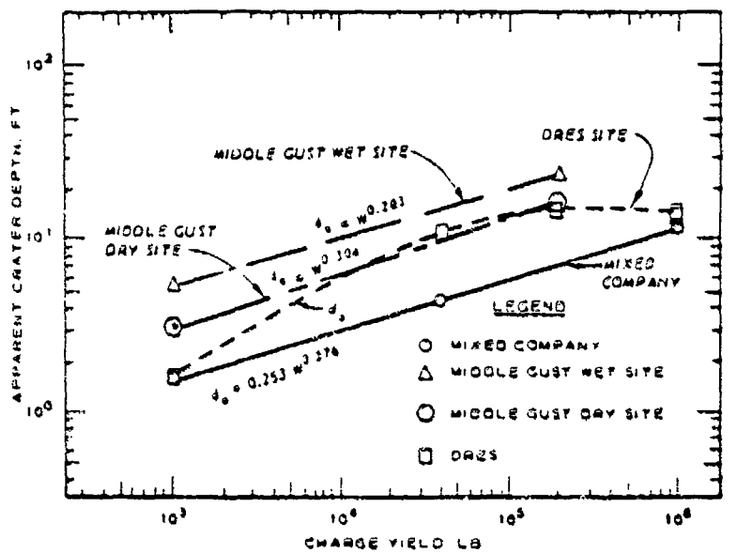

b. APPARENT CRATER AVERAGE MAXIMUM DEPTH VERSUS CHARGE YIELD

Figure 8. Apparent Crater Dimensions Versus Charge Yield for Mixed Company Scaled Overburden ST Events MC-3, MC-2, and MCC-5; Middle Gust Wet and Dry Site ST Events; and Spherical Charge ST Events Conducted at the DRES Site

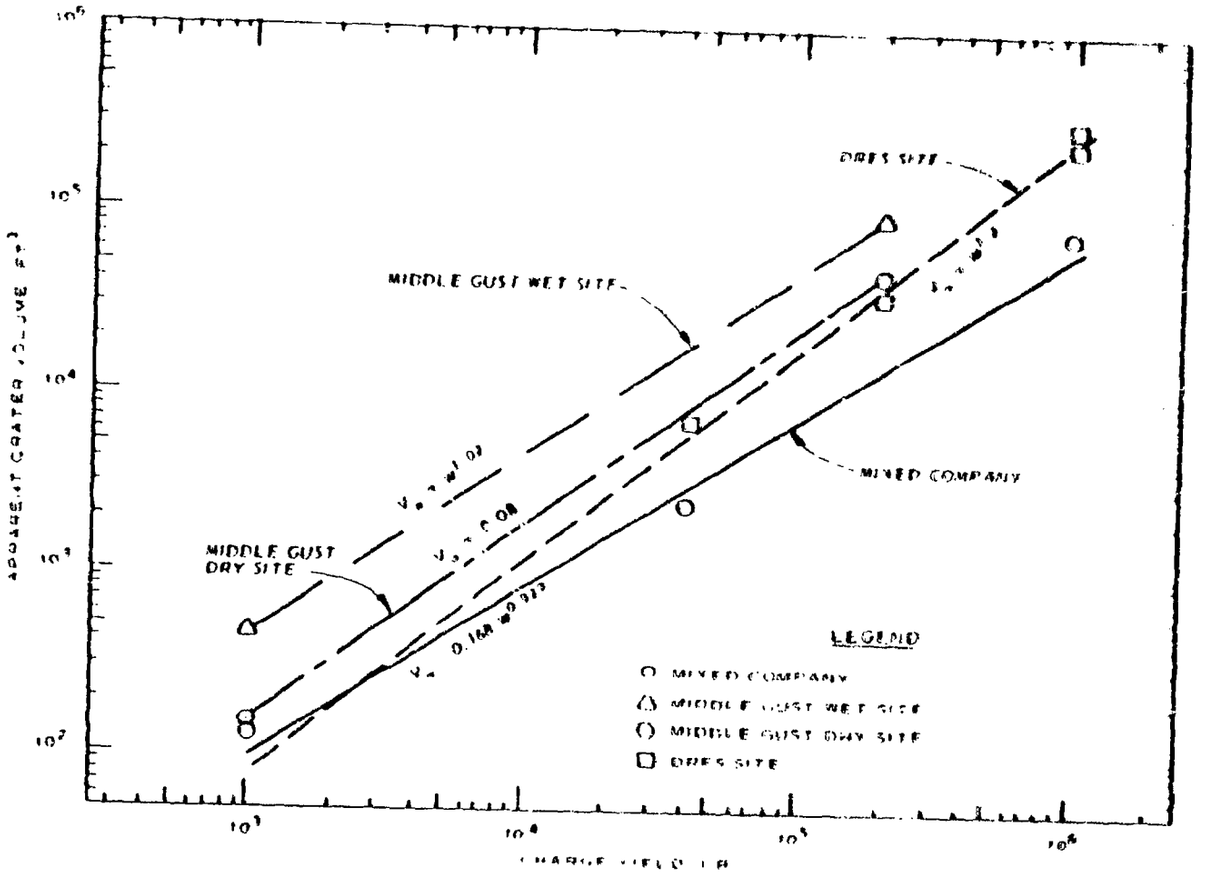

Figure 9. Apparent Crater Volume Versus Charge Yield for Mixed Company Scaled Overburden ST Events MC-3, MC-2, and MCC-5; Middle Gust Wet and Dry Site ST Events; and Spherical Charge ST Events Conducted at the DRES Site.

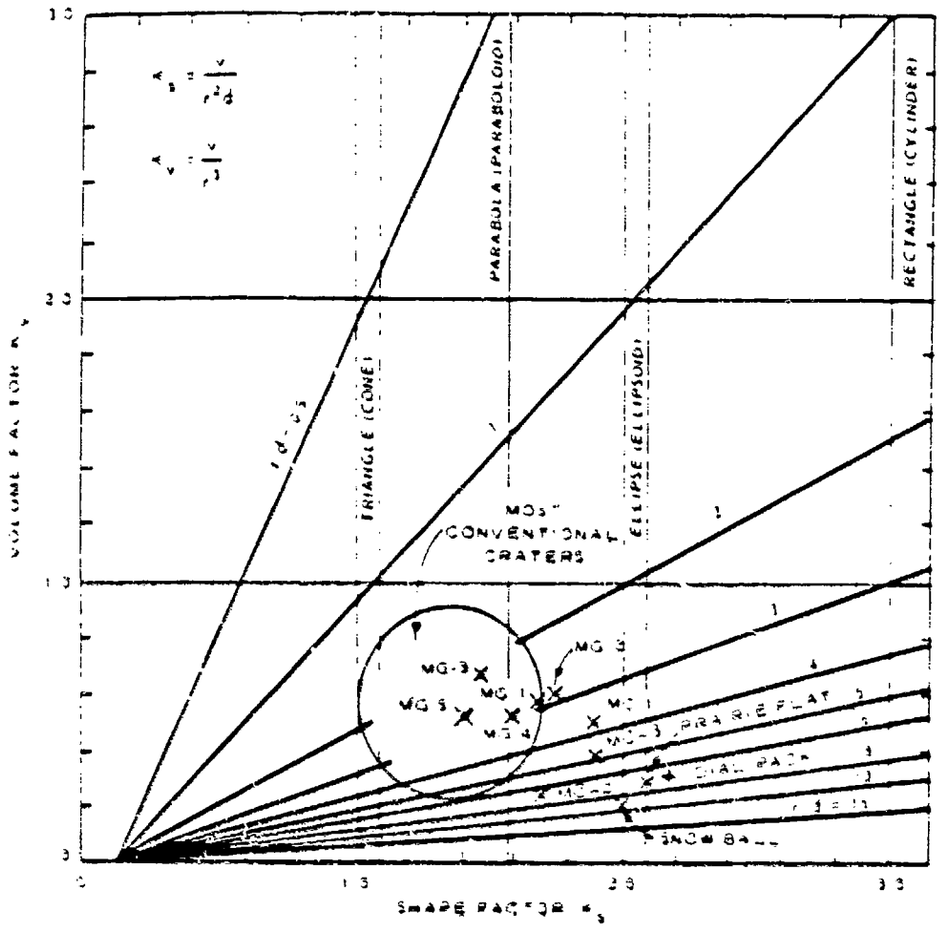

Figure 10. Crater Shape Factors for Conventionally Shaped Craters in Solid and Rock as Compared with those for Events MC-1, MC-2, and MC-3; the Middle Gust Events; and the Events Conducted at DRES. Plots are based upon apparent dimensions; maximum depths have been used for Craters in which a central mound was formed.

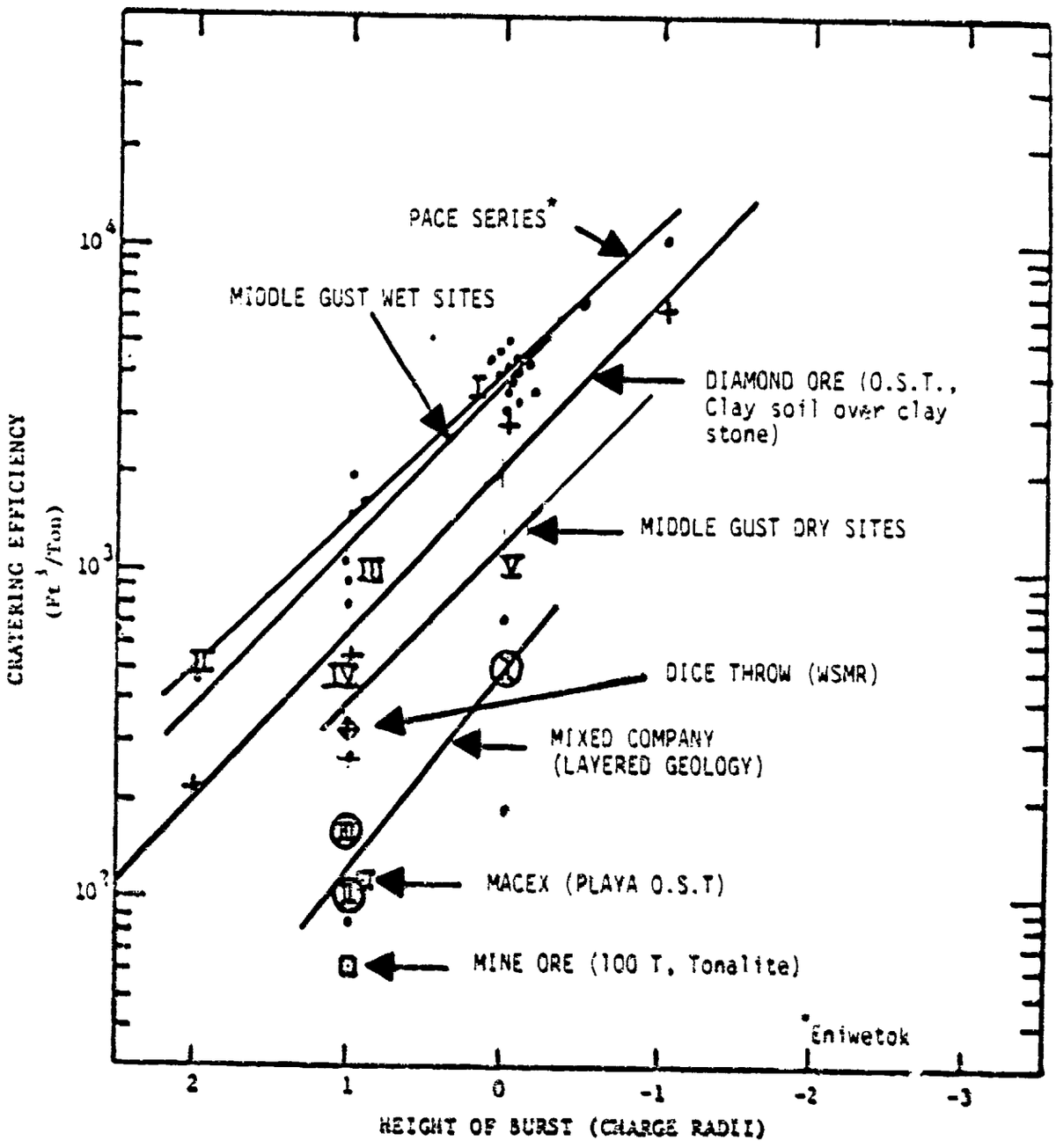

Figure 11. Cratering Efficiency as a Function of Height of Burst (Charge Radii)

TABLE 13

ESTIMATED PARAMETERS FOR SHELLS AND MORTARS

Item	Soil Type; Condition	$c_r/W^{1/3}$	$c_d/W^{1/3}$	γ (ft^3/lb)	m_Q
1	Sod & soil; wet*	$.7W^{-.03}$	$.71W^{-.04}$	.55	90%
	Sod & soil; dry	$.72W^{-.04}$	$1.0W^{-.03}$	.33	75%
2	Clay; wet	1.44	.72	2.0	90%
	Clay; dry	.5	.3	.72	75%
3	Sandy clay; wet	1.6	.56	2.5	90%
	Sandy clay; dry	.55	.32	.75	75%
4	Silt stone; wet	.04	.43	.55	90%
	Silt stone; dry	.9	.2	.32	75%
5	WSMR soil; wet	1.3	.50	1.67	90%
	WSMR soil; dry	.96	.45	.87	75%
6	Alluvial soil; moist	.71	.31	.33	50%

*Crater may be larger at the surface, we assume here an effective crater.

-155-mm live shell.

3.2 THERMAL EFFECTS

3.2.1 General Discussion

The detonation of a high-explosive charge generates a high-temperature environment including shock-heated air. The environment is a high-temperature, low-pressure bubble (fireball) which expands and rises. It is responsible for the later stages of the dust cloud behavior and the radiant power history. Here we will discuss the temperature sources and the emitted thermal radiation and attempt to estimate the late, low temperature, characteristics of the cloud that are important to thermal electro-optical systems.

First let us consider the shock wave effects on the ambient air that occur at times $\leq 10W^{1/3}$ msec. Several significant variables are given in Table 14.

TABLE 14

SPATIAL DISTRIBUTION OF SHOCK-HEATED AIR FOR ATMOSPHERIC DETONATION

Reduced Radial Distance ($ft/W^{1/3}$)	Peak Shock Overpressure (psi)	Peak Shock Temperature (°C)	Residual Temperature (°C)
3.93	250	911	245
4.31	100	399	101
5.52	50	225	53
6.38	30	153	37
7.59	20	114	30
10.0	10	74	26

The shock-heated air will be engulfed by the dust cloud at later times. As will be shown later, the cloud radius is $\sim 5.5W^{1/3}$ at $t = 0.1W^{1/3}$ sec and $> 10W^{1/3}$ (ft) at $t \sim 0.35W^{1/3}$ sec. Since we are concerned about longer time periods ($\sim 4W^{1/3}$ sec), the fireball effect or heated cloud is of greater significance.

The luminous cloud has a definitive thermal pulse--a first peak,* second peak, and a later third peak resulting from the rising TNT debris afterburning. We can write for the peaks the following scaling laws:

$$t_1 = 12W^{1/3} \text{ (μsec)}$$

$$t_2 = 150W^{1/3} \text{ (μsec)}$$

$$t_3 = 2.5W^{1/3} \text{ (msec)}$$

The radiated power (for an HOB = 1) normalized to t_2 is shown in Fig. 12, and the integrated value in Fig. 13. Although the latter implies that the normal radiation is ~10% of the blast yield, the probable value is closer to 30% since the sensors measure primarily visible and near-infrared radiation.[8]

Let us now consider surface heating. For a 1000-lb charge the fireball radius, at 10 msec, is ~3.6 m. For a 500-ton charge we observe a value of ~39 m at 100 msec. Thus the $W^{1/3}$ scaling agrees with the observed results. These times correspond approximately to times of their respective second peak. Hence, if scaling holds, we have a 1-lb charge, a sphere (fireball) whose radius is 0.36 m. At this time scale ~10% of the total energy is radiated.

For a 155-mm shell, W = 7 kg, the fireball radius is 0.88 m at 2.26 msec. Hence, the energy radiated is

*It should be noted that it takes about 6 μsec for the detonation wave to reach the surface of a 1-lb spherical charge.

[8]See discussion in F. B. Porzel, Introduction to a Unified Theory of Explosions, NOL TR-72-209, September 1972.

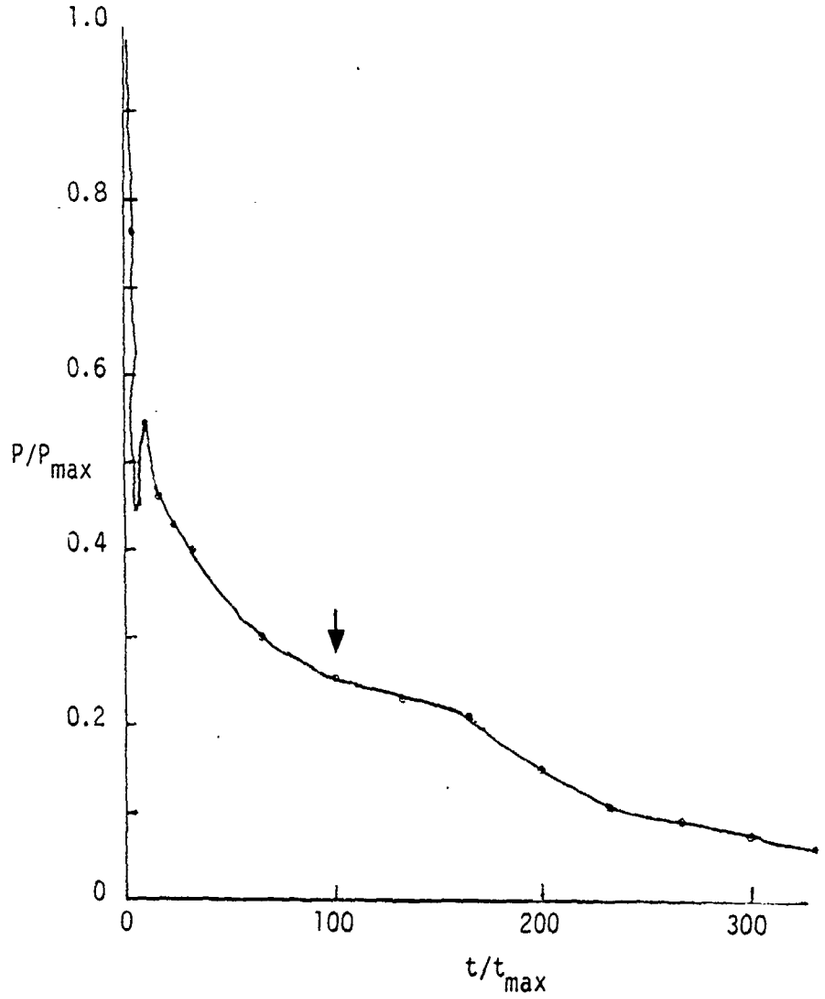

Figure 12. Normalized Radiated Power History

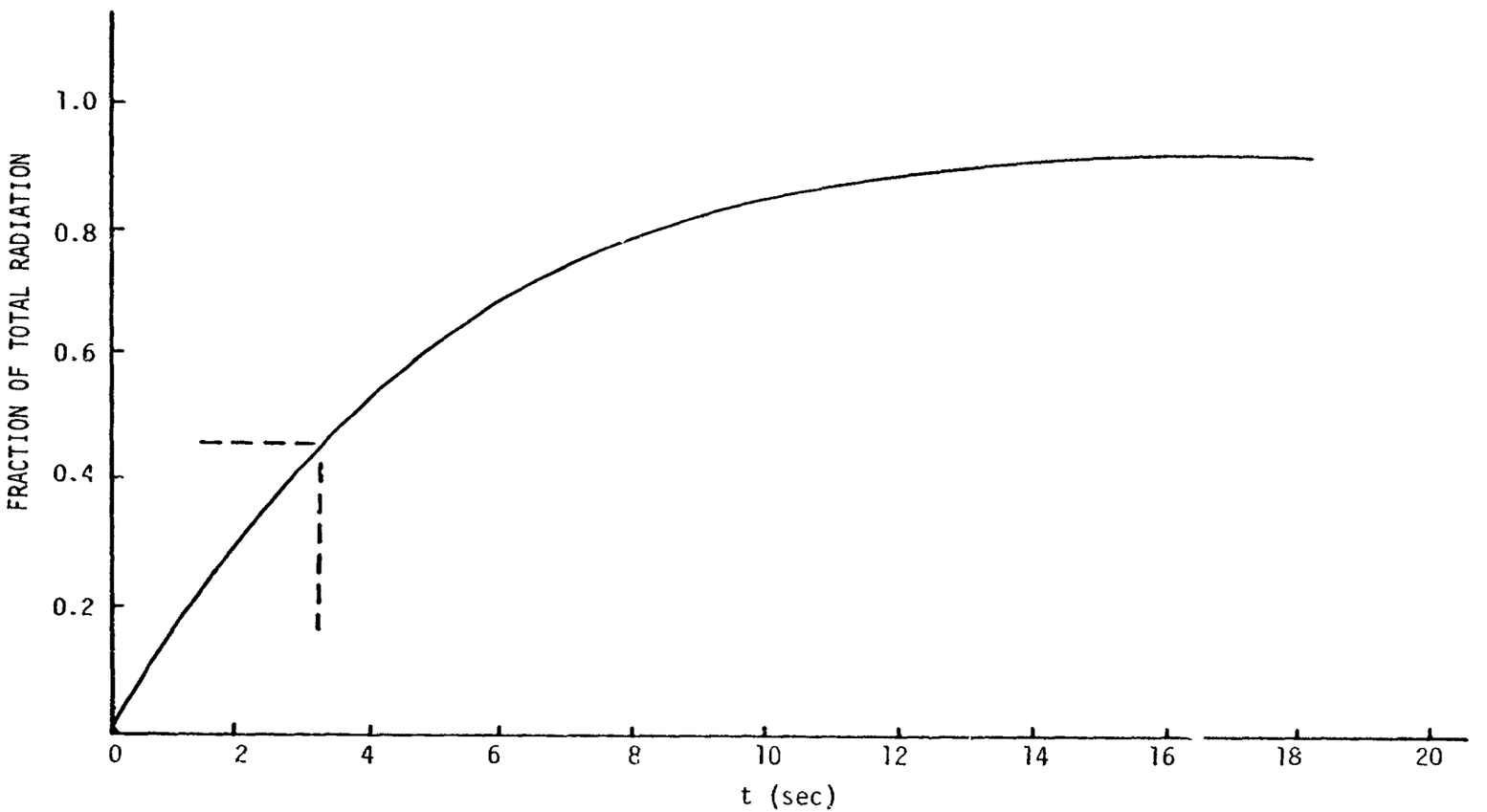

Figure 13. Thermal Yield as a Function of Time

$$Q = (0.1)(0.1)W \times 10^6 \text{ cal/kg} \tag{18}$$

$$= 7 \times 10^4 \text{ cal}$$

where the thermal power is 10% of the explosive yield. The ground irradiance is therefore

$$H = \frac{Q}{\pi r^2} \text{ cal/cm}^2 = \frac{7 \times 10^4}{4\pi(88)^2} \tag{19}$$

Consider this input to 1 cm^2 of surface of thickness, t; then the temperature rise is

$$0.72 \text{ cal/cm}^2 = \rho c_p \Delta T \tag{20}$$

where ρ = soil density

c_p = specific heat

or, for t = 1 cm

$$\Delta T = 0.72/(2.6)(0.22) = 1.26°C \tag{21}$$

Since the irradiation occurs at shorter times and radii, the increase may be $\lesssim 3°C$ which under most conditions is unimportant.

Thus we suggest that the surface heating for explosive events of interest to this study (artillery/mortar munitions) is unimportant in calculating the overall cloud thermal effects. There is semi-quantitative evidence that the crater is warm. Long-term observations (42 min) after a multi-ton event showed that in the near field, i.e., 2× crater radius, the surface temperature was characteristic of the subsurface ambient temperature and then dropped to the normal ambient surface temperatures at 5× crater radius. This implies that background temperatures can be disturbed by the explosion for long periods, and furthermore, may depend upon the season of the year.

The work done by the explosive on the soil and the hot cloud fallout into the crater can contribute to the warm crater temperature.

3.2.2 Cloud Temperature

Above, we have shown that the ground heating and shocked heated air is not significant since the fireball heating of the dust cloud, which includes the latter, is the dominant mechanism. The temperature history is important for two reasons: (1) residual heat to generate a buoyant cloud; and (2) target obscuration.

Quantitative measurements of thermal radiation produced by high-explosive detonations are limited and these, until recently, to relatively large events. In Fig. 14 we present the power-time results from a 500-ton event in the spectral bands $\lambda \leq 2.5$ μm and $\lambda \leq 4.5$ μm. The effect at ~4 sec is due to either afterburning or uncovering of low temperature debris.* Correspondingly, the mean temperature of cloud vs. time is shown in Fig. 15. The extrapolation to lower temperatures is a complex problem; however, this has been done analytically (see Fig. 16) and can be used for other charge weights by using the scaling factor $(W/15.6)^{1/3}$.

The cooling of the hot → warm dust cloud is given by a relationship of the form

$$\Delta T \propto \Delta T_0 \exp\left[-(3h/\rho c_p r)t\right] \tag{22}$$

where h = thermal transfer coefficient (cal/cm^2 sec °C)

ρ = particle density, g/cc

c_p = particle specific heat, cal/g °C

r = particle radius, cm

*We note here that even at t = 30 sec, there is an amount of thermal radiation emitted at wavelengths of interest to some thermal systems.

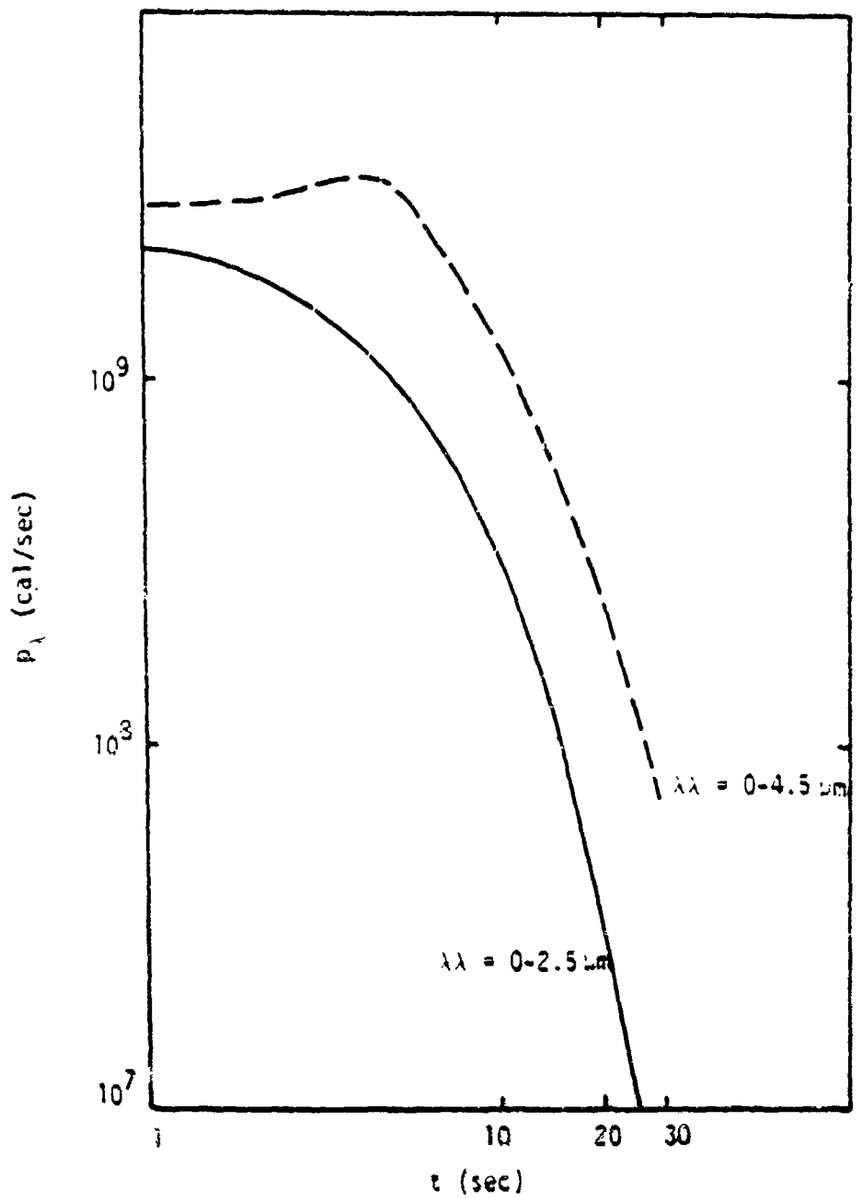

Figure 14. Spectral Power vs. Time for Two Bands (500 Tons HE)

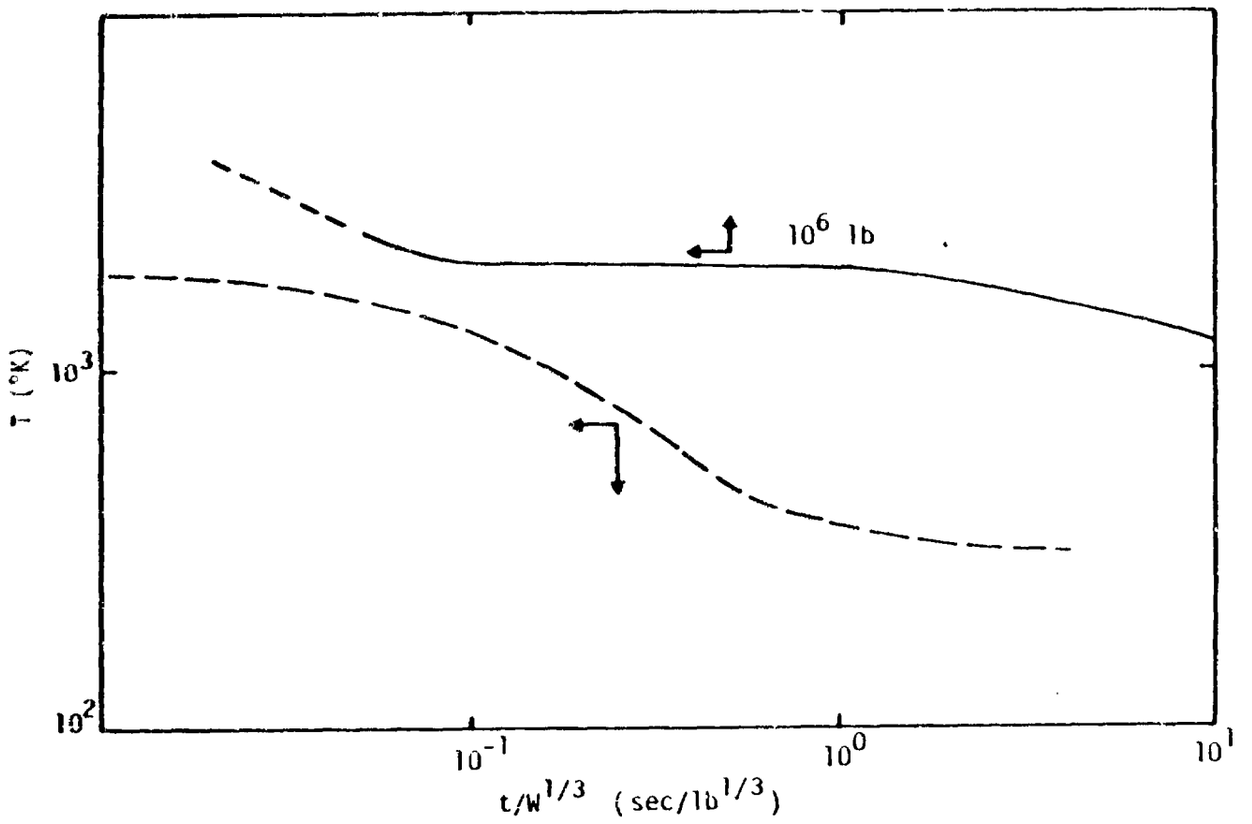

Figure 15. Mean Cloud Temperature Vs. Scaled Time

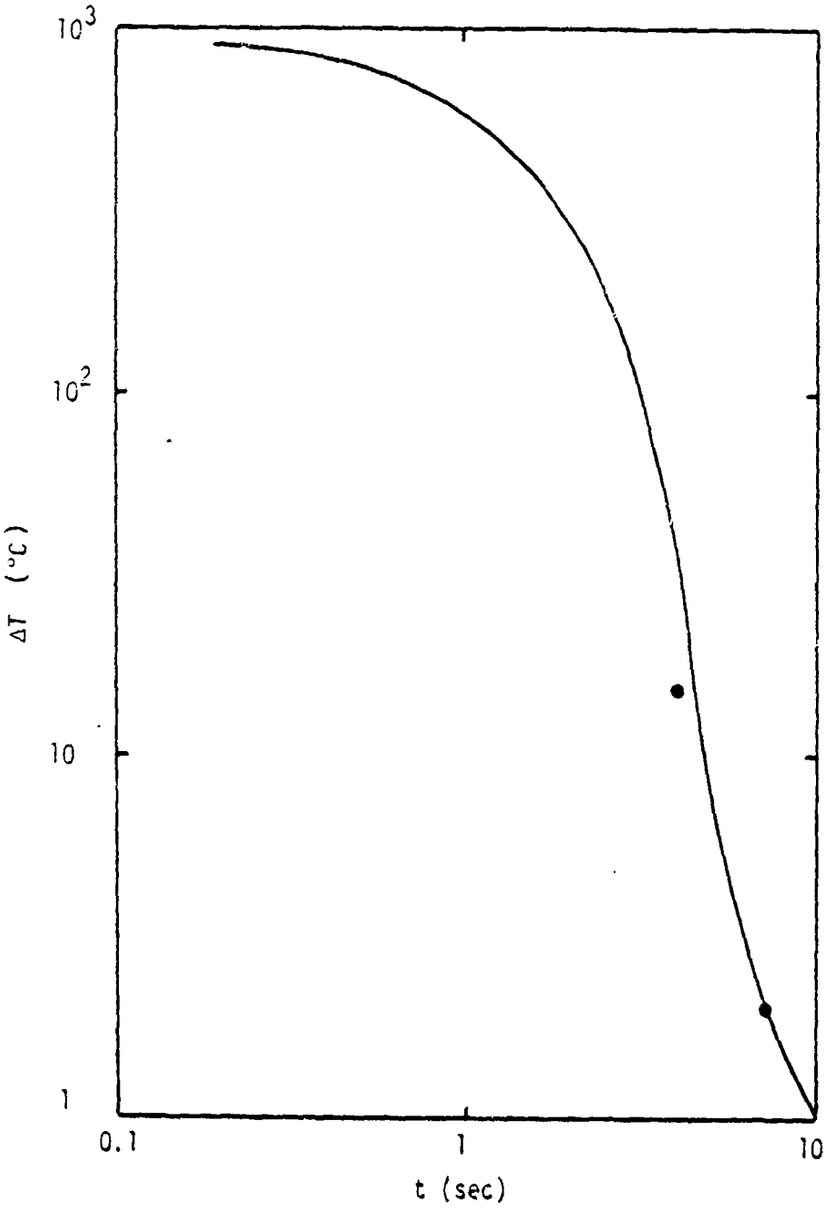

Figure 16. Cloud Temperature Differential vs. Time for 155 mm Shell, Background Temperature = 1°C

The exponent is $\sim(3 \times 1.356 \times 10^4/(2.6)r = 6.51/r$, where r is in micrometers, and therefore, the $(\Delta T_{10}/\Delta T_1)$ for $\bar{r} \simeq 10$ μm is $\sim 0.521/1.49 \times 10^{-4} \simeq 1/350$ and 1/671 for $\Delta T_{(11)}/\Delta T_1$. These values do not disagree with observed values for the 155-mm event, and the curve scaled from large TNT charges; see Fig. 16. For $\bar{r}$ different than 10 μm, the times may be faster or slower if less or greater than 10 μm, respectively.

For buoyant plume calculations we assume that 300 cal/g of TNT is the appropriate quantity and the duration is $t\ (\text{sec}) \simeq 4.1W^{1/3}$. This quantity does not scale precisely since for larger events the cloud penetrates to greater altitudes, i.e., to lower temperatures, giving greater buoyancy. For example, a 100-ton event was reported to stabilize at an altitude of ~8000 ft after 300-480 sec, whereas the above expression would suggest ~240 sec.

Alternatively we can use Fig. 16 in the following fashion: if the mean cloud temperature > ΔT of the ambient air temperature corresponding to cloud Δz (temperature at cloud top minus temperature at cloud base), it is buoyant.

Although the above is directly applicable to an explosion on the surface, extension to near-surface bursts will introduce smaller errors than other uncertainties. For example in the HOB = -1 case, the high-temperature bubble will be non-spherical due to the initial venting process. Also the crater will be hotter than for HOB = +1.

For events like Fort Sill, i.e., small particles, the cooling should be faster.

3.3 CLOUD DISPERSAL

In Ref. 6 the generation of the dust cloud and dispersion of this cloud are described in detail for the case of HOB = 1. The results are given in Sec. 3.4; that is, for the lofted crater mass.

3.4 INITIAL CLOUD VOLUME

The second stage is defined when an initial volume is lofted into the atmosphere, forming a parabolic dust cloud. This stage occurs within a scaled time, $t \leq 0.1W^{1/3}$. Hence, the volume is

$$V_{c\ell}(t) = \frac{\pi}{8} D_{c\ell}^{2}(t) \cdot H_{c\ell}(t) \tag{23}$$

where $D_{c\ell}$, $H_{c\ell}$ are specified in Fig. 17.

For example, at $t = 0.1W^{1/3}$, $D/W^{1/3} = 10.8$ ft/(lb)$^{1/3}$ and $H/W^{1/3} = 6.6$ ft/(lb)$^{1/3}$; therefore

$$V_{c\ell}(0.1W^{1/3}) = 320W \tag{24}$$

Hence, for an explosive charge of weight W = 15 lb for wet terrain, the concentration C is $\sim 3.5 \times 10^{3}$ g/m^{3}.*

3.5 GROWTH OF MAIN CLOUD AND STEM

For the time period $0.1W^{1/3} \leq t \leq 0.3W^{1/3}$, we treat the growth of the stem and the main cloud separately.

The stem diameter is considered to be ≈ 2 crater diameters. We consider, for computational reasons, that the stem is a cylinder.

The main cloud is also defined as a cylinder whose volume is given by the expression

$$V_{c\ell}(t) = \frac{\pi}{4} D_{c\ell}^{2}(t) \cdot T(t) \tag{25}$$

where T(t) is the cloud thickness; see Fig. 17. The stem value is defined as

*Note ft/(lb)^{3} = 1.6×10^{-6} g/m^{3}.

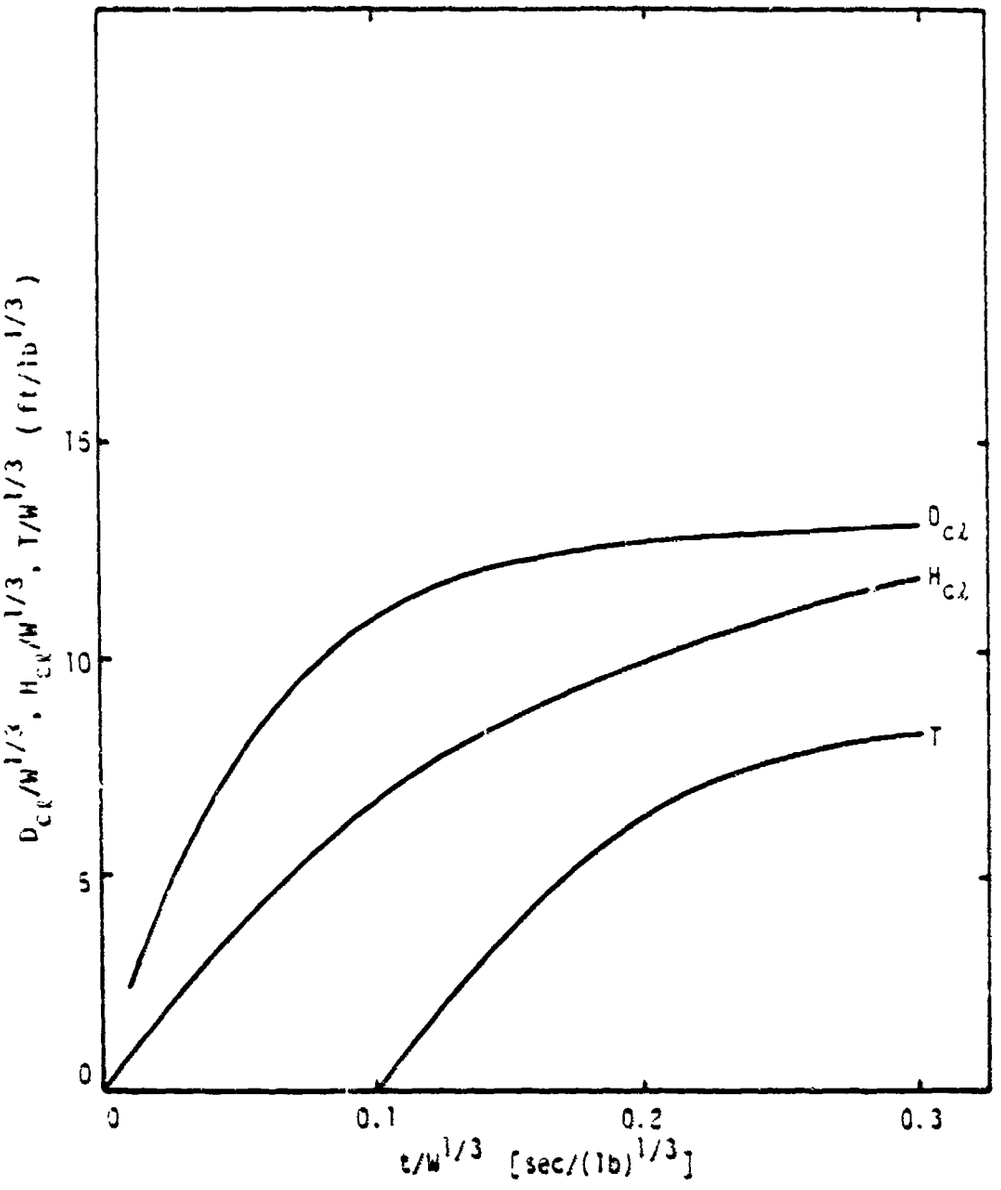

Figure 17. Main Cloud Parameters Vs. Time

$$V_s(t) = 4\tau C_r^2 \cdot H_s(t) \tag{26}$$

where $H_s(t)$ is the stem height and given in Fig. 18. The overall cloud height is $H_s(t) + T(t)$.

At this time we assume that the cloud has stabilized at a height defined by W only; that is, we include the effect of lapse rate as part of the plume.

The buoyant plume in still air is a special case, see discussion in Part 1. On the basis of limited data and analysis one may estimate that the height of the cloud is given by the value

$$H = 3.7F^{1/4} \quad (m) \tag{27}$$

where $F = 3.6 \times 10^{-5}$ Q (cal/sec) and $Q = (10^3$ cal/gm TNT) $\cdot$ 454W $\div$ $0.3W^{1/3}$ or $Q = (1.5 \times 10^6$ cal)$W^{2/3}$, where W is in pounds.

3.6 CLOUD DISPERSION

For times greater than $t = 0.3W^{1/3}$ we assume the dust cloud is dispersed like a low-order thermal, stationary source.[9]

For the present we limit the discussion for dust cloud dimensions at or near stabilization when HOB = 0 and -1. These are listed in Table 15. Like the dispersion of the HOB = 1 case, the dust clouds for HOB = 0 and -1 are dispersed by the methodology described in Part 1. This includes the thermal effect described in Sec. 3.2, namely 300 cal/g of TNT is available for a time $t = 4.1W^{1/3}$ sec.

Again we assume to a first approximation the mass concentration is uniform. In the next subsection we consider qualitatively the subject of non-uniform distribution.

---

[9] Zirkind, R., An Obscuring Aerosol Dispersion Model, General Research Corporation Report CR-231, December 1978.

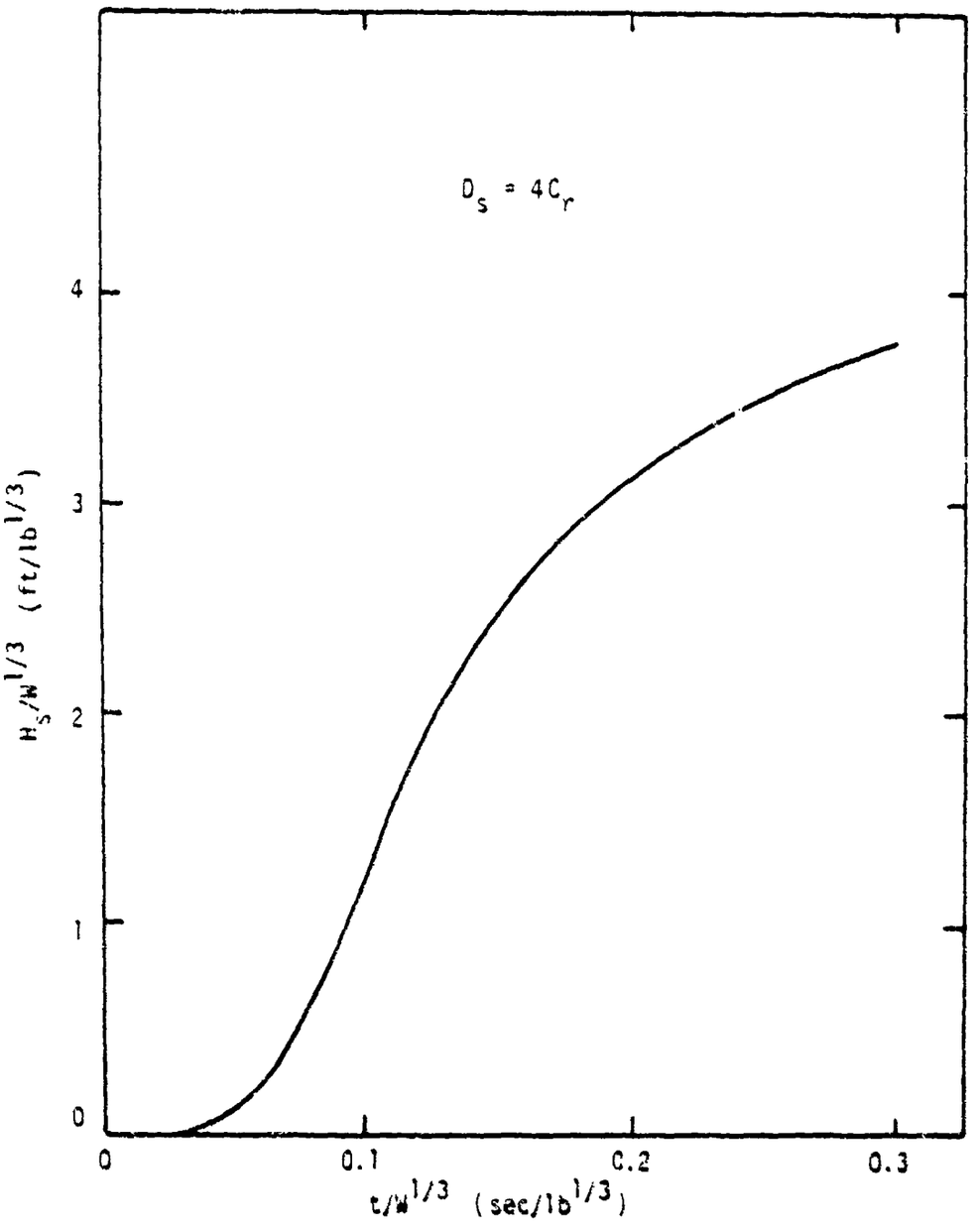

Figure 18. Stem Height vs. Time

TABLE 15

CLOUD DIMENSIONS FOR HOB = 0, -1

	HOB = 0	HOB = -1
Cloud Height ($ft/W^{1/3}$)	7	6.2
Cloud Diameter ($ft/W^{1/3}$)	6.84	5.5
Stem Diameter ($ft/W^{1/3}$)	1.14	1.0
Stem Height ($ft/W^{1/3}$)	2.28	2.0

3.7 MASS DISTRIBUTION

One of the uncertainties in explosive-related phenomena is the spatial-temporal history of the lofted dust. Although the early history is responsible for the flow field internal to the dust cloud and the dust distribution, our interest is in the later stages. Experimental data are limited particularly for artillery/mortar munitions; however, the general behavior is reasonably understood. It should be noted that the data from large HE detonations are not directly applicable in view of the heights reached, thousands of feet above ground level, to which the dust cloud rises--the vertical atmospheric wind and temperature structure are different. Nevertheless, the creation of a cloud stem and a rising vortex in the main cloud are also characteristic of near-surface explosions.

Observations for large detonations after the initial rise indicate that the horizontal distribution in the cloud has a form shown below; that

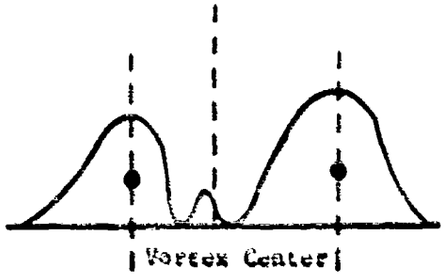

is, the primary mass is located in the vicinity of the vortex center, and a relatively small amount of dust is concentrated around the axis. The stem distribution will have a form similar to the one shown below: the stem extremities (x) are increased

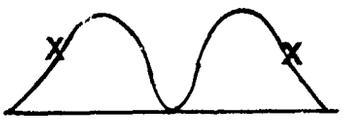

due to limited quantities of upswept ground dust. The vertical distribution is a result of the vertical motion and the sedimentation.

3.8 MASS CONCENTRATION

The swept-up dust is part of the stem and increases the outer radius somewhat.

From the above sampling results the vortex center appears to exist equidistant from the axis, and we may assume the vertical location is the center of the cloud. In time, turbulence will vertically mix the particulates in the cloud. On the other hand, sedimentation (fallout) plays an important role in altering the mass and size distribution in the cloud and stem; that is, the larger particles settle out by inertial forces. This is illustrated in Fig. 19 for a 100-ton event, HOB = 1. The mass values given are for a horizontal column of unit area at that altitude and time.

On the basis of the above, for charge weights of battlefield munitions, we consider that for normal wet soil about 90% of the soil ejected will settle early and therefore, 10% will constitute the dust cloud and stem. In fact most particles in excess of 100 μm will fall out in the first 10 sec. On the other hand, if the soil in the dust cloud is made of small particles, as exemplified by Fort Sill, the large fraction of the ejected mass may remain aloft.

If there is a need to establish a non-uniform concentration then for the main cloud, above the stem height plus 3 m, we suggest the vertical

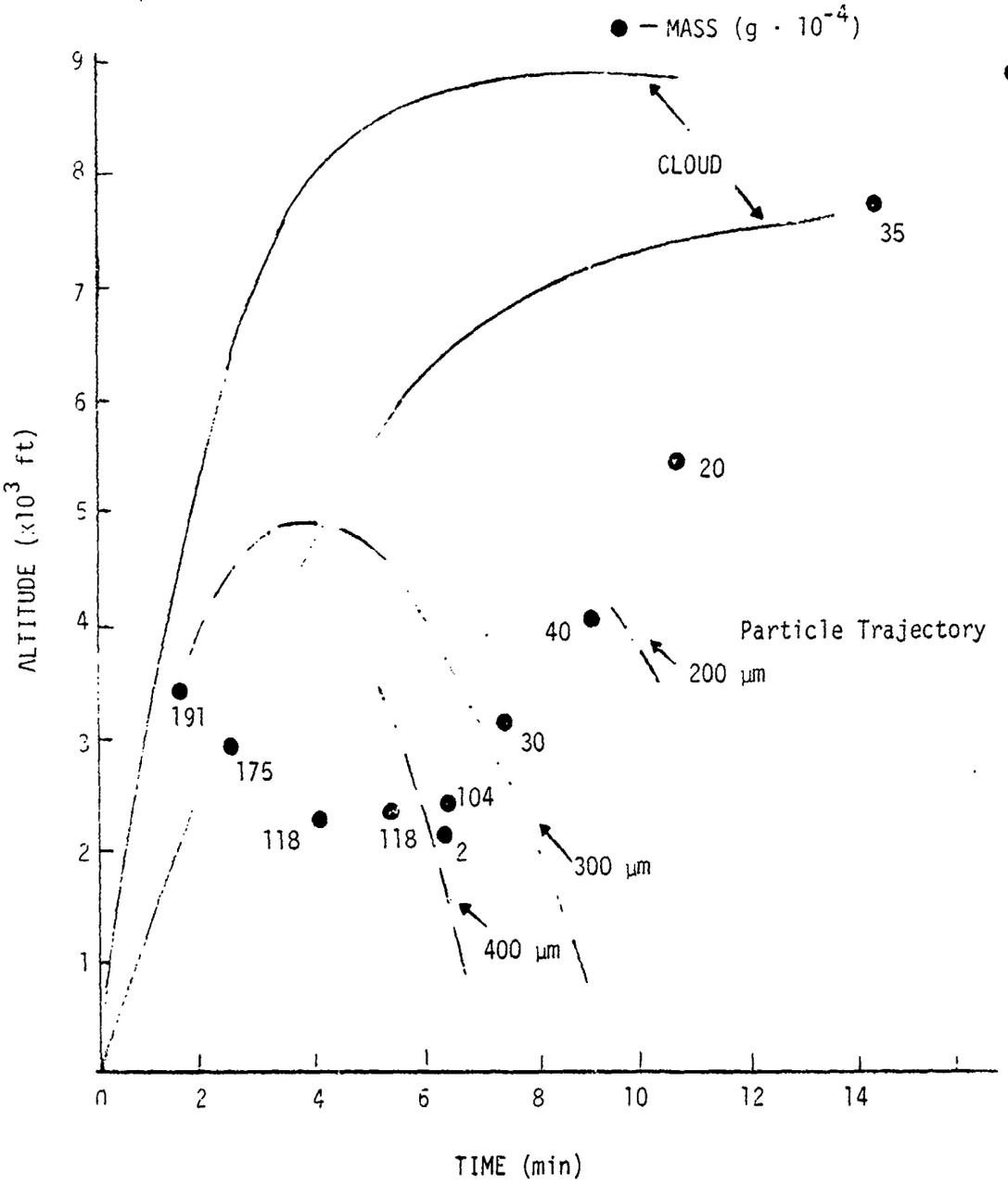

Figure 19. Cloud History for Middle Gust III; (100 T), HOB = 1

mass distribution is of Gaussian form with the halfwidth about the cloud toroid center equal to toroid thickness/2. Similarly, for the horizontal distribution, we may assume the shape as shown above with the same halfwidth as the vertical distribution. Since turbulent vertical and horizontal mixing will exist, uniform concentration occurs after a time ~20-30 sec.

For the model presented here we assume uniform concentration in the cloud and stem; however, the mass differences will yield different concentrations for both.

Since the height of the clouds attain values of 30-40 m, we disperse the cloud in the following manner: (1) stem, (2) top layer, and (3) cloud center. Obviously the cloud height is established from the top-layer behavior, the overall width from the stem and cloud widths. The dispersion algorithms require the mean wind speeds at the respective heights. Thus we use an average $\bar{u}$ for the stem at ~2 m. To find the values at the different altitudes we can suggest the following:

$$\text{Stem:} \quad \bar{u}(z) = \frac{V_x}{0.4} \ln (z/z_0) \tag{28}$$

where V_x = frictional velocity = $(1/2)C_d\bar{u}_1^2$ $(C_d \sim 4 \times 10^{-2})$

z_0 = surface roughness; see Table 8, Part 1

$\bar{u}$ = mean speed at 0.5 m

For heights >4 m, employ the power law:

$$\bar{u} = \bar{u}_1(z/z_1)^p \tag{29}$$

where z_1 is 4 m and $\bar{u}_1$ is the mean speed at 4 m. The values for p are the following: neutral - 0.142; unstable - 0.1; stability G - 0.8. Values of 0.3 and 0.5 are suggested for stability classes E and F.

Although a surface surge is associated with the shock wave, we will neglect this effect for several reasons:

1. The height of the surge cloud can be expressed as

$$H\ (ft) = 2 \cdot \Delta P \cdot t\ (sec)$$

and, since we are interested in $\Delta Ps \sim 0.1$ psi and $t \sim .003$ sec, $H\ (ft) = 2.(0.1)(0.003) \simeq 0$. Further, the shock strength would be too weak to raise significant dust from the compacted soil.

2. The material velocity of the air behind the shock wave is only ~ 1.7 m/sec.

3. The effect of the asymmetric jets should be more important on the near-surface obscuration.

Hence any dust raised by the surface surge will for modeling purposes be considered as an integral part of the initial cloud.

3.8.1 Settling Speed

The particulate material within the cloud will settle out provided the vertical downward velocity exceeds the upward wind speed where the latter is approximately one-fifth the mean horizontal wind speed.

Consider a spherical particle to be acted on by gravity. The force is then defined by

$$F = \frac{4\pi r^3}{3} g(\rho_p - \rho_a) \tag{30}$$

where r = particle radius, cm

$g = 981\ cm/sec^2$

ρ_p = particle density, g/cc

ρ_a = air density, g/cc

For particles at constant velocity we can apply Stokes Law to define the resistance force; i.e.,

$$R = 6\pi\eta \cdot r \cdot v \tag{31}$$

where η = coefficient of viscosity (1.8×10^{-4} g/cm sec)

v = particle velocity

At this point we need to examine the character of Stokes Law. The drag can be defined by the expression

$$R = (1/2)\rho_a v^2 C_D A \tag{32}$$

where C_D = drag coefficient

A = particle area

or, for the Stokes case,

$$C_D = 24/Re \tag{33}$$

where Re is Reynolds number = $\rho vD/\eta$. One may show when Re > 1 that the Stokes value for C_D underestimates the drag, and a more appropriate expression is

$$C_D = 0.06 + \frac{36}{Re} \tag{34}$$

To find the settling speed for Stokes particles, neglecting ρ_a, we have $F - R = 0$ or,

$$v = \frac{2}{9}\frac{g}{\eta}\rho_p r^2 \tag{35}$$

Substituting the values for g, η and $\rho_p r^2$, we have for a 2 g/cc particle,

$$v = 2.5 \times 10^6 r^2 \tag{36}$$

Hence, for a 10-μm particle, v = 2.5 cm/sec. For a 100-μm particle, v = 2.4 m/sec. Experiments have shown that the terminal velocities for 100-μm,

1000-μm, and 1-cm particles are 0.5 m/sec, 6 m/sec, and 22 m/sec, respectively.* For our use here we assume Stokes Law for $r \leq 50$ μm ($v \lesssim 0.5$ m/sec) and the experimental values for $r > 50$ μm. If this is the situation, then in 10 sec all particles with $r \gtrsim 50$ μm at heights ≤ 5 m will settle out.

Alvarez[11] examined the effect of relative humidity on precipitation of ambient hygroscopic particles.† His data indicate that, if the relative humidity > 74%, the suspended particles approach precipitation weight and by 91% the particles are heavy enough to precipitate. This situation may be exascerbated in a dust cloud. Again, there is little data on the relative humidity within the dust cloud; however, the local value must be elevated above ambient conditions.

---

*The general equation of motion is defined as

$$\ddot{y} = -g - (18\mu/\rho D^2)\dot{y}$$

$$\ddot{x} = -(18\mu/\rho D^2)\dot{x}$$

from which we obtain

$$x = x_0 + \frac{\bar{u}}{a}(1 - e^{-at})$$

$$y = y_0 - \frac{gt}{a} + (V_0/a + g/a^2)(1 - e^{-at})$$

where $\bar{u}_2$ = mean horizontal speed, V_0 = initial vertical velocity, and $a = 18\,\mu/\rho D^2 = 18\,\eta/D^2$.

[11] Alvarez, R., "A Study in the Changes on the Quantity of Aerosol Particles in the Ambient Medium as a Result of Fluctuations in the Relative Humidity of the Air," Izv, Atmospheric & Oceanic Physics, Vol. 13, No. 12, 1977. p. 911.

†It should be noted that this effect on hygroscopic smokes has not been examined and may affect the yield of phosphorus-derived smoke clouds. Also ambient particles are ≤ 10 μm, whereas dust particles are primarily > 10 μm.

4 VALIDATION TESTS

As in Part 1, we present here several tests of the dust model discussed earlier. Unfortunately, the many tests performed to data have limitations; that is, the data are unavailable (Grafenwohr 1979, DIRT-1); the data are not complete (Grafenwohr 1978 and others); for live firings the exact detonation location relative to the samplers are unknown. Further, few tests of single or multi-individual rounds are available for analysis. If the test consists of several adjacent rounds, ≤ 25 m*, then interactive affects occur that are difficult to model accurately. Notwithstanding the above, we will present several cases.

Test 1 - Grafenwohr - November 1978: NV & EO LAB

Input Conditions:

$\bar{u}$	- 3.35 m/sec
Pasquill Category	- C
Ground level	- 960 mb
Munition	- One 155-mm shell artillery delivered

The data provided were limited to semi-quantitative cloud geometry and the transmission to the 8-12 μm spectral region.

In Fig. 20 we show that the cloud height is accurately predicted when the buoyancy (heat added) is taken into account. In Fig. 21, we present the calculated concentration and transmission and the measured transmission. Although the practical implication between the two transmissions are small, the measured value is 2× the calculated. There are several possible explanations: (1) the extinction coefficient is too large; (2) the concentration is too high; or (3) both. The underlying reason is that the transmissometer is near the cloud base and consequently, the particle sizes may be different (larger) than in the other parts of the cloud, and the parts of the line of sight are not filled with dust.

*Half distance.

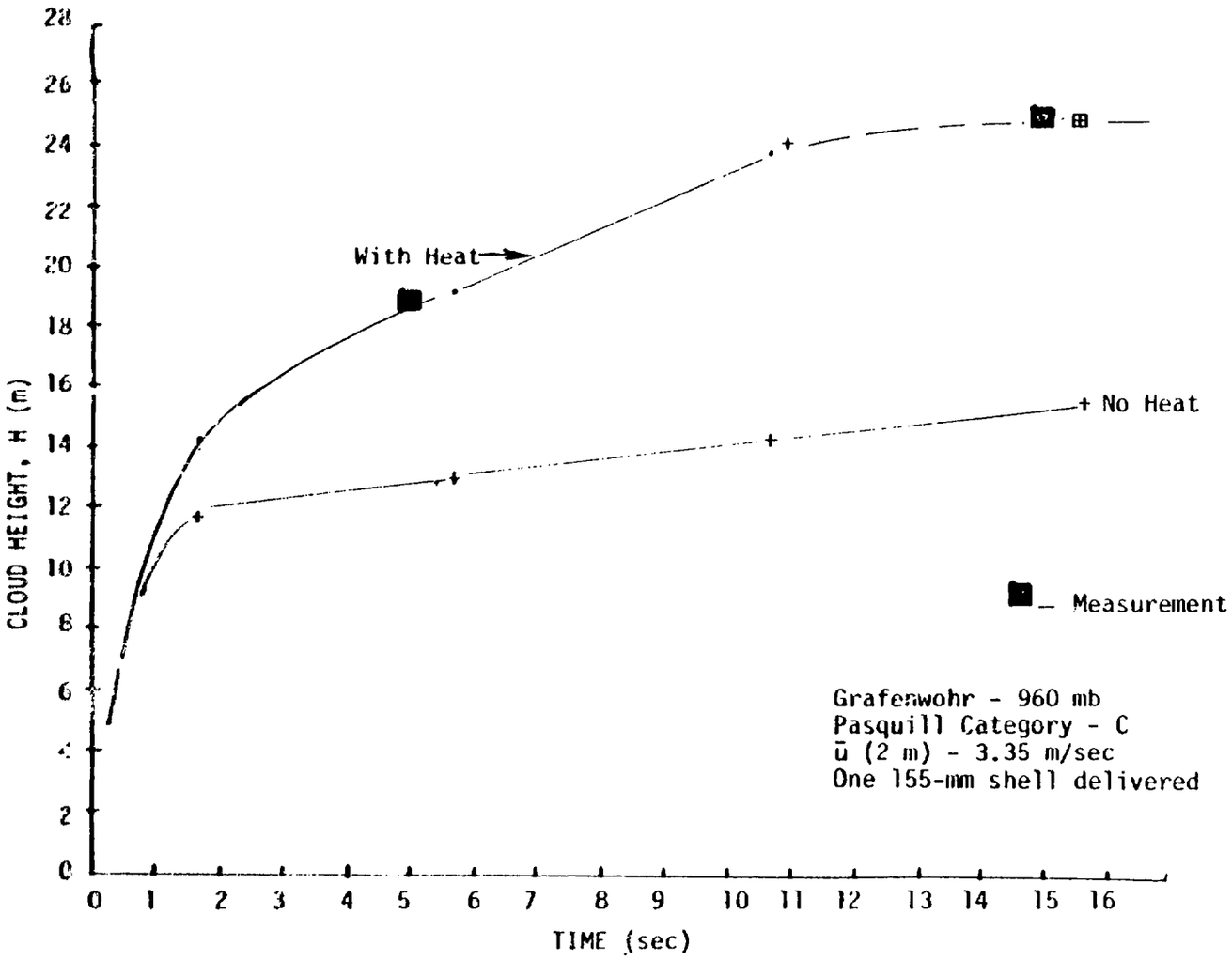

Figure 20. Cloud Height as a Function of Time

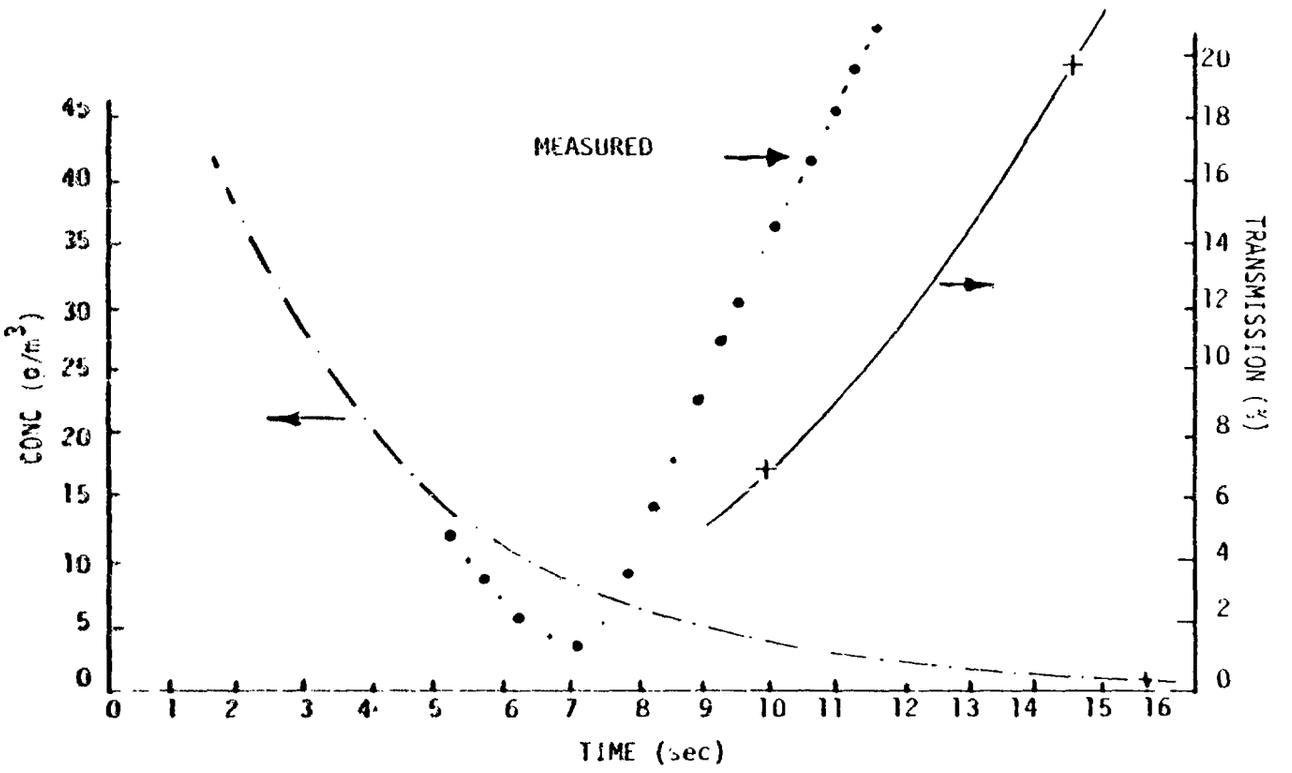

Figure 21. Concentration, Transmission vs. Time for one 155-mm Shell

Test 2 - Grafenwohr - November 1978

Input Data:

$\bar{u}$	- 2.5 m/sec
Pasquill Category	- C
Visibility	- 2 km (high humidity)
Ground temperature	- 1°C
Munitions	- Two 155-mm artillery shells delivered; detonations 25 m apart

Results

Apparently the two events occurred simultaneously, and therefore, the shock interacts at ~12.5 m at 97 msec. A Mach shock will form at an altitude of ~5 m and then propagate in both directions. The wave will reach the ejecting mass at 125 msec at a velocity of ~40 m/sec. The wave will interact with the dust cloud for 0.02 sec in the direction of air flow. Vectorial considerations yield an average displacement of 1.7 m due to the wind; i.e., the average ejecta velocity is ~40 m/sec at 45° to the vertical. The horizontal displacement ≥ 2 m and ≤ 5 m, and the cloud diameter is increased ~3.4 m. The effect on cloud height is small, ≤ 1 m.

The calculated initial cloud dimensions are as follows:

t (sec)	D (m)	H (m)
0.061	3.72	1.49
0.122	5.58	2.79
0.742	13.2	10.0

Subsequent dimensions are determined by conventional expressions for Pasquill Category C.

In Fig. 22 the cloud height, as measured by a silicon TV and 8-12 μm FLIR, is presented as a function of time. The calculated values are presented as well as the settling location for particles ≥100 μm. The decrease of the height at infrared wavelengths is due to the cooling of the dust cloud.

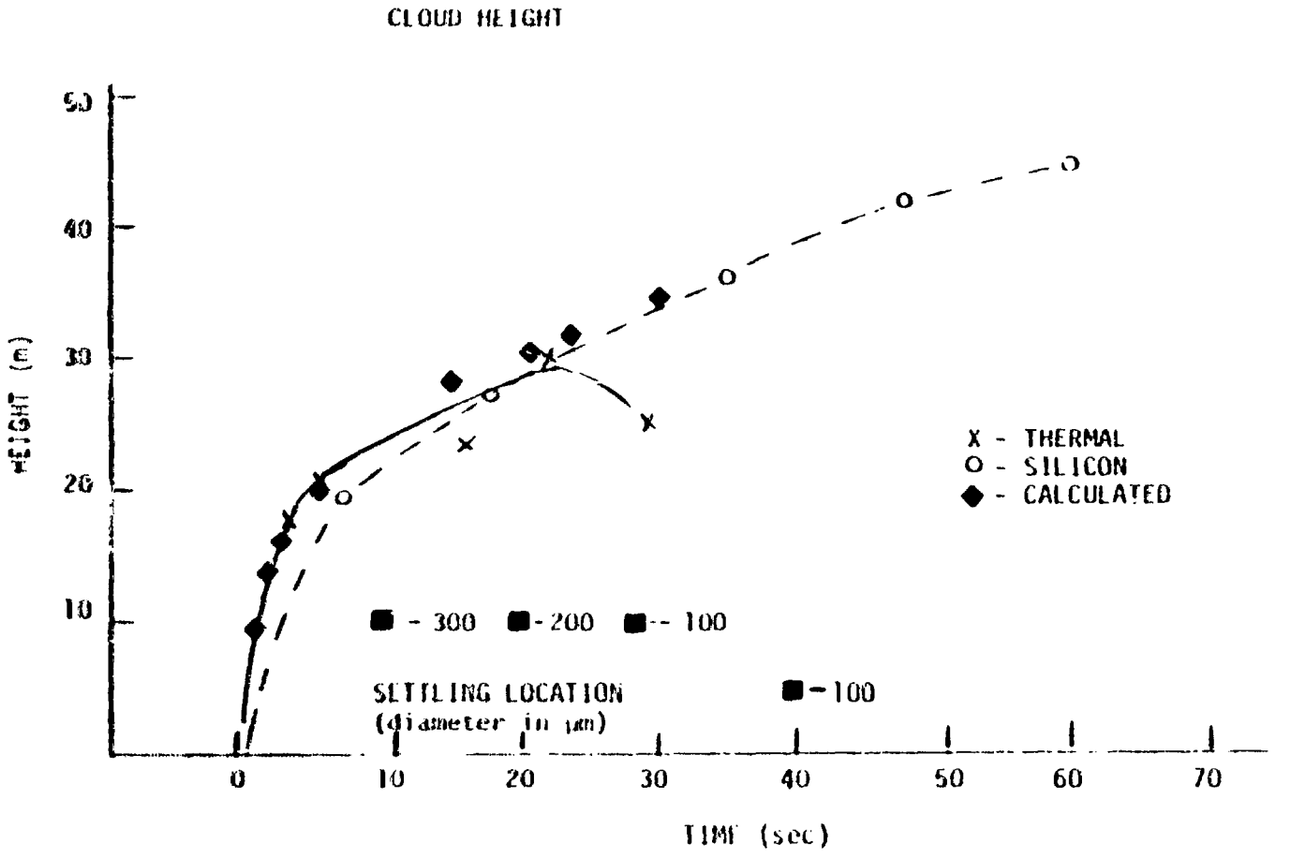

Figure 22. Cloud Height History in Silicon and 8-12 μm Region

The cloud width comparative results are shown in Fig. 23. These and the above show good agreement. One must recognize that the measured results are subject to some error.

Finally, the calculated and measured transmissions through the cloud are presented in Fig. 24. The thermal transmission agrees reasonably well; however, the silicon region appears to have a lower extinction coefficient than theoretically estimated.

Test 3 - SWII - Trial 29

The input data are given in Fig. 25, where the second row was detonated 5 sec after row A. The distance of S, C, and N transmissometers were 40, 90, 140 m from row A, respectively.

The calculated and measured C · L for the three transmissometers are shown in Fig. 26. It should be noted that the shock interaction has been taken into account; i.e., intra and inter row.

The agreement between the two C · L curves is excellent.

Test 4 - Ft. Sill, DPI-005-T3

In Fig. 27, we present the initial conditions, the measured C · L (solid) and the calculated results. If the arrival time is displaced several seconds then the agreement is improved. The methodology used here is as described in the text.

Test 5 - Ft. Sill, DPI-005-T19

The available input conditions are given below:

$\bar{u}$	- 6 m/sec
Relative Humidity	- 87%
Time	- 1141
Sky	- Overcast
Pasquill Category	- (Estimated) D
Munition	- 1, M-1, 105-mm artillery shell delivered

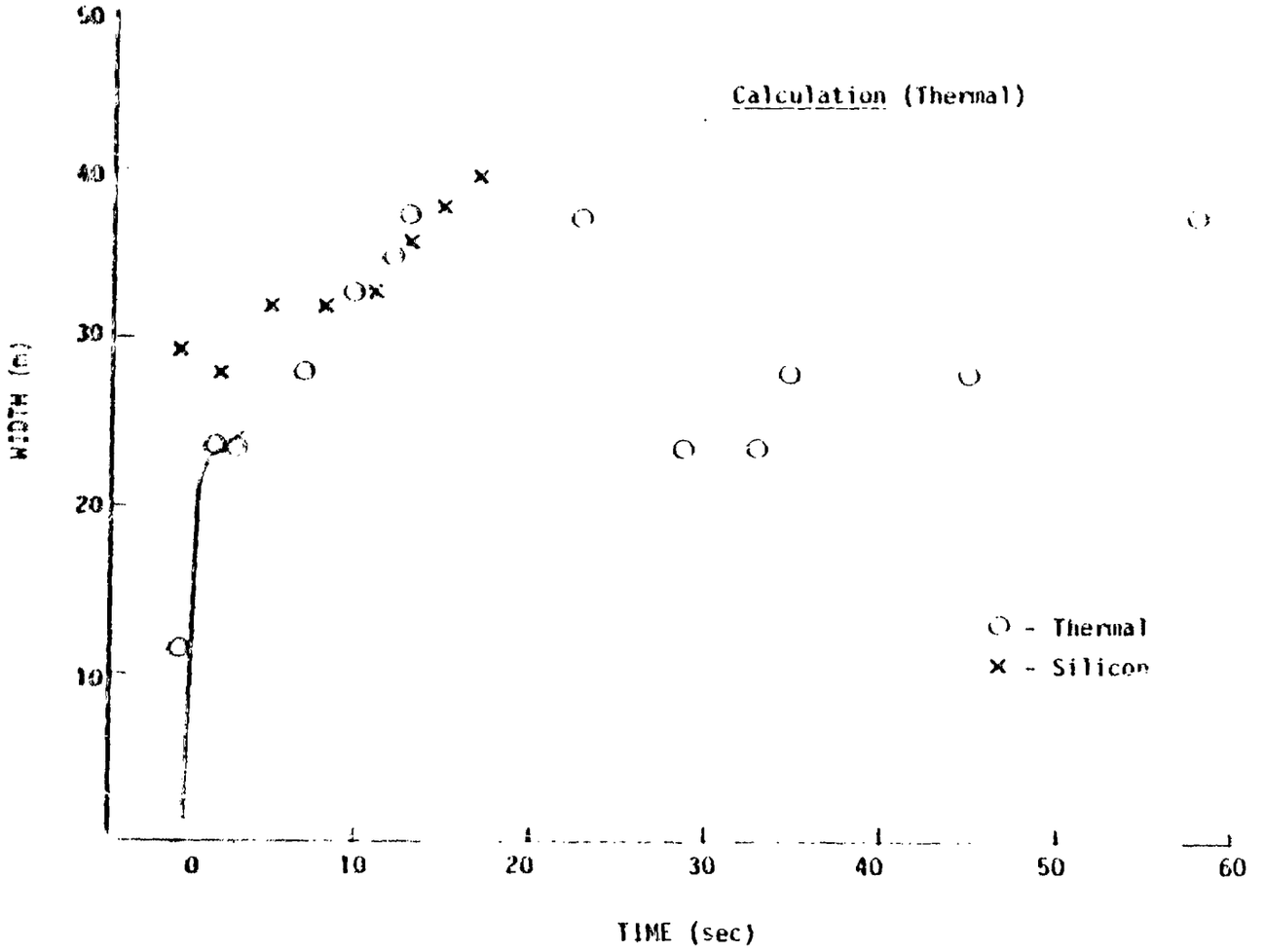

Figure 21. Cloud Width History in Silicon and Thermal Region Measurements

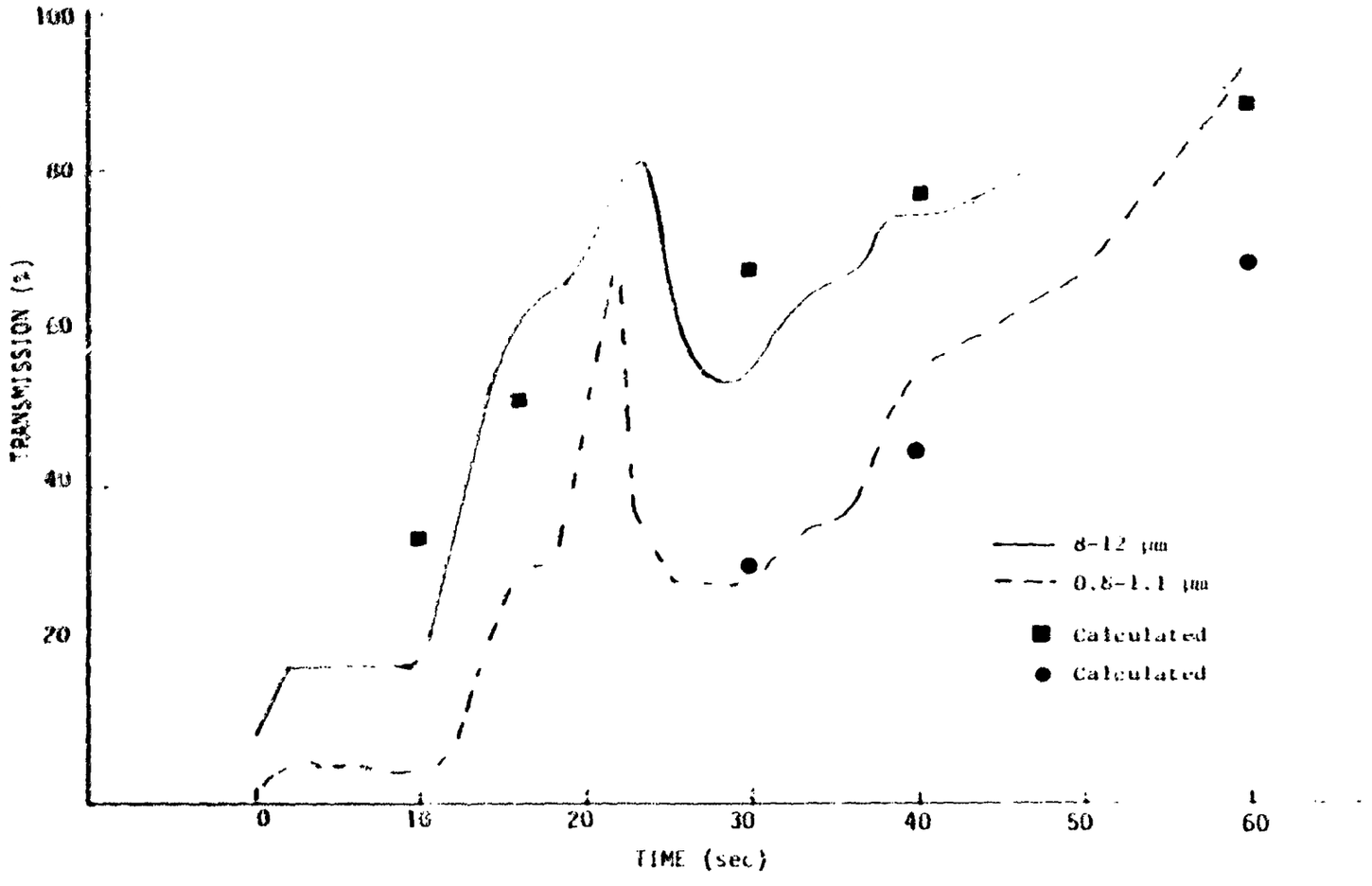

Figure 24. Comparison of Measured Relative Transmission and Calculated Values

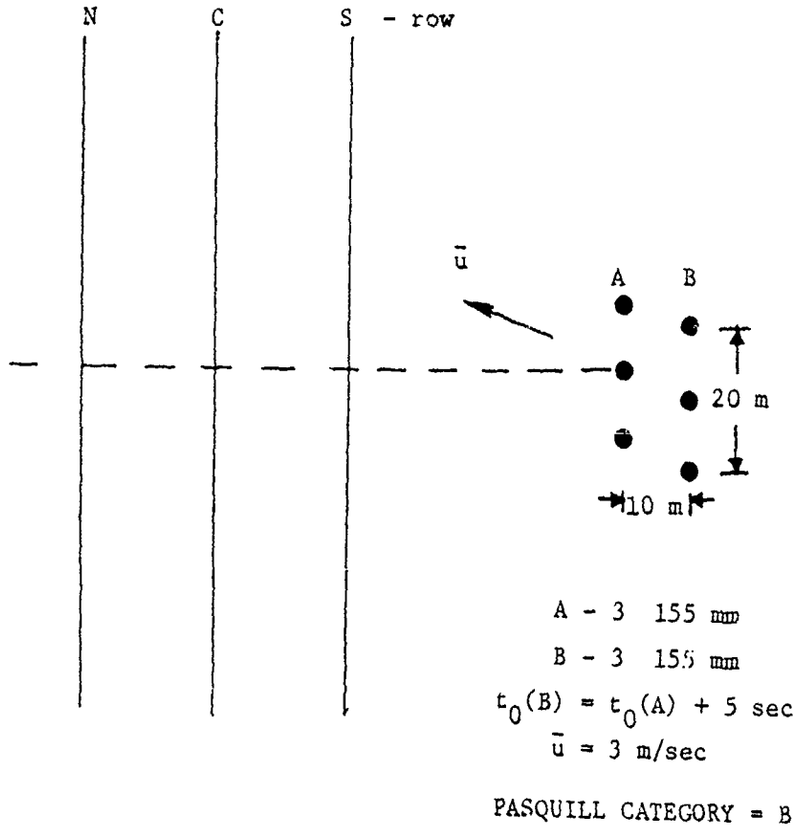

Figure 25. Layout of SWII-29 Event

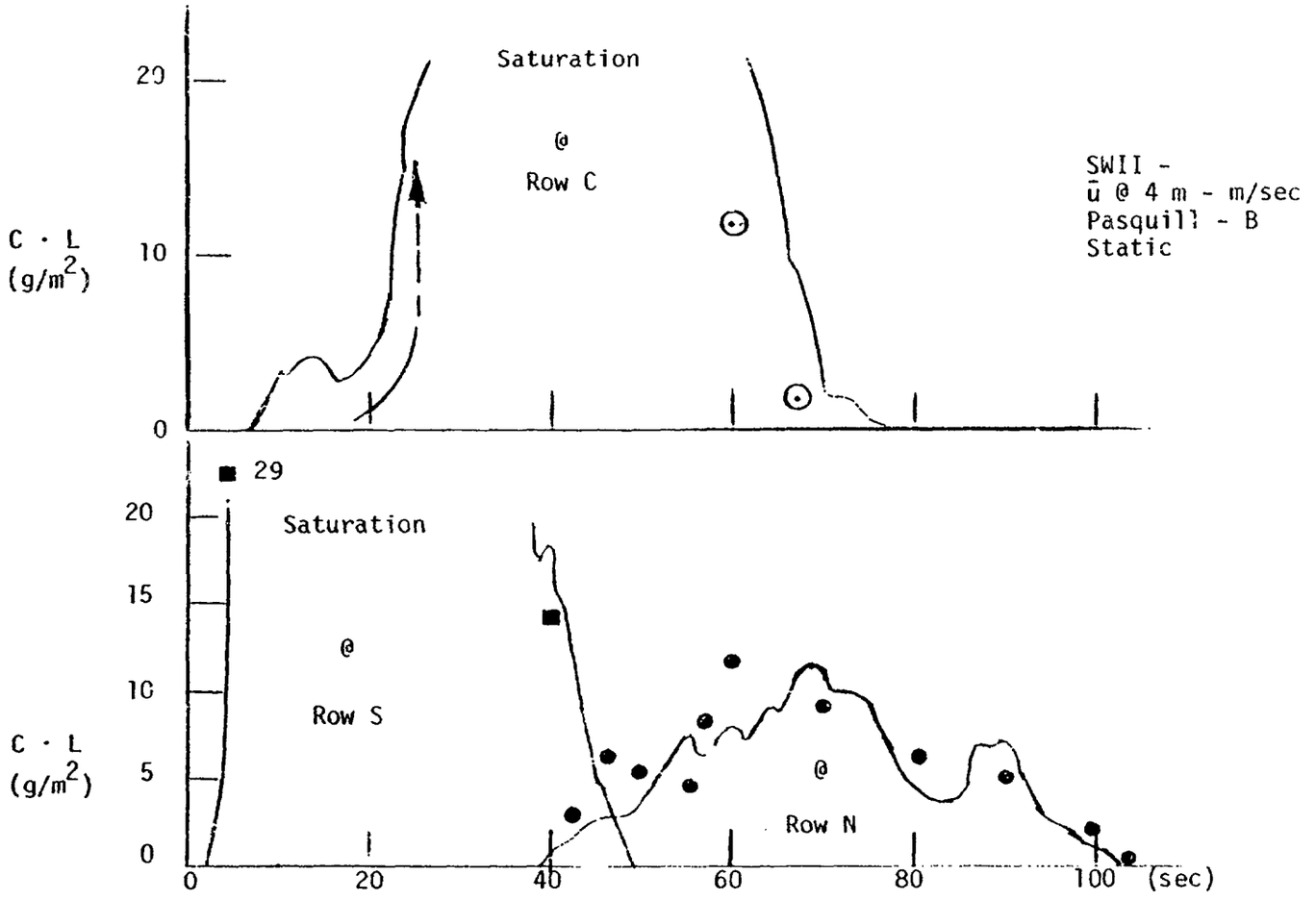

Figure 26. Comparison of Measured and Calculated C · L Histories at Three Lines
(■ , ● , ⊙ - Calculated Values)

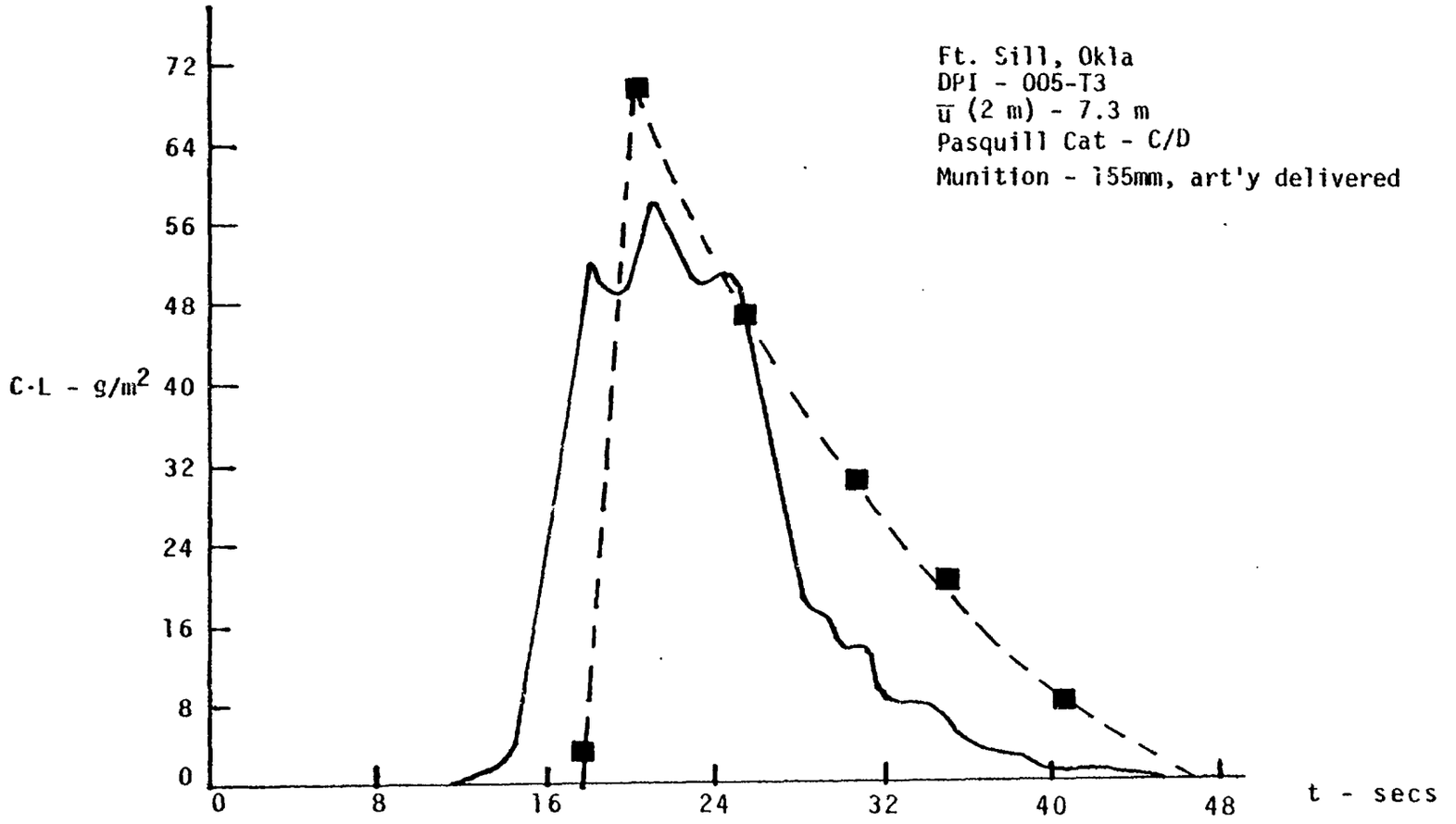

Figure 27. Comparison of Measured and Calculated C · L History
(■ - Calculated)

In Fig. 28 we present the calculated and observed cloud height and width. The results are in fair agreement in spite of the limited input data to establish the prevailing meteorological conditions. In Fig. 29 we present the comparative results for C · L, and the results are in good agreement.

On the basis of the above we conclude that the proposed model can provide a good estimate of the dust obscuration generated by explosive munitions.

With respect to the detailed explosive dust model presented here, a form suitable for operational use is described. For specific calculations where the actual burst height, soil type, etc., are known, the reader can obtain the necessary cratering expressions from the basic text.

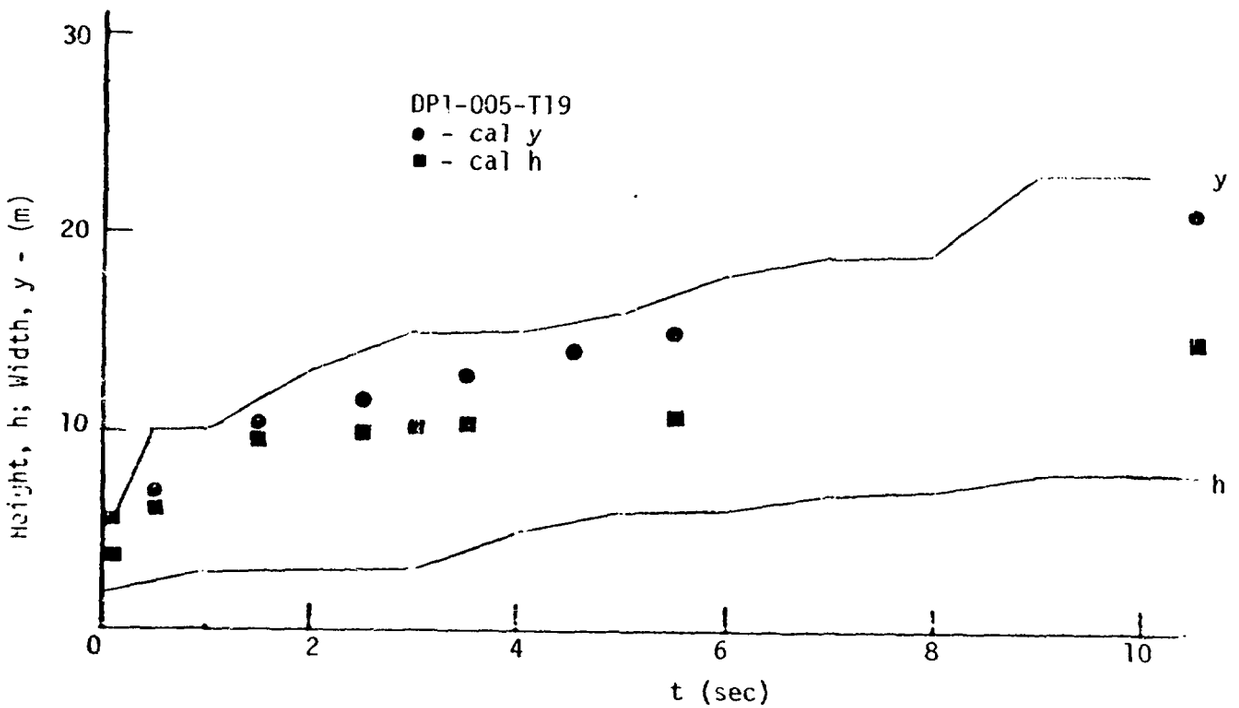

Figure 28. Comparison of Calculated and Measured Cloud Height and Width vs. Time

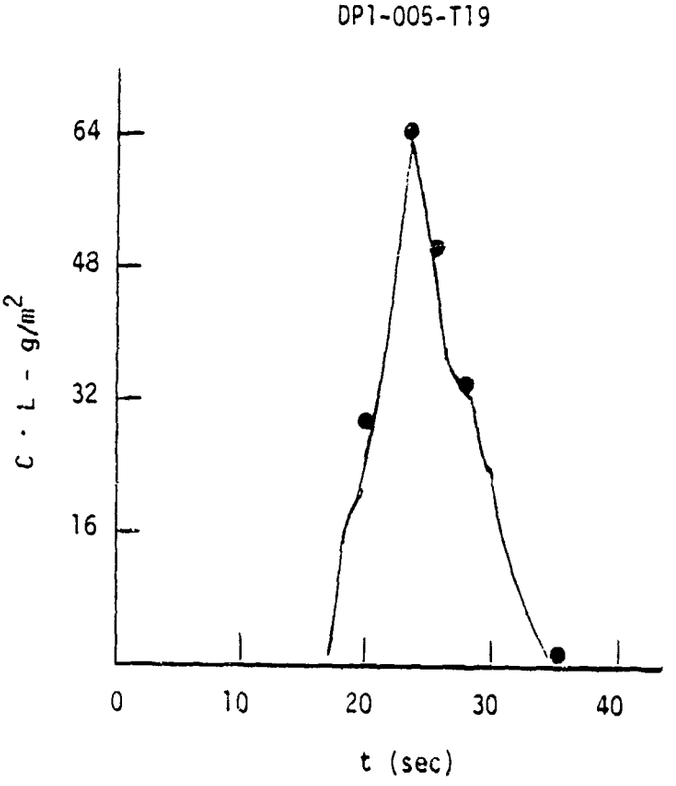

Figure 29. Comparison of Calculated and Measured C · L History (● - model predictions)

5 MODEL STRUCTURE FOR EXPLOSIVE DUST

5.1 GROUND INPUT DATA

A. Scenario

Line of sight

Munition deployment plan

Munition rate

Sensor type and operational wavelength

B. Munition Characteristics

Type (caliber, Mk No.)

HE material and weight

Fuze type and setting

C. Meteorological Conditions

Time of day

Cloud cover

Mean wind speed (m/sec) - surface to 10 m

Temperature T(°C) - 0.5 m and 10 m

Elevated inversion layer

Wind direction

D. Terrain Characteristics

Soil moisture conditions

Soil type and gradation

Vegetation

E. Optical Properties

(1) Effective Charge Weight Calculation

W_{eff} = W (pressure at sea level/pressure at detonation alt)

W = a (explosive weight)

a = 1 for TNT

= 1.19 for Comp B

= 1.1 for C-4

= 0.86 for Explosive D

(2) For ambient conditions and explosives used, compute W_{eff} and $(W_{eff})^{1/3}$.

(3) Establish soil type and condition, enter Table 16, and find scaled parameters, $\bar{r}$ and m_0. From (2) obtain crater radius and depth. The latter is only for general interest.

TABLE 16

ESTIMATED PARAMETERS FOR SHELLS AND MORTARS

Item	Soil Type; Condition	$C_r/W^{1/3}$	$C_d/W^{1/3}$	$\bar{r}$ ($ft^3/\#$)	m_0*
1	Sod and soil; wet†	$0.7W^{.03}$	$0.71W^{-.04}$	0.55	90%
	Sod and soil; dry	$0.72W.04$	$1.0W^{-.03}$	0.33	75%
2	Clay; wet	1.44	0.72	2.0	90%
	Clay; dry	0.50	0.30	0.72	75%
3	Sandy clay; wet	1.60	0.56	2.50	90%
	Sandy clay; dry	0.55	0.32	0.75	75%
4	Silt stone; wet	1.04	0.43	0.55	90%
	Silt stone; dry	0.90	0.20	0.32	75%
5	WSMR soil; wet	1.30	0.50	1.67	90%
	WSMR soil; dry	0.96	0.45	0.87‡	75%
6	Alluvial soil; moist	0.71	0.31	0.25	50%

*Fallout fraction (%).

†Crater may be larger at the surface, we assume here an effective crater.

‡155-mm live shell.

(a) Determine ejected weight = $\gamma \cdot \eta \cdot$ charge weight (lb)

η - See Table 16

γ(lb/ft^3) - soil type

100	Alluvium moist
35	Sod, dry
70	Sod, wet
125	Clay, wet
100	Clay, dry
100	Sandy clay, dry
125	Sandy clay, wet
140	Sandy clay and gravel
125	Siltstone, wet
90	Siltstone, dry

(b) Lofted weight = $(1 - m_0)$ · ejected weight

(c) Main cloud dust weight = (0.9) · lofted weight
Stem dust weight = (0.1) · lofted weight

Retain above for use to find concentration and <u>particle distribution, if desired</u>.

(4) Cloud History - Initial

(a) Enter Fig. 30, find $D_{cl}(t)$ and $H_{cl}(t)$ for $t \leq 0.1\ W^{1/3}$

(b) Enter Fig. 30, for $D_{cl}(t)$, $H_{cl}(t)$ $T(t)$ when $t > 0.1\ W^{1/3}$ and $\leq 0.3\ W^{1/3}$

(c) Enter Fig. 31, for stem height and stem diameter, i.e., $D_s = 4C_r$.

(d) From (a) we get Vol = $(\pi/8)D_{cl}^2(t) \cdot H_{cl}(t)$

(e) From (b) and (c) we have Vol = $(\pi/8)D_s^2(t) \cdot T(t)$

$V_s = 4\pi\, C_r^2 \cdot H_s(t)$

<u>Note</u>: $Z = T + H_s$ at $t = 0.3\ W^{1/3}$ (sec)

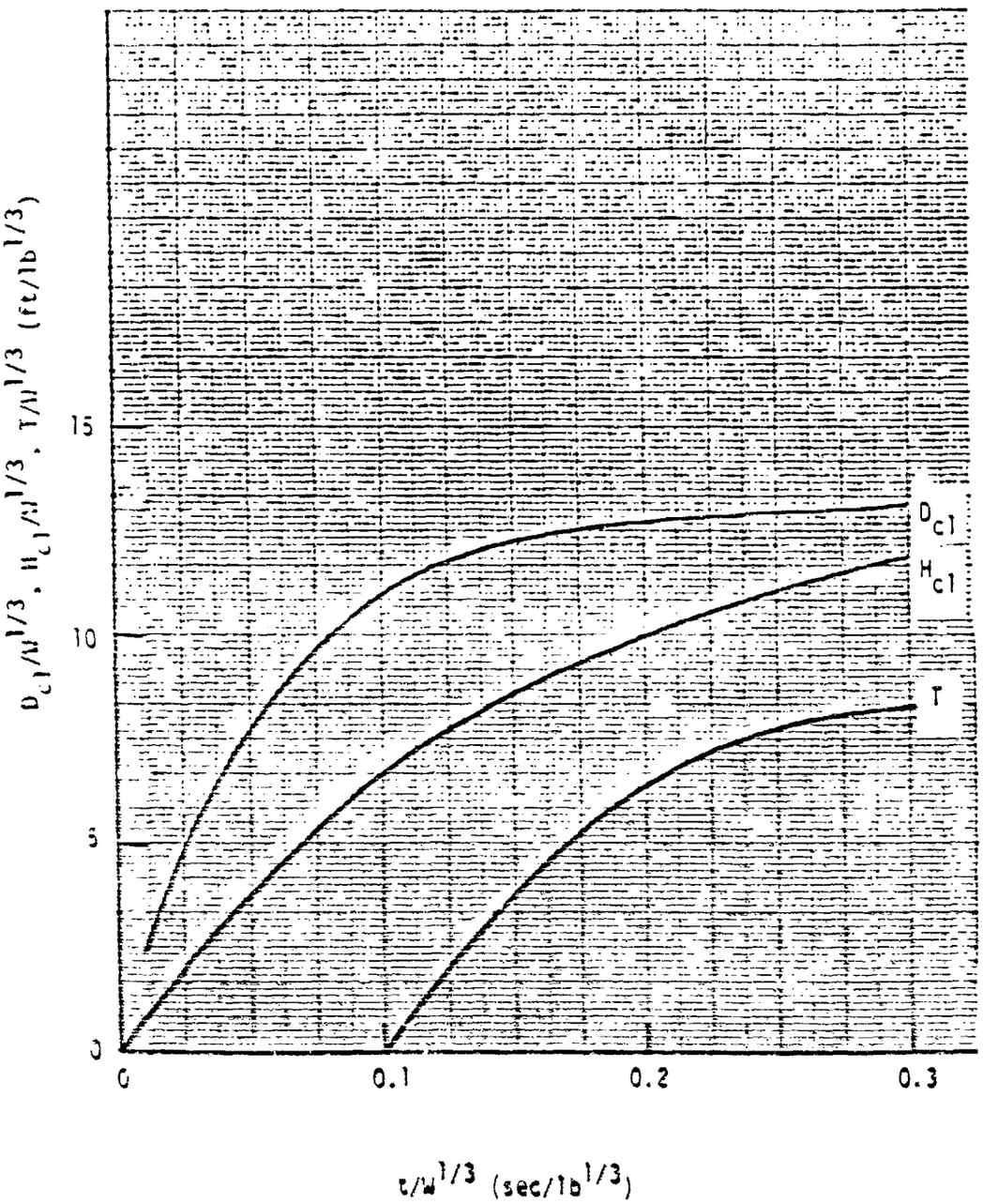

Figure 30. Main Cloud Parameters vs. Time

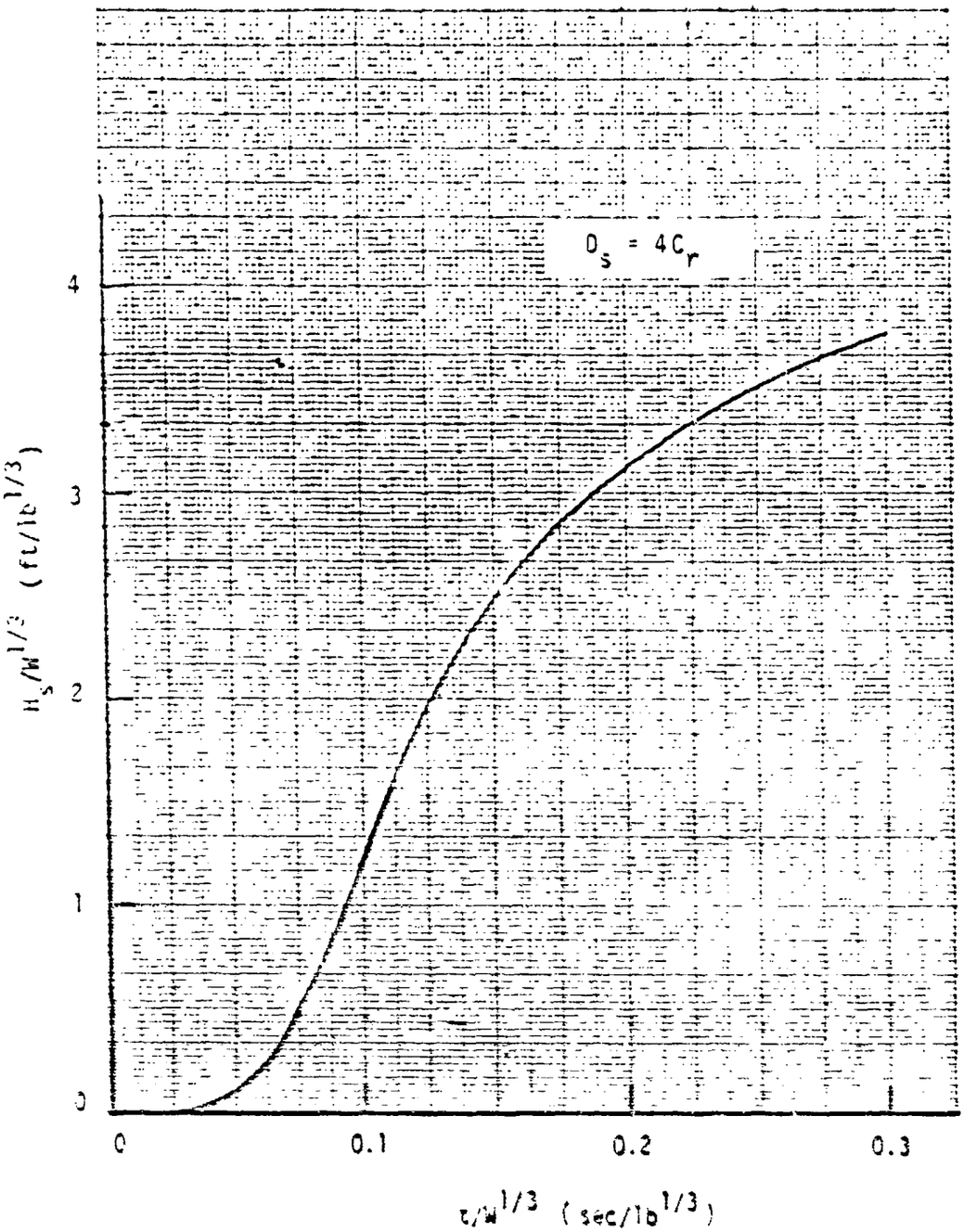

Figure 31. Stem Height Vs. Time

(5) Concentration - Initial

$$C = \frac{0.9 \text{ Loft Weight (g)}}{\pi/4 \cdot D_{ci}^2 \cdot T} \text{ g/m}^3$$

$$C = \frac{0.1 \text{ Loft Weight (g)}}{4\pi C_r^2 \cdot H_s} \text{ g/m}^3$$

We next consider the dispersion of the main cloud and stem, realizing that the cloud is still buoyant.

(6) Cloud History - Buoyant Phase

(a) Calculate $t_b = 4.1W^{1/3}$, resultant is time for buoyant phase of major cloud only.

(b) Calculate $F = 3.6 \cdot 10^{-5} (300 \cdot g \text{ HE} \div t_b)$

(c) Pasquill Category A, B, and C

$$\Delta h = \frac{1.6 F^{1/2} x^{2/3}}{\bar{u}}$$

$\bar{u}$ at 4 m

(d) Pasquill Category D

$$\Delta h = 1.6F^{1/2}x^{2/3}\left[0.4 + 0.64\frac{x}{x_*} + 1.2\left(\frac{x}{x_*}\right)^2\right] \div \bar{u}\left[1 + 0.81\left(\frac{x}{x_*}\right)^2\right]$$

$$x_* = 14F^{5/8} \qquad F < 55 \text{ m}^4/\text{sec}^3$$

$$= 34F^{0.4} \qquad F \geq 55 \text{ m}^4/\text{sec}^3$$

(e) $(\Delta h)_{max} = 1.6F^{1/2}x^{2/3} \div u$

where $x = 3.5x_*$ for Pasquill Category A, B, C, and D

(f) Cat E, F, etc.

Compute $s \simeq \frac{g}{T_0}\left[\frac{\Delta T}{\Delta z} + 0.098\right]$; T is actual temperature

Compute $x_1 = 2.4\ \bar{u}/s^{0.5}$

$\Delta h = 1.6\ F^{1/2} x^{2/3} \div \bar{u}$ for $x \leq x_1$ $\bar{u} \simeq 9$ 4m

$\Delta h_{max} = 2.9\ (F/\bar{u}s)^{1/3}$

(g) $\bar{u} = 0$

$H_{max} = 1.87Q^{0.25}$ (m)

$Q = 4.2 \cdot 10^6 \cdot W$ (kg); W = TNT equivalent weight

Note: The dimensions here are given by a right circular cone where top radius = $0.5 \cdot H_{max}$ and the cone half-angle is 26°.

(7) Stem: Momentum Dispersion Phase ($\bar{u} > 0$)

(a) From input data and the table determine Pasquill Category.

PASQUILL STABILITY CATEGORIES

Surface Wind Speed at 10 m ($m\ sec^{-1}$)	Insolation			Night	
	Strong	Moderate	Slight	Thinly Overcast or ≥4/8 Low Cloud	≤3/8 Cloud
2	A	A-B	B	--	--
2-3	A-B	B	C	E	F
3-5	B	B-C	C	D	E
5-6	C	C-D	D	D	D
>6	C	D	D	D	D

(b) $x = \bar{u}t$, $\bar{u} \geq 2$ m

(c) Cloud Width, $\bar{y}$

From (a) enter table and compute $\bar{y}$.

Pasquill Category - A	$\bar{y} = 9.1 + 0.419x$
Pasquill Category - B	$= 9.1 + 0.328x$
Pasquill Category - C	$= 9.1 + 0.238x$
Pasquill Category - D	$= 9.1 + 0.20x$
Pasquill Category - E	$= 9.1 + 0.18x$
Pasquill Category - F	$= 9.1 + 0.146x$

(d) Cloud Rise, $\bar{z}$

Note: The stem dust will penetrate the main cloud base

From (a) enter table and find $\bar{z}$.

$\bar{z}(x) = 2.73 + 0.39x$	$\bar{u} = 0.5$ m/sec	Cat - A
$= 2.73 + 0.35x$	$= 1.0$ m/sec	Cat - A
$= 2.73 + 0.18x$	$= 1.5$ m/sec	Cat - A
$= 2.73 + 0.15x$	$= 2.0$ m/sec	Cat - A
$= 2.73 + 0.137x$	2.0 m/sec	Cat - A
$= 2.73 + 0.11x$		Cat - B
$= 2.73 + 0.073x$		Cat - C
$= 2.73 + 0.06x$		Cat - D
$= 2.73 + 0.053x$		Cat - E
$= 2.73 + 0.046x$		Cat - F

(e) Cloud Volume: Stem

$$V(t) = (\pi/6)\, x \cdot \bar{y}^1 \cdot \bar{z}^1$$

$$x = \bar{u}t + D_s/2$$

$$\bar{y}^1 = \bar{y}(t) + D_s$$

$$z^1 = \bar{z}(t) + H_s$$

(f) Concentration (t) $= 0.1 \dfrac{\text{Loft Weight}}{V(t)}$ g/m^3

(8) Main Cloud Dispersion

(a) Compute $\bar{u}(z)$

$$\bar{u}(z) = \bar{u}\ (4\,m) \cdot (z/4)^p$$

p = 0.1, [illegible], B, and C

p = 0.142, Cat D

p = 0.3, Cat E

p = 0.5, Cat F

p = 0.8, Cat G (+3, Table 1)

(b) For unstable and neutral, cloud sheared at base (4 m), H (top) and $(H_{cl} - 4) \div 2$.

For stable categories, shear only top.

From input data, find Pasquill Category, see (7a).

$x = \bar{u}t$ where $\bar{u}$ is given by above rules

$\bar{y}$, see (7c), again use appropriate value of x.

$\bar{z}$, see (7d), again use appropriate value of x.

(c) Inversion layers can be treated as defined for smoke.

(9) Main Cloud Dimensions

$$x = \bar{u}t + D_{cl}/2$$

$$\bar{y}^1 = \bar{y}(t) + D_{cl}$$

$$Z(t) = \Delta h(t) + \bar{z}(t)$$

(10) Main Cloud Volume

A simple approach is to assume an ellipsoidal shape; i.e., ellipsoid ÷ 4, where $\bar{x}$, $\bar{y}$, and $\bar{Z}(t)$ are defined for the top layer. This will give a somewhat larger volume. Otherwise, we can treat the volume in two parts, the top layer and the remainder.

For top, insert, compute values for x, $\bar{y}$, $\bar{Z}$

$$V_1 = (\pi/6)\, x\bar{y}^{-1}\, \bar{Z}(t)$$

For remainder

$$V_2 = \frac{\pi D_{c1}^2 T}{8} + (1/3)\, y^1(t) \cdot \bar{Z}(t) \cdot \bar{u} \cdot t$$

where $\bar{u}$ is at cloud center.

(11) Main Cloud Concentration

$$\text{Concentration} = 0.9 \text{ loft weight} \div (V_1 + V_2)$$

Note: The validations in the main text were performed using the simple procedure.

(12) Particle Size Distribution

Follow procedure described in main text.

(13) For a precise calculation where the charge center height is known explicitly, then the crater dimensions and crater efficiency can be estimated from material in text and appendix D. The remainder of the procedure is as given above.

The values in Fig. 4, Part 2, are for free air explosions. For the condition HOB < 0 the reader must employ the relation

$$W_{air} = W(\text{charge}) \cdot \exp(-3\rho\lambda_d)$$

where ρ = soil specific gravity and λ_d = charge depth/$W^{1/3}$.

(14) Multi-Munitions

In the above procedure, we assumed each explosion is mutually independent. This is correct provided the charges are about 50 m apart, or the material velocity (see Fig. 4) is comparable to the ambient $\bar{u}$. Otherwise, there are shock interactions. Since operationally there is no a priori knowledge of detonation locations and lapse time between these events; i.e., space and time must be considered, the effects cannot be modeled until a detailed study of the statistical characteristics are made.

Again the basic data to analyze the interactive event is contained in the text, and the reader may analyze any particular event.

PART 3
VEHICULAR DUST OBSCURANT MODEL*

*Note: The basic work was performed under sponsorship of the Defense Advanced Research Projects Agency and is incorporated herein for completeness.

1 INTRODUCTION

Experience has shown that military tracked vehicles and wheeled vehicles raise considerable dust as evidenced at Proving Grounds and in combat areas. Under some conditions, the generated obscuration creates a serious problem for offensive systems. We will consider this problem of vehicle dust obscuration.

Ground vehicles can raise loose surface material (dust, water, etc.). The atmospheric loading of this material is dependent on the type of vehicle, vehicle speeds, fender arrangement, etc. For dust, we must add the soil type, soil cohesiveness, grain size, and related factors. The launching speed and angle in combination with atmospheric conditions, wind speed, and stability, will affect the dust cloud behavior. For example, particles of $\lesssim 7$ μm launched at a minimum speed of ~ 7 m/sec will be transported with airflow motion; larger particles are propagated by a process called saltation.* The latter is a looping action where the particle impacts the soil and launches additional soil particles.

The quantity and quality of data on dust created by vehicles are extremely limited; that is, there are no real controlled experiments nor sufficient statistical data to generate a comprehensive model. Further, the soil types are limited, namely, to those of Army Proving Grounds. The general configuration of the vehicle will affect the dust cloud geometry. For the available data, this parameter has not been specifically defined except in a general sense, i.e., light or heavy wheeled, heavy track. Nevertheless, an attempt has been made here to provide several algorithms to permit an estimate of vehicle dust.

---

*See Bagnold's Blown Sand & Desert Dunes (1934).

2 TECHNICAL DISCUSSION

First, to generate a dust cloud relatively loose, dry soil is required. Second, the soil particle size distribution affects not only the attenuation coefficient but also the dust concentration lofted into air and staying aloft. In Fig. 1 is presented the relation between concentration and p, percent by weight of particles with d < 74 μm, where the areas define the cloud visibility at ~25 ft from the source. We see if p ≤ 10%, there is unrestricted visibility except for high concentration. On the other hand, if p ≥ 24%, the visibility reduces to ≃ 0 ft. This is understandable since the more loose powder in the surface and subsurface layers, the denser the dust cloud. Thus we suggest Fig. 1 is a general plot which may, however, differ somewhat for a specific situation.

In Part 2, Table 6, we presented the particle size fractions at several US Army facilities. The fraction of particles ≤74 μm falls into the category of dust cloud potential. Similarly, we have shown that at Grafenwohr the soil has been sufficiently pulverized at a number of sites to allow dust cloud generation. Of course, the soil should be relatively dry to be conducive for dust making. It should be noted that clay soils tend to have large particle sizes (MMD ≃ 650 μm) and high cohesiveness when wet. Therefore, the likelihood for dust generation differs radically depending on locale.

From Fig 1 we can estimate that the photopic extinction coefficient (in m^2/g) will vary significantly; see Table 1.

TABLE 1

EXTINCTION COEFFICIENT AS A FUNCTION p

p(% < 74 μm)	$\alpha_e (m^2/g)$
>21	>0.93
9-21	<0.093-0.93
<9	≥0.093

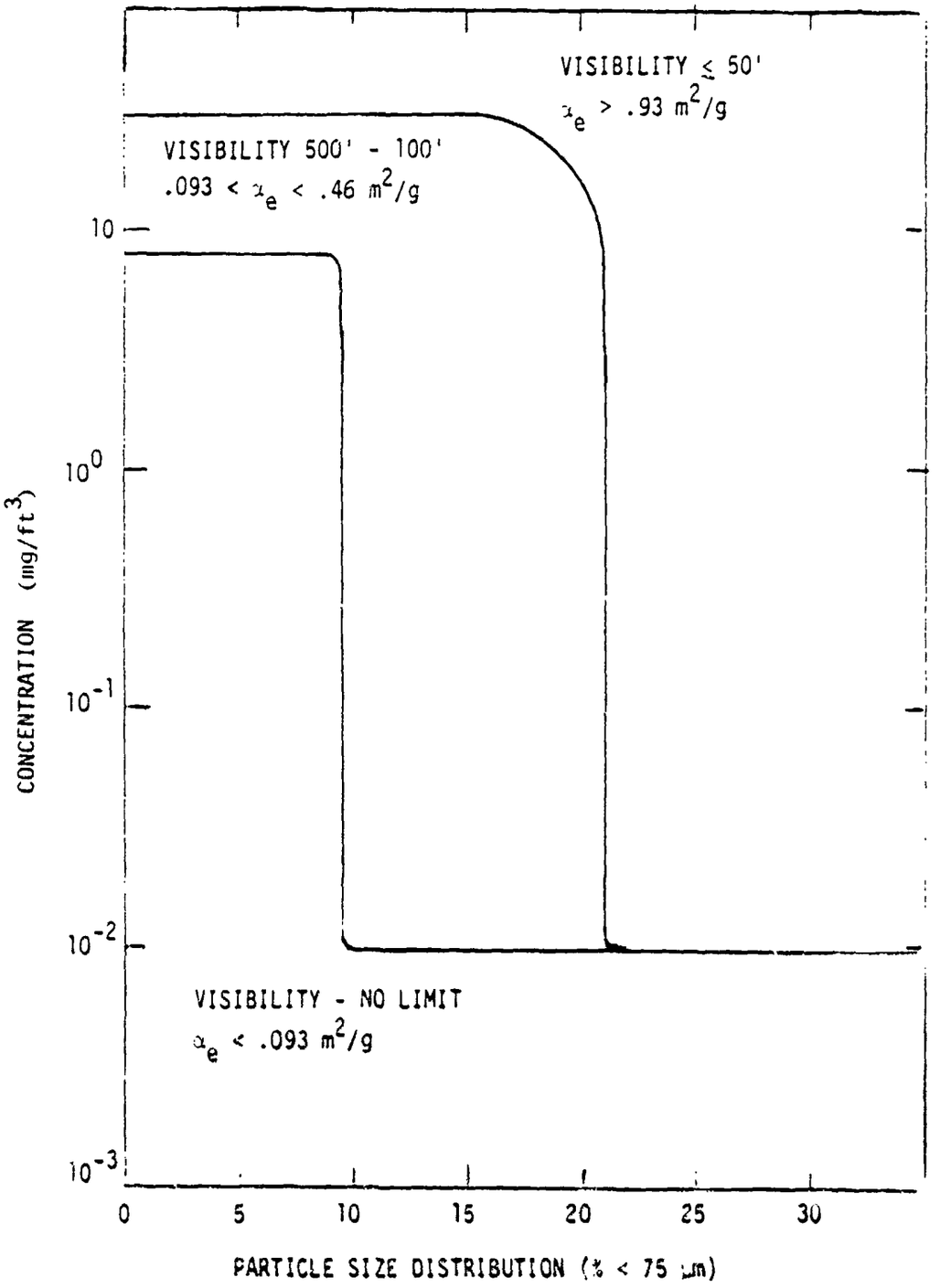

Figure 1. Visibility Zones as a Function of Concentration and p (Estimates of Extinction Coefficients Are Provided)

It should be noted that for typical soil p ~ 15% and, therefore, $\alpha \simeq .46\ m^2/g$ is a valid number. The spread in Table 1 is very interesting; it shows an order-of-magnitude difference in extinction coefficient; see Part 2.

Next, we analyzed the concentration as a function of distance for heavy wheeled and heavy-tracked vehicles, where the vehicle speeds were between 15 and 35 mph and heavy dust conditions existed. The expressions are given below where the concentration is constant from vehicle axis to edge (halfwidth).

Wheeled Vehicle:

$$C\ (g/m^3) = 6.9489/d^{5.32} \tag{1}$$

Heavy Track:

$$C\ (g/m^3) = 525.3/d^{2.367} \tag{2}$$

where d is the distance in meters from the vehicle velocity vector and is $\geq$ vehicle width/2. When the surface dust is light, the values are reduced by an order of magnitude.

Lastly, we have reduced a set of data for heavy-wheeled vehicles in light soil that related the number of vehicles in a convoy, vehicle speed, duration of dust, and distance from vehicle route, i.e., N, u (mph), t (sec), and d (ft), respectively.

The general form of the expression is

$$N/t = (N/t)_{asy}\ [1 - e^{-\beta u/d}] \tag{3}$$

where β is an empirical determined constant. The preliminary values of (N/t) asymptotic, i.e., limiting value, and β are

Vehicle Type	Soil Type	$(N/t)_{asy}$	β
Heavy Wheel	Light/Moderate	0.2	1.8
Light Track	Moderate	0.24	2.86
Light Wheel	Light	0.14	2.0
Heavy Track	Heavy	0.28	5.0

The soil types are defined as follows:

Light	$p < 5\%$
Moderate	$p < 9\%$
Heavy	$p > 10\%$

One should note that t and d are positive (non-zero). Lastly, the effect of wind is minor and included in the above, i.e., for winds $\leq$ 5 m/sec.

The several expressions given above provides an initial approach to the modeling of vehicle dust. Basically, the visual observation produced by generated dust has a duration comparable to the time the vehicle passes through the line of sight. Secondly, the extrapolation to another wavelength, λ, the required concentration, would have to be increased (decreased) directly proportional to the ratio of the extinction coefficients. Finally, the above algorithms are valid to cloud heights of 3 m.

3 MODEL STRUCTURE

To apply the above expressions, we suggest the following procedure.

Inputs:

Vehicle Speed - u (mph)

Vehicle Type - wheeled or tracked

Vehicle Size - light, heavy

Soil Condition - light, heavy

Soil Type - p, % wt of particles ($d \leq 74$ μm)

Number of Vehicles - N

Steps:

1. If the soil is either wet or $u \leq 10$ mph or $p < 90\%$, then the concentration = 0.

2. Establish value of p, soil condition, location from source edge d, type of vehicle.

   Enter Eqs. 1 and 2 and find concentration. (Note: $g/m^3 = 35\ g/ft^3$.)

   If concentration $< 10^{-5}\ g/ft^3$ and $d \geq 25$ ft, terminate.

   If concentration $> 10^{-5}\ g/ft^3$, find C vs. d. $C \cdot \bar{L}$ is determined by geometry.

3. To find transmission:

   Multiply $C \cdot L$ by appropriate extinction coefficient. If the region of interest is the photopic, then enter Fig. 1 and find visibility range.

4. To find the duration:

   Enter Eq. 3 with N, u, and d and $(N/t)_{asy}$ and β and compute t.

APPENDIX A

MUNITIONS CHARACTERISTICS

Table A1

TYPES OF FILL AND FILL WEIGHTS FOR SMOKE MUNITIONS

SYSTEM	AMMUNITION	FILL TYPE	FILL WEIGHT (LBS)
Hand Grenade, Smoke[1]	AN-M8(STD.A)	HC	1.2
Hand Grenade, Smoke	M15(STD.C)	WP	0.9
Hand Grenade, Smoke	M18(STD.A)	Colored Smoke	0.71
Hand Grenade, Smoke	M34(STD.A)	WP	0.94
Rifle Grenade, Smoke[1]	M19A1(STD.C)	WP	0.53
3.5 inch Rocket[1]	M30(C&T)*	WP	2.23
40 mm[2]	M675(T25) (STD.B)	Red Smoke	0.21
40 mm	XM676(L.P.)**	Yellow Smoke	0.13
57 mm Cannon[2]	M306A1(C&T)	WP	0.37
60 mm Mortar[2]	M302A1(C&T)	WP	0.75
	M302(C&T)	WP	0.75
75 mm Rifle[2]	M311, M311A1(C&T)	WP	1.35
76 mm Gun[2]	M361A1(STD.A)	WP	1.38
81 mm Mortar	M57(Obsolete)	FS	4.59
	M57, M57A1(STD.C)	WP	4.06

Ammunition Handbook, Department of the Army Field Manual FM9-13, Headquarters, Department of the Army, March 1973.

Table A1 (Cont'd)

TYPES OF FILL AND FILL WEIGHTS FOR SHORT ROUNDS

SYSTEM	AMMUNITION	FILL TYPE	FILL WEIGHT (LBS)
81 mm Mortar (Cont)	M370(STD.B) M375(STD.B) M375A1(STD.B) M375A2(STD.A)	WP WP WP WP	1.68 1.75 1.75 1.75
90 mm Tank Gun	M313C(STD, STD.B)	WP	1.97
105 mm Tank Gun	M416(STD.A)	WP	6.00
105 mm Howitzer	M60(STD.A) M508A1, M84(STD.A) M508E1 Yellow Red Green Violet M841(TP)	WP HC HC HC HC HC HC	3.83 7.50 4.92 5.21 5.13 5.13 12.30
155 mm Gun Howitzer Howitzer Howitzer Howitzer	M104(STD.B) M116A1 Smoke Projectile M110(STD.A) M116(STD.B) M116A1 (any color)	WP WP FS HC HC	15.60 15.66 17.47 25.84 17.19
175 mm Gun	M557 Projectile	WP	7.2

Ammunition Handbook, Department of the Army Field Manual FM9-13, Headquarters, Department of the Army, March 1973.

Table A1 (Cont'd)

TYPES OF FILL AND FILL WEIGHTS FOR SMOKE MUNITIONS

SYSTEM	AMMUNITION	FILL TYPE	FILL WEIGHT (LBS)
4.2 Inch Mortar[2]	M2A1 Smoke Cartridge " M328(SID.B) M328A1(SID.A) M2(SID.B) M2(Obsolete)	WP PWP WP WP WP FS	7.50 7.50 7.50 8.14 7.50 7.50
5 Inch Gun[2]	5-Inch/38-cal. Projectile 5-Inch/54-cal. Projectile	WP WP	7.10 8.34
100-lb Smoke Bomb[3]	AN M47A2	WP PWP	100.00 74.00
100-lb-T1 Smoke Bomb[4]	M904A1(E87)	Red Smoke	72.0
250-lb-T1 " "	M93(SID.)		
250-lb-T1 " "	M93(SID.)	Red Smoke Green Yellow	16.6 16.8 13.9

Ammunition Handbook, Department of the Army Field Manual FM9-13, Headquarters, Department of the Army, March 1971.

Table A1 (Cont'd)

TYPES OF FILL AND FILL WEIGHTS FOR SMOKE MUNITIONS

SYSTEM	AMMUNITION	FILL TYPE	FILL WEIGHT (LBS)
250-lb-TI Smoke Bomb	M106(STD.)	Red-Green Smoke Yellow-Green Red-Yellow	70.1 66.1 58.9
250-lb-TI " "	M89(C&T)	Red Smoke Green Yellow	61.4 71.8 56.7
250-lb-TI " "	M90(C&T)	Red Smoke Green Yellow	59.3 66.1 53.0
250-lb-TI " "	M88(C&T)	Red Smoke Green Yellow	32.2 35.9 28.8
CBU-11A[3]	261 BLU-16/B Smoke Bombs	WP	Cluster 265.00 Bomb 1.00
CBU-12/A	261 BLU-17/B Smoke Bombs	WP	Cluster 315.00 Bomb 1.20

Ammunition Handbook, Department of the Army Field Manual FM9-13, Headquarters, Department of the Army, March 1973.

Table A1 (Cont'd)

TYPES OF FILL AND FILL WEIGHTS FOR SMOKE MUNITIONS

SYSTEM	AMMUNITION	FILL TYPE	FILL WEIGHT (LBS)
CBU-12A/B***	213 BLU-17/B Smoke Bombs	HC	Cluster 256.00 Bomb 1.20
CBU-13/A	130 BLU-16/B 131 BLU-17/B Smoke Bombs	HC WP	Cluster 130.00 Bomb 1.00 Cluster 158.00 Bomb 1.20

*Contingency & Training
**Limited Production
***Adapted for F-4 Aircraft

(1) "Logistics Complete Round Charts, Grenades, Mines, Pyrotechnics, Rockets, Rocket Motors, Demolition Material," AMCP 700-3-5, March, 1970.
(2) "Logistics Complete Round Charts. Artillery Ammunition. "AMCP 700-3-3, Nov., 1970
(3) JMEM Effectiveness Manual (Air-To-Surface) Weapons Characteristics Handbook, 1965
(4) "Logistics. Complete Round Charts. Bombs "AMCP 700-3-4, Dec., 1968

NOTE: [illegible] meters x MK12 Mod 0 Smoke Tank (Navy) which can produce a 300 meter screen in 30 secs with a duration of 5-15 minutes.

Ammunition Handbook, Department of the Army Field Manual FM9-13, Headquarters, Department of the Army, March 1973.

Table A2

Some Smoke Generators and Pots

Smoke	Type	Fill	Fill Wt/Flow Rate
Smoke Generator	M3	Fog Oil	25-50 gal/hr
Smoke Pot	AN-M7	Fog Oil (SGF)	–
	AN-M7A1	Fog Oil (SGF)	–
Smoke Pot	M1	HC	10.0
	ABC-M5	HC	3.0
Air Smoke Pot	M4A2		

Table A3

UK Grenades

Smoke Screen Type	Range (m)	Burn Time (sec)	Source	Smoke	Time (sec)	Fill
L5A1,2,3,4	70 (grd)	55-75	Point ground	White	8	
L7A1	70 (grd)	30-50	Point ground	Green		
XL7E2	120 (grd)	30-50	Point ground	Green		
XL3E1 (Curtain) L3A1	30	60-90	8 m air, ground	-	2	RP-butyl rubber
XL13E1 (for L8A1 practice)	120		10 m air, ground			$TiCl_4$-silica
XL19E1	110	8-10		Green		

APPENDIX B

A STABILITY CLASSIFICATION BASED ON HOURLY AIRPORT OBSERVATIONS

A STABILITY CLASSIFICATION BASED ON HOURLY AIRPORT OBSERVATIONS*

This system of classifying stability on an hourly basis for research in air pollution is based upon work accomplished by Dr. F. Pasquill of the British Meteorological Office (see reference 1 of text). Stability near the ground is dependent primarily upon net radiation and wind speed. Without the influence of clouds, insolation (incoming radiation) during the day is dependent upon solar altitude, which is a function of time of day and time of year. When clouds exist, their cover and thickness decrease incoming and outgoing radiation. In this system insolation is estimated by solar altitude and modified for existing conditions of total cloud cover and cloud ceiling height. At night, estimates of outgoing radiation are made by considering cloud cover. This stability classification system has been made completely objective so that an electronic computer can be used to compute stability classes. The stability classes are as follows: (A) Extremely Unstable, (B) Unstable, (C) Slightly Unstable, (D) Neutral, (E) Slightly Stable, (F) Stable, (G) Extremely Stable. Table B-1 gives the stability class as a function of wind speed and net radiation. The net radiation index ranges from 4, highest positive net radiation (directed toward the ground), to -2, highest negative net radiation (directed away from the earth). Instability occurs with high positive net radiation and low wind speed, stability with high negative net radiation and light winds, and neutral conditions with cloudy skies or high wind speeds.

The net radiation index used with wind speed to obtain stability class is determined by the following procedure:

---

* The following explanation of the Pasquill Stability classification has been extracted from an article by D. Bruce Turner in the February 1964 Journal of Applied Meteorology

(1) If the total cloud cover is 10/10 and the ceiling is less than 7000 feet, use net radiation index equal to 0 (whether day or night).

(2) For nighttime (night is defined as the period from one hour before sunset to one hour after sunrise):

a. If total cloud cover ≤4/10, use net radiation index equal to -2.

b. If total cloud cover >4/10, use net radiation index equal to -1.

(3) For daytime:

a. Determine the insolation class number as a function of solar altitude from Table B-2.

b. If total cloud cover ≤5/10, use the net radiation index in Table A-1 corresponding to the insolation class number.

c. If cloud cover >5/10, modify the insolation class number by following these six steps:

(1) Ceiling < 7000 ft., subtract 2.

(2) Ceiling ≥7000 ft. but < 16000 ft., subtract 1.

(3) Total cloud cover equal 10/10, subtract 1. (This will only apply to ceilings ≥ 7000 ft. since cases with 10/10 coverage below 7000 ft. are considered in item 1 above).

(4) If insolation class number has not been modified by steps (1), (2), or (3) above, assume modified class number equal to insolation class number.

(5) If modified insolation class number is less than 1, let it equal 1.

(6) Use the net radiation index in Table B-1 corresponding to the modified insolation class number.

TABLE B-1 STABILITY CLASS AS A FUNCTION OF NET RADIATION AND WIND SPEED

WIND SPEED (KNOTS)	NET RADIATION INDEX 4	3	2	1	0	-1	-2
0, 1	A	A	B	C	D	F	G
2, 3	A	B	B	C	D	F	G
4, 5	A	B	C	D	D	E	F
6	B	B	C	D	D	E	F
7	B	B	C	D	D	D	E
8, 9	B	C	C	D	D	D	E
10	C	C	D	D	D	D	E
11	C	C	D	D	D	D	D
≥ 12	C	D	D	D	D	D	D

TABLE B-2 INSOLATION AS A FUNCTION OF SOLAR ALTITUDE

SOLAR ALTITUDE (a)	INSOLATION	INSOLATION CLASS NUMBER
60° < a	Strong	4
35° < a ≤ 60	Moderate	3
15° < a ≤ 35	Slight	2
a ≤ 15°	Weak	1

APPENDIX C

CONTINUOUS VALUES FOR PLUME DISPERSION PARAMETERS PLUME HEIGHT

In Table 10 of Part 1 we have defined the vertical rise as $2.73 + A \cdot x$, where A depends upon Pasquill category. For modeling purposes we have proposed a fixed value for each category. Actually the parameter varies continuously with mean wind speed, $\bar{u}$, for values ≤ 5 m/sec. Although smoke normally is not discharged when $\bar{u} \leq 2$ m/sec because the horizontal coverage is low, for completeness we present the value of A for $0.5 \leq \bar{u} \leq 5$ m/sec (Fig. C.1). Similarly, we provided an estimate of the continuous values for the lateral dispersion, $\bar{y} = 9.1 + B \cdot x$.

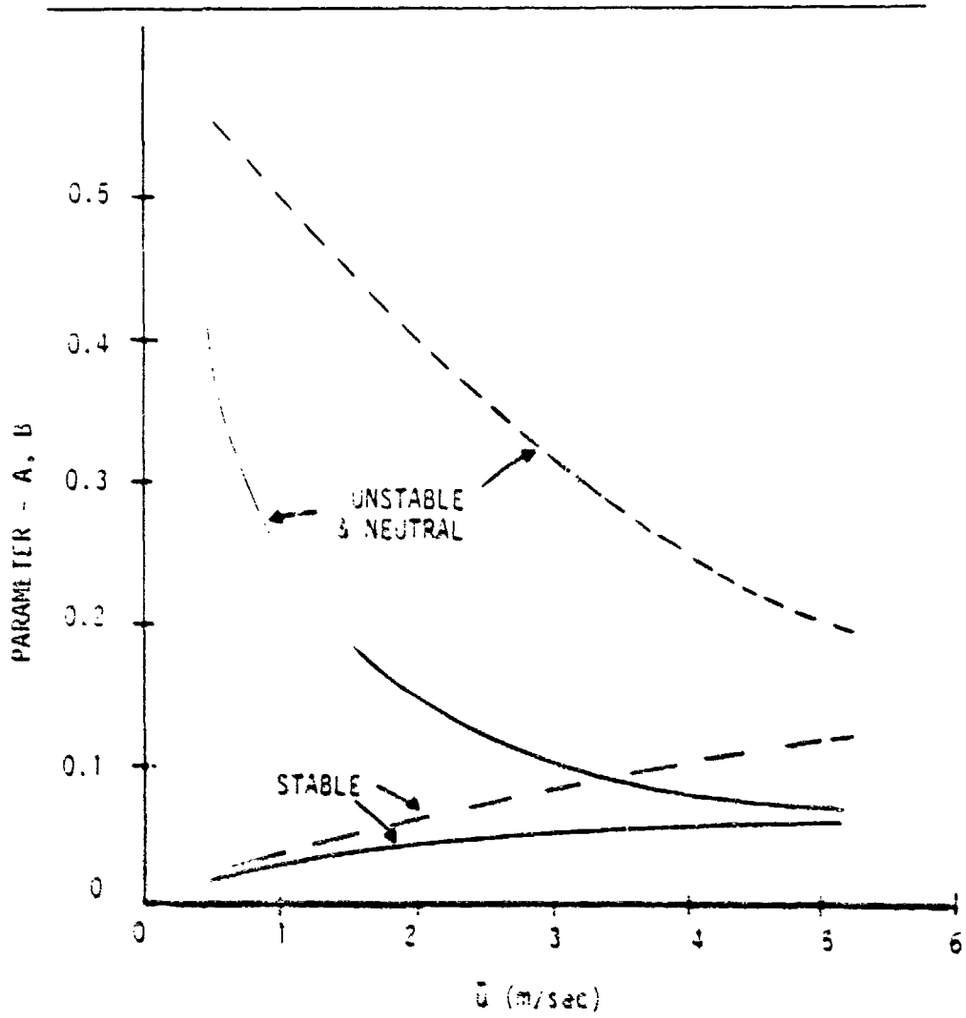

Figure C.1. Plume Parameters at Low Wind Speeds: Rise (A) ——; Lateral Spread (B) — —

APPENDIX D

ADDITIONAL CRATERING DATA

The US Army, Waterways Experimental Station, analyzed the available data through 1960 and reported the results in Ref. 1. The data included results from various explosives including shaped charges, various soils and terrain conditions, and charge weights from ≤ 1 lb to 10^6 lb. The results, in algebraic form, are given in Table D.1, where λ_c = scaled charge center location in units of ft/charge weight$^{1/3}$. It should be noted that the 3σ values for the crater radii and depths vary between 1.5× to 4× the mean value.

In this appendix several nomographs, Figs. D.1 and D.2, are reproduced here from Ref. 1 that show the differences between wet and dry soil types.

Additional data are provided in Tables D.2 and D.3 and Figs. D.3 and D.4.

---

[1] US Army, Waterways Experiment Station (WES), Analysis of Crater Data, Technical Report 2-547, Report 2, June 1961.

TABLE D-1

CRATER DATA

Material	Scaled Height, Depth ($\lambda/W^{1/3}$)	Crater Depth (ft)	Crater Radius (ft)
Various Soils	$\lambda_c = 0$	$.57W^{.35}$	$1.54W^{.32}$
Various Soils	$.7 \geq \lambda_c \geq 0$	$.24W^{.43}$	$.72W^{.34}$
Various Soils	$0 \geq \lambda_c \geq -1$	$1.01W^{.31}$	$2.15W^{.31}$
Various Soils	$-.45 \geq \lambda_c \geq -.55$	$1.32W^{.30}$	$2.3W^{.31}$
Various Soils	$-.9 \geq \lambda_c \geq -1.1$	$1.38W^{.29}$	$2.62W^{.29}$
Various Soils	$-1 \geq \lambda_c \geq -2$	$1.01W^{.34}$	$2.7W^{.30}$
Clay	$\lambda_c = 0$	$.93W^{.32}$	$1.87W^{.27}$
Clay	$0 \geq \lambda_c \geq -1$	$1.32W^{.31}$	$2.38W^{.30}$
Clay	$-.45 \geq \lambda_c \geq .55$	$1.49W^{.29}$	$2.28W^{.30}$
Clay	$-.9 \geq \lambda_c \geq -1.1$	$1.29W^{.32}$	$2.31W^{.33}$
Sand	$\lambda_c = 0$	$.64W^{.3}$	$1.67W^{.3}$
Sand	$0 \geq \lambda_c \geq -1$	$.95W^{.27}$	$2.08W^{.29}$
Sand	$-.45 \geq \lambda_c \geq -.55$	$1.16W^{.28}$	$2.31W^{.31}$
Sand	$-0.9 \geq \lambda_c \geq -1.1$	$1.64W^{.29}$	$2.78W^{.27}$

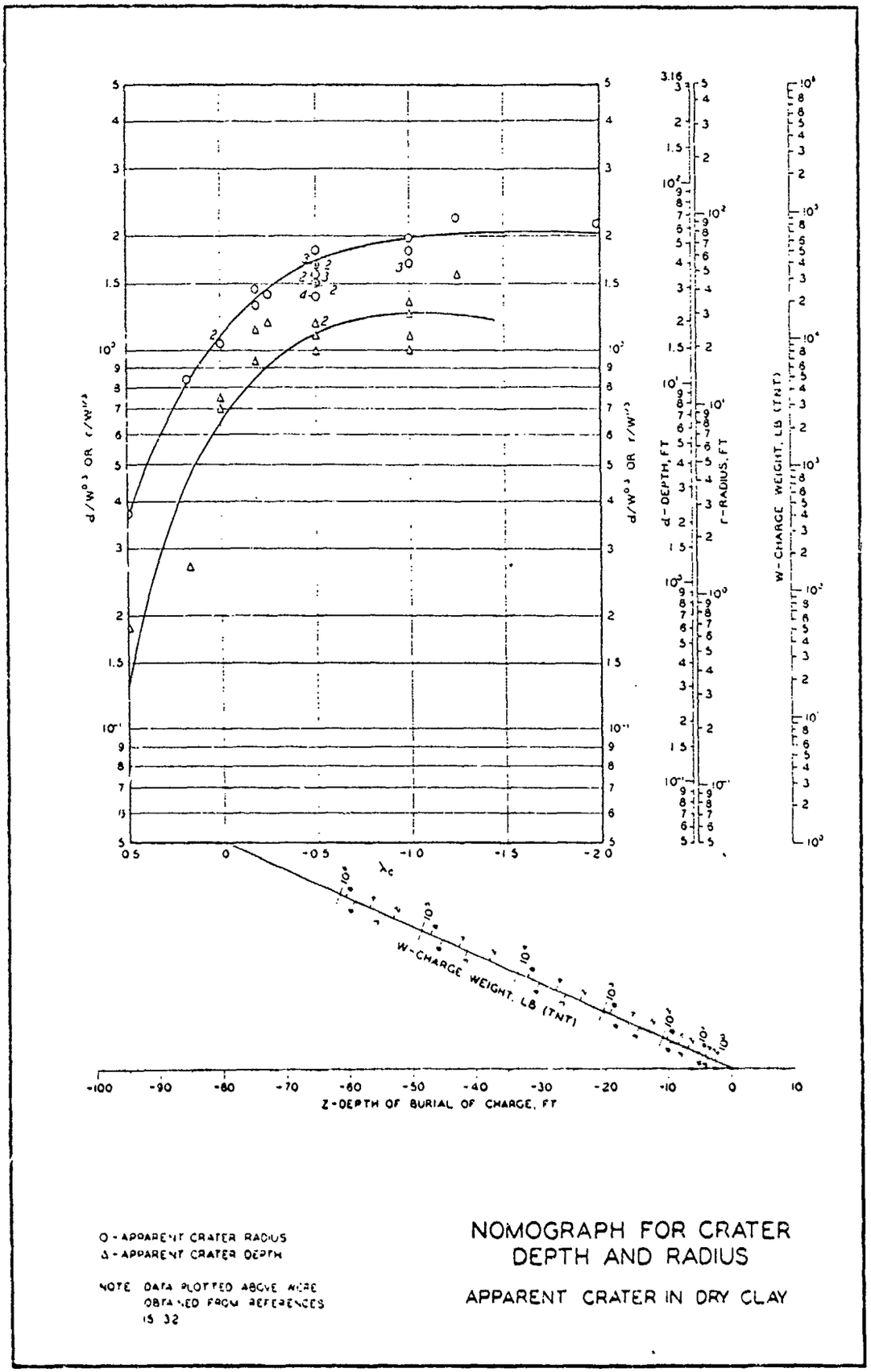

Figure D.1. Nomograph for Crater Depth and Radius (US Army, Waterways Experiment Station (WES), Analysis of Crater Data, Technical Report, 2-547, Report 2, June 1961.

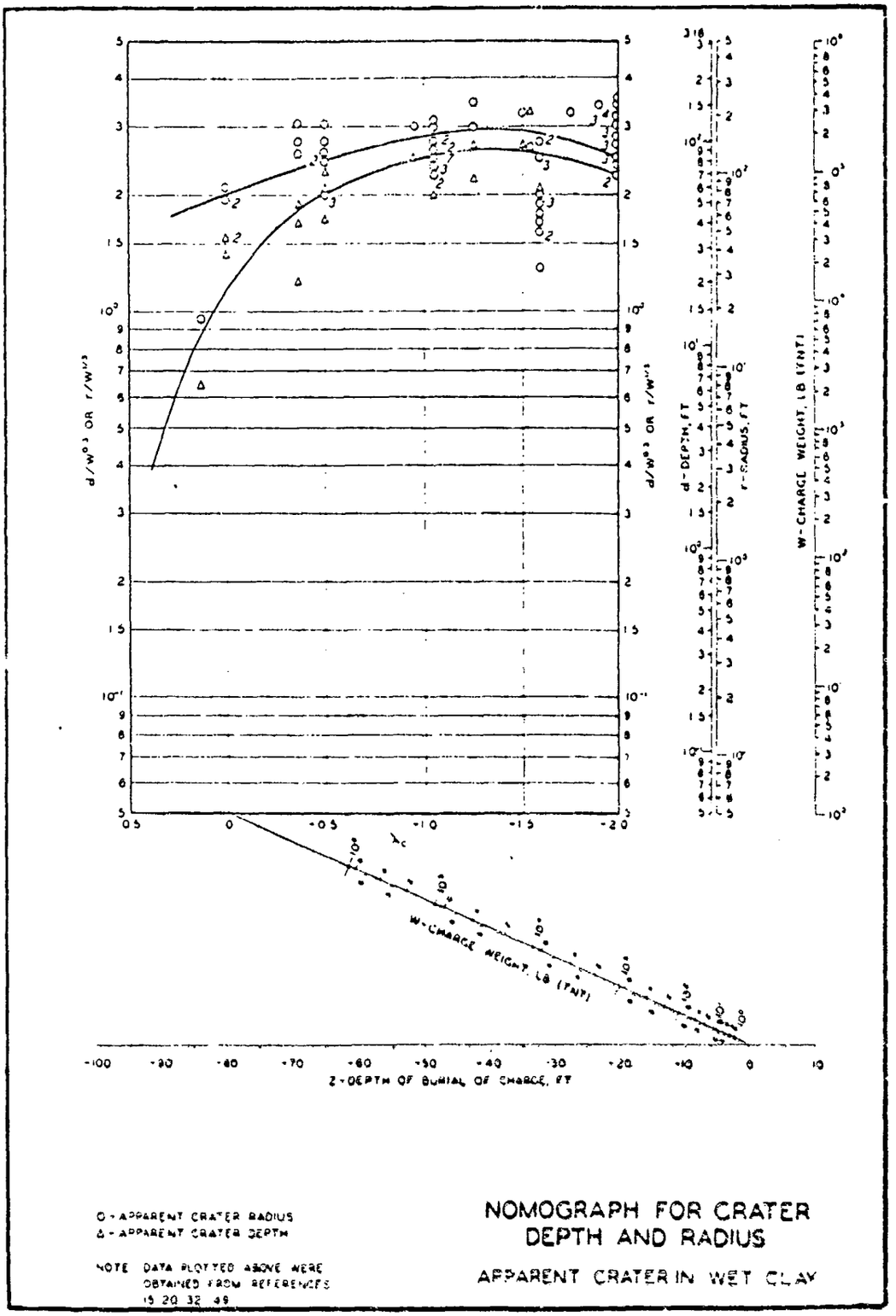

Figure D.2. Nomograph for Crater Depth and Radius (US Army, Waterways Experiment Station (WES), Analysis of Crater Data, Technical Report, 2-547, Report 2, June 1961.

TABLE D-2

MIDDLE GUST 1000 lb CRATERING DATA

EVENT	YIELD	HOB (Ft)	CONFIG.	R_a (Ft)	D_a (Ft)	V_a (Ft^3)	V_a (Ft^3) / W-TON	GEOLOGIC ENVIRONMENT
1	1000 lb	1.33	Ω	6.64	2.88	138	276	2 Ft Silty Clay over Weathered Shale
2	"	-17.0	o	25.93	9.21	10100	20200	9 Ft Sandy Clay over Weathered Shale. Water Table at -5 Ft.
3	"	0	⊖	16.23	5.56	2540	5080	" " " " " " "
3a	"	0	⊖	14.37	7.15	2080	4160	Shot in Clay Soil - No Overburden Removed - Water Table 4 Ft Down
3b	"	0	⊖	13.11	6.65	1620	3240	" " " " " " "
3c	"	0	⊖	16.13	4.74	2240	4480	" " " " " " "
3d	"	0	⊖	13.04	7.00	1560	3120	Shot in Clay Soil - No Overburden Removed - Water Table 4 Ft Down
4	"	1.33	Ω	8.04	5.27	401	802	9 Ft Sandy Clay over Weathered Shale. Water Table at -5 Ft.
5	"	1.33	Ω	11.67	5.01	741	1482	4 Ft Overburden Removed - in Sandy Clay Soil - Water Table 1 Ft Down
6	"	0	⊖	13.67	7.00	1970	3940	" " " " " " " "
6a	"	0	⊖	13.99	6.99	2040	4080	4 Ft Overburden Removed - in Clay Soil - Water Table at Surface
7	"	1.33	Ω	8.98	4.25	470	940	9 Ft Overburden Removed - in Weathered Shale - Water Table at Surface
8	"	0	⊖	14.92	7.35	2140	4280	" " " " " " "
9	"	0	⊖	15.09	5.00	1810	3620	16 Ft Overburden Removed - on Pierre Shale - Saturated

TABLE D-3

MIXED COMPANY 1000 lb CRATERING DATA

EVENT	YIELD	HOB (Ft)	CONFIG.	R_e (Ft)	D_a (Ft)	V_a (Ft^3)	$\frac{V_a (Ft^3)}{W\text{-ton}}$	GEOLOGIC ENVIRONMENT
1	1000 Lb	1.33	Ω	4.94	1.81	40.8	81.6	6-8 Ft Alluvial Sandy Soil over Sandstone, ρ = 112 Lb/Ft
2	"	0	⊖	5.56	2.60	87.7	175	" " " " " " " "
3	"	1.33	Ω	3.28	1.42	17.4	34.8	2 Ft Overburden Removed on Hard Sandstone, ρ = 137 Lb/Ft^3
4	"	0	⊖	8.69	3.49	339	678	" " " " " " "
5	"	1.33	Ω	7.90	1.70	130	260	0.65 Alluvial Sandy Soil over Sandstone - Alluvial Soil put Over Sandstone and Packed Down

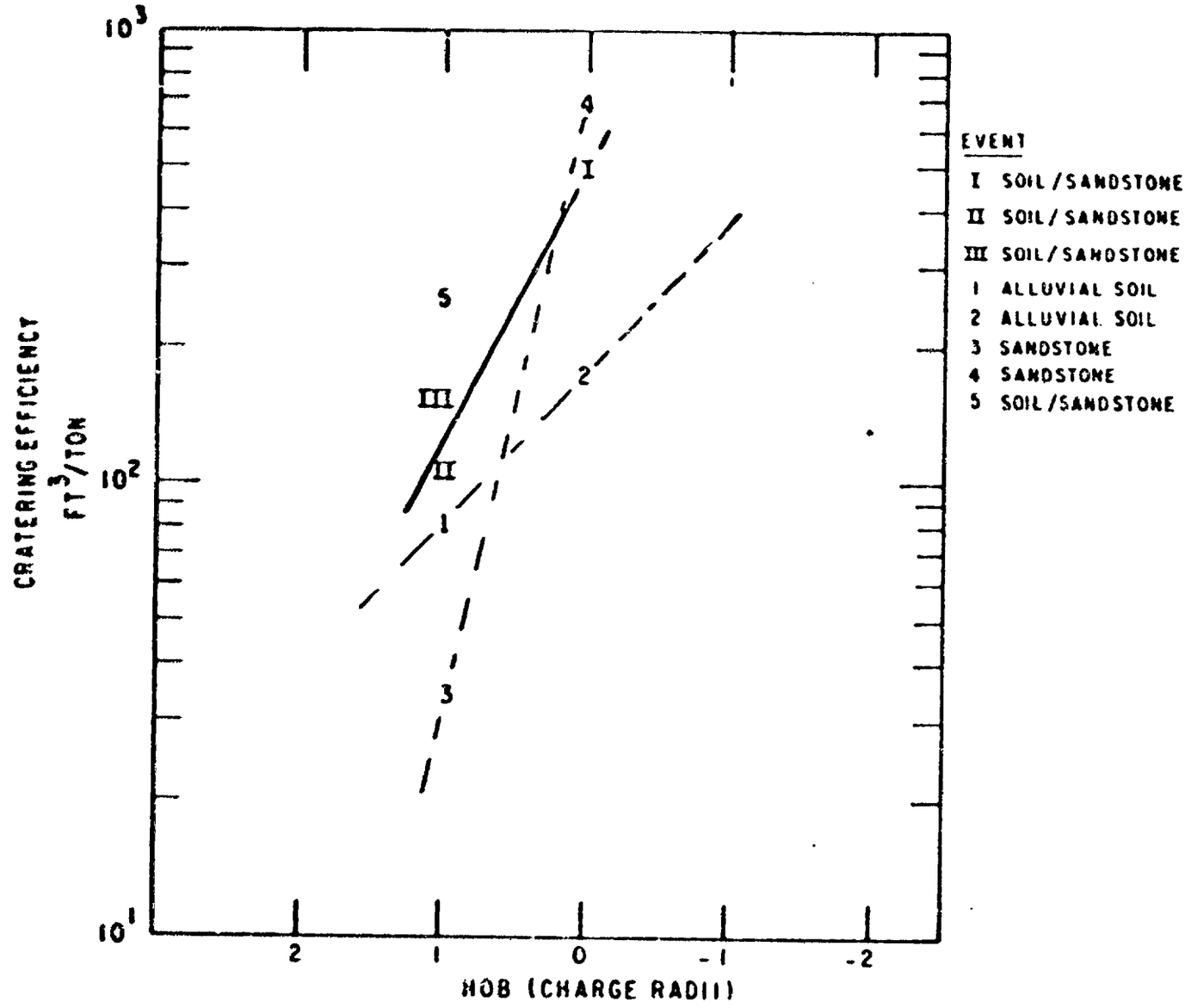

Figure D.3. Mixed Company Series

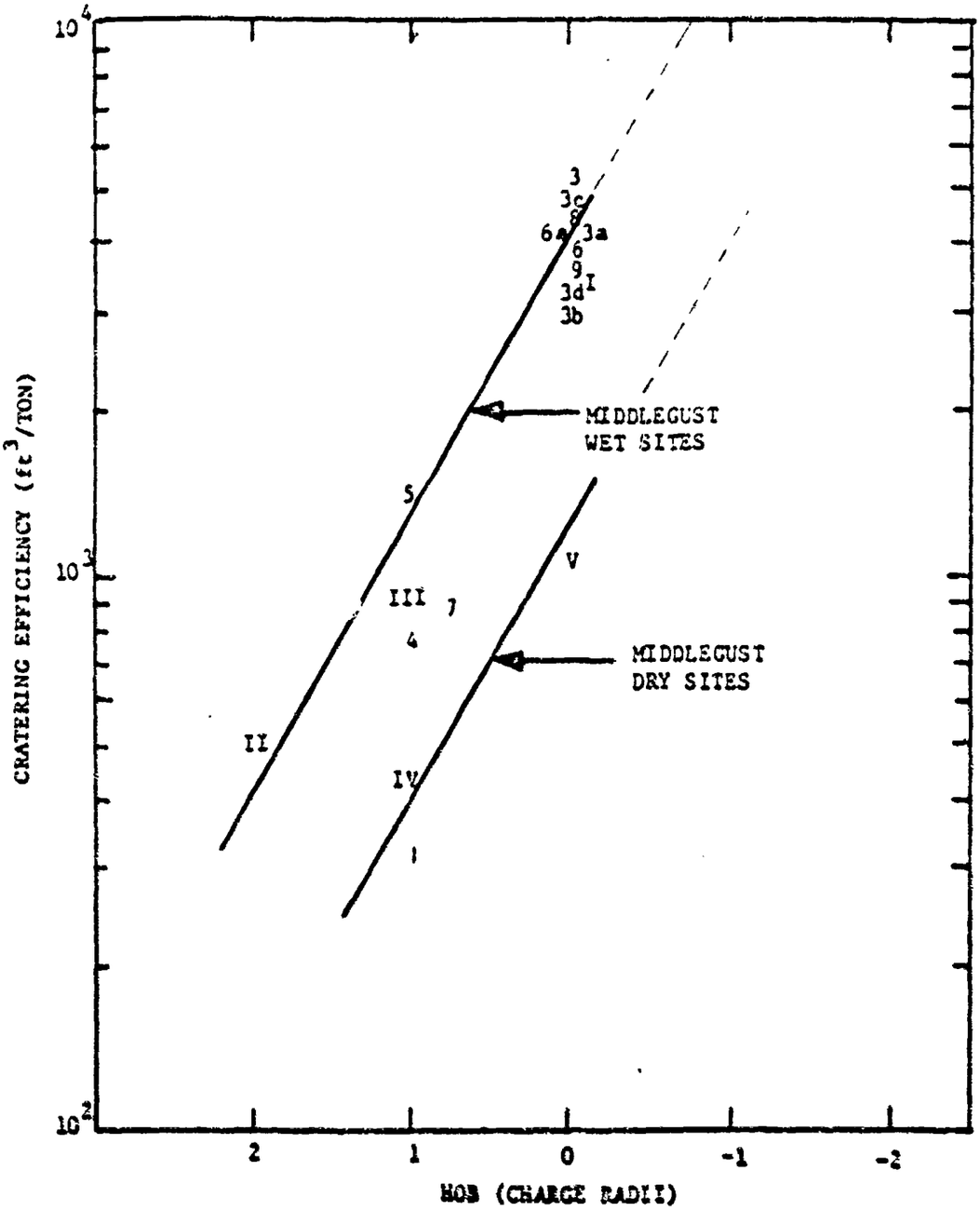

Figure D.4. Middlegust Series